UNIVERSITY OF CALIFORNIA SAN DIEGO

Brainstem control of voluntary urination

A dissertation submitted in partial satisfaction of the
requirements for the Degree Doctor of Philosophy

in

Neurosciences with a Specialization in Computational Neurosciences

by

Jason A. Keller

Committee in charge:

Professor Lisa Stowers, Chair
Professor William Kristan, Co-Chair
Professor David Kleinfeld
Professor Byung Kook Lim
Professor Sam Pfaff

2018

The dissertation of Jason A. Keller is approved, and it is acceptable in quality and form for publication on microfilm and electronically:

_____

_____

_____

_____

Co-Chair

_____

Chair

University of California San Diego

2018

DEDICATION

To Eli and Owen, who with great irony provided the human potty training data (N = 2).

EPIGRAPH

‘Forward now!' we inwardly cry, 'though the heavens fall.' This reckless and exultant espousal of an energy so little premeditated by us that we feel rather like passive spectators cheering on the display of some extraneous force than like voluntary agents, is a type of decision too abrupt and tumultuous to occur often in humdrum and cool-blooded natures. But it is probably frequent in persons of strong emotional endowment and unstable or vacillating character. And in men of the world-shaking type, the Napoleons, Luthers, etc., in whom tenacious passion combines with ebullient activity, when by any chance the passion's outlet has been dammed by scruples or apprehensions, the resolution is probably often of this catastrophic kind. *The flood breaks quite unexpectedly through the dam*.

William James, 1890

Nothing in neurobiology makes sense – except in the light of behavior.

Gordon Shepherd, 1983

TABLE OF CONTENTS

LIST OF FIGURES

LIST OF SUPPLEMENTAL VIDEOS

Supplementary Video 1: Awake photostimulation of Bar$^{ESR1\text{-}ChR2}$ neurons at five different frequencies. Top and bottom views of a freely moving Bar$^{ESR1\text{-}ChR2}$ mouse urinating in response to light pulses at five frequencies: 1, 5, 10, 25, 50 Hz. Photostimulation occurs when white frequency letters appear on middle-left. Video condensed to 4X speed.

Supplementary Video 2: Awake photostimulation of Bar$^{CRH\text{-}ChR2}$ neurons at five different frequencies. Top and bottom views of a freely moving Bar$^{CRH\text{-}ChR2}$ mouse urinating in response to light pulses at five frequencies: 1, 5, 10, 25, 50 Hz. Photostimulation occurs when white frequency letters appear on middle-left. Video condensed to 4X speed.

Supplementary Video 3: Anesthetized photostimulation of Bar$^{ESR1\text{-}ChR2}$ neurons. Top and bottom views of an anesthetized Bar$^{ESR1\text{-}ChR2}$ mouse urinating in response to three 50 Hz photostimulation bouts, separated by 1 min intervals. Subject is moved between stimulations to observe and record urine excreted during each photoperiod. Video condensed to 4X speed.

Supplementary Video 4: Photostimulation of Bar$^{ESR1\text{-}ChR2}$ neurons during cystometry. Urine output during Bar$^{ESR1\text{-}ChR2}$ photostimulation while recording bladder pressure (top yellow trace) and urethral sphincter EMG (bottom red trace). Blue shading on plots and blue light shadow behind mouse delineate photostimulation period. Video slowed to 0.67X speed.

Supplementary Video 5: Photostimulation of Bar$^{CRH\text{-}ChR2}$ neurons during cystometry. Urine output during Bar$^{CRH\text{-}ChR2}$ photostimulation while recording bladder pressure (top yellow trace) and urethral sphincter EMG (bottom red trace). Blue shading on plots and blue light shadow behind mouse delineate photostimulation period. Video slowed to 0.67X speed.

Supplementary Video 6: Odor motivated urination assay. Example urine marking behavior under UV light in response to control odor (1.5 - 2 min.) and female odor (2 - 4 min.) in a 4 min. assay. Video condensed to 4X speed.

Supplementary Video 7: Photoinhibition of Bar$^{ESR1\text{-}ArchT}$ neurons prevents rapid, odor-evoked urination. Bar$^{ESR1\text{-}ArchT}$ mouse before, during, and after a 2 min. photoinhibition period during which female urine was presented. Video condensed to 4X speed.

ACKNOWLEDGEMENTS

Thank you first to my advisor, Lisa Stowers, for providing just the right balance of mentorship and resources, intellectual freedom, and prudence when things veer off track. I also owe a great debt to the entire Stowers Lab over the past few years, particularly: Marisol Chacon, Natasha Weaver, and Angela Asaro, who provided administrative support, Angel Kaur, who started scent marking behavior in the lab, and Jingyi Chen, who kept my sanity during paternity leave and has been invaluable to this project.

The Dorris Neuroscience Center community at The Scripps Research Institute is an incredible privilege to share. Thank you to Denyse Huff and Jessie Lat for keeping the mice happy, to Kathy Spencer for keeping a spare everything, to Ardem Patapoutian and Bruno Conti for lending data acquisition hardware and resources, and to Sierra Simpson, an expert mouse urologist that fate would make my neighbor and friend. Thank you to Helen Dorris for backing it all.

Thank you to my thesis committee members for your valuable time and advice, as well as sharing your lab's expertise. In particular, Ariel Levine helped with spinal techniques, Eric Wang helped with fiber photometry, and Varoth Lilascharoen performed slice recordings and made virus. The greater mesa neurosciences community and the Neurosciences Graduate Program have been instrumental not only for this project but for my personal growth as well. Tom Hnasko generously provided transgenic mice. Many administrators, particularly Erin Gilbert and Linh Vandermar, provided critical support and made it a pleasure to navigate as a graduate student parent. Thank you to everyone who caught a few gamma waves with me.

Thank you to the many other teachers and mentors who allowed me to get to UCSD, especially LaVonne Neal, Dixie Ross, Steve Stotts, Heidi Frock, Jeremy Cook, Paola

Pedarzani, Micheal Haüsser, Spencer Smith, Karel Svoboda, Mac Hooks, Vjay Iyer, and Simon Peron. The National Science Foundation generously supported my research (NSF-GRFP DGE-1144086), and I am forever grateful for their support of basic science.

Last but not least, thank you to my family, for your love, support, and sacrifice. Dad, thanks for showing me around the garage, and Mom, thanks for teaching me to work hard and aim high. To my wife Emily – none of this is possible without you. From simple editing to cheering me up to making me think about how brains and bladders deal with child-bearing, you make me a better scientist and person and deserve so much credit.

The Results, in part, are a reprint of material as it appears in bioRxiv, available at: https://doi.org/10.1101/270801. This material, in part, has also been submitted for publication in Nature Neuroscience, 2018. Keller JA, Chen J, Simpson S, Wang E, Lilascharoen V, George O, Lim B, Stowers L, 2018. The dissertation author was the primary investigator and author of these papers.

VITA

2000-2004 Bachelor of Science, Electrical Engineering, The University of Texas at Austin

2005-2008 Hardware Engineer, National Instruments Corporation

2008-2011 Bachelor of Science, Neuroscience, University College London

2011-2018 Doctor of Philosophy, Neurosciences, University of California San Diego

PUBLICATIONS

Keller JA, Chen J, Simpson S, Wang E, Lilascharoen V, George O, Lim B, Stowers L. (2018). Brainstem control of urethral sphincter relaxation and scent marking behavior. bioRxiv. Available at: https://doi.org/10.1101/270801.

Stowers L, Cameron P, Keller JA (2012). Ominous odors: olfactory control of fear and aggression in mice. Curr. Opin. Neurobiol. 23, 339-345.

ABSTRACT OF THE DISSERTATION

Brainstem control of voluntary urination

by

Jason A. Keller

Doctor of Philosophy in Neurosciences with a Specialization in Computational Neurosciences

University of California San Diego, 2018

Professor Lisa Stowers, Chair
Professor William Kristan, Co-Chair

Scent marking behavior in male mice can simultaneously address two important gaps in neuroscience: (1) the need for a simple and ethologically relevant output to make sense of the neural activity driving it, and (2) the need for better models of voluntary urination to take us beyond a coarse understanding of prevalent medical issues. Uncontrolled urination, or

incontinence, is a common problem that stems from disruption at the two main muscles responsible, the bladder wall and external urethral sphincter (EUS). Lesion studies have shown that these muscles switch from urine storage to release via control from a small region in the brainstem known as Barrington's nucleus (Bar). Although we know some cellular details of bladder control, specific neurons that relax the EUS and ultimately enable urine flow are unknown, partly because this is a voluntary, striated muscle, and adequate animal models of voluntary urination do not exist. Here we establish a scent marking assay in which male mice rapidly urinate when presented with female odor. This allows measurement and manipulation of neural activity in Bar while quantifying voluntary urination, and led us to identify a small subset of novel Bar neurons that control the EUS. These excitatory neurons express estrogen receptor 1 (Bar^{ESR1}), project to sphincter-relaxing interneurons in the spinal cord, and have increased activity during natural urination. Optogenetic stimulation of Bar^{ESR1} neurons rapidly initiates sphincter bursting and efficient voiding in anesthetized and behaving animals. Conversely, optogenetic and chemogenetic inhibition reveals their necessity in motivated urination behavior. The identification of these cells provides an expanded model for the control of voluntary urination and its dysfunction, as well as a tractable anchor from which to study upstream control. Because scent marking behavior is regulated by age, sex, competing interests, and learning, this paradigm provides a powerful avenue for future studies examining more general mechanisms of behavioral control in mammals.

INTRODUCTION

Two fundamental problems motivate this thesis. First, behavior is complicated beyond comprehension. Moving your arm generally requires tens of muscles controlling the skeletal system against external forces such as gravity, along with millions of neurons at the premotor level, distributed throughout the brain and spinal cord. The inputs that trigger such a movement are often dynamic and require structured memory resources, for example someone asks you to move your arm using learned human language, or throws a ball at your arm. Is there a simpler behavior, with low-dimensional input and output, but still enough variability to generalize it, that can aid our understanding of the underlying neural mechanisms? Here I will argue that urination (aka. micturition), a behavior requiring coordination of only two principle muscles, the bladder wall and urethral sphincter[1–10], can fulfill this role.

The second problem relates to urination as a fundamental need to eliminate nitrogenous liquid waste. Although humans urinate involuntarily at birth, voluntary urination is achieved with learning and development. Involuntary urination affects one in three adults worldwide at some point in their lives and remains an enormous healthcare burden[11]. However, the neurons in the brain that control this process remain obscure, at least in part because most studies on the neural control of urination have focused on *reflex* urination, where bladder filling and voiding can be easily controlled and monitored in anesthetized animals. However, *voluntary* urination occurs before the bladder reaches capacity and must be studied in awake, behaving animals. Because of these experimental complications, there is little understanding of the neural substrates underlying natural, voluntary urination behavior

and continence. Here I contend that this problem can be addressed by a particular type of voluntary urination, common in many animal models.

House pets commonly demonstrate that many animals learn to control urination behavior, in addition to humans. Moreover, territorial males of many wild animals including fish[12,13], rodents[14–24], and primates[25] deliberately urinate their domain to transmit social information in the form of pheromones. Male mice in particular scent-mark prolifically in order to attract female mating partners[18,14,26]. However, exuberant urination behavior is metabolically wasteful[27] and may attract other aggressive males[28] or predators[29–33]. Mice offset these risks by limiting voluntary scent marks to critical social environments such as those most likely to contain females[14,22]. Therefore, the use of female odor to promote rapid and robust scent marking behavior in the male mouse serves as an experimental platform to identify neurons controlling voluntary urination.

The switch from urine storage to deliberate elimination is known to depend on brain input, as spinal cord injury acutely prevents voluntary urination. Barrington's nucleus (Bar, aka. pontine micturition center, PMC, M-region), is a well-conserved and heterogeneous population of neurons in the dorsal pons that was identified as the major brain center regulating urination almost a century ago[34–36]. Since then, multiple lines of evidence have converged to support the role of Bar in reflex urination under anesthetized conditions[1,36]. Recent evidence also implicates Bar in other functions requiring pelvic muscles such as defecation, childbirth, and sexual activity[4,5,37], thus raising the question of whether functional heterogeneity in Bar is reflected at the cellular and molecular levels. Bar contains at least three different cell types defined by physiology[38–41], gene expression[36,42], and histology[36,43,44]. The best-studied among these express corticotropin releasing hormone/factor (CRH or

CRF)[45–49,3]. Bar^{CRH} neurons increase their firing rate during anesthetized bladder and colon distension as well as awake, diuretic-induced urination[50,42]. However, about half of the Bar neurons projecting to the spinal cord lack CRH expression[47], and their molecular identity and functions are unknown[36]. Current models of Bar[1,42] assume a single projection to the spinal cord controlling bladder and urethra, and this work sought to clarify the functional consequences of cellular heterogeneity in Bar.

Although Bar^{CRH} neurons can increase bladder pressure when optogenetically stimulated in anesthetized mice[42], it is not known if any Bar cell type can drive urination in awake animals. The smooth muscle of the bladder wall (i.e. the detrusor muscle) contracts slowly via autonomic, involuntary control, which alone is not sufficient for voiding. Urine release is gated by the external urethral sphincter (EUS, or urethral rhabdosphincter[51,52]), which is normally constricted, but relaxes to allow urine flow (Figure 1a). In humans, this relaxation precedes bladder contraction and initiates voluntary urination[53–56]. An increase of bladder pressure without sphincter relaxation leads to the guarding reflex, which is a compensatory tonic contraction of the EUS to prevent unwanted urination. The EUS is composed of striated muscle to permit fast control via somatic, voluntary motoneurons. It is monosynaptically inhibited by interneurons in the dorsal grey commissure (DGC) in the spinal cord[57,58]. Broad electrical or chemical stimulation of Bar drives urination[59–61], but it is not known if any subset of Bar neurons is sufficient to control voiding by relaxing the urethral sphincter.

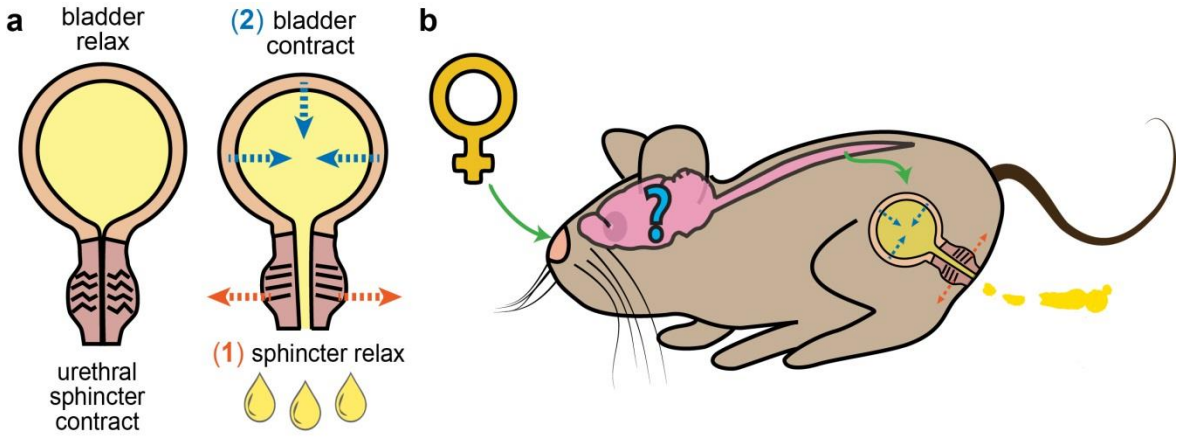

Figure 1. Urination muscles are endpoints in a relatively simple CNS circuit.
a, Release of urine requires urethral sphincter relaxation (voluntary striated muscle) followed by bladder contraction (autonomic smooth muscle). **b,** Urination muscles are the final output in a complete sensory-to-motor circuit in the male mouse, with female odor as the input**.**

Rodents use a specific bursting mechanism to relax the EUS for efficient urination[62–68], which is believed to be necessary to overcome surface tension in the urethra[69], and some have speculated a specific role in scent marking behavior[70,4]. This distinct bursting pattern in a single striated muscle can also be considered as the objective and simple output of a reductionist circuit through the central nervous system (CNS), having female odor as the input (Figure 1b). Its muscular simplicity, relative to other behaviors, provides a key advantage for untangling upstream control mechanisms. The rodent EUS has no skeletal connections to move against external forces, and the duration of muscle relaxation correlates well with observable urine output[67,63]. Identifying the substrate of urethral relaxation in the brain could thus give hope for unraveling the inherent complexities in a brain circuit containing billions of interacting cells.

Because of these complexities, this “nose-to-sphincter” circuit is not merely a reflex; it includes many properties that can address fundamental topics in neuroscience: sexual dimorphism[71], developmental regulation[72], plus modulation by social status[28], environmental

risk[29–33], and learning[73]. Olfaction is well-studied in mice and provides more direct input to the core of the brain known as the "limbic system", compared to other sensory sytems[74]. A variety of evidence supports the importance of limbic neurons, some of the most well-connected neurons in the CNS (e.g. extended amygdala and hypothalamus), in many behavioral tradeoffs. Yet rigorous inquiry into the neural mechanisms at hand requires a *complete* circuit, since interactions that affect information transfer from input to output could occur at any one node or combination of nodes. No functional circuit has been established from sensory input to motor output that traverses the aforementioned brain areas, and consequently this thesis originated to lay the groundwork with behavior and brainstem motor control in such a circuit in the mouse.

The present work establishes a rapid scent marking assay in male mice and shows that this voluntary urination depends upon a subpopulation of spatially clustered neurons in Bar that express high amounts of estrogen receptor 1 (Bar^{ESR1}). These neurons project heavily and distinctly to the DGC and increase their activity during voluntary scent marking urination in freely behaving mice. Bar^{ESR1} neurons drive efficient voiding when photostimulated in awake animals, and urinary muscle recordings in anesthetized animals indicate a mechanistic role in urethral sphincter relaxation. Chemogenetic inhibition of Bar^{ESR1} but not Bar^{CRH} neurons abolishes natural scent-marking urination, and acute Bar^{ESR1} photoinhibition abruptly terminates ongoing EUS relaxation. Thus, Bar^{ESR1} neurons are necessary and sufficient to drive urethral relaxation and voluntary urination in male mice and provide an expanded model for the supraspinal control of urination and its dysfunction, as well as a critical node in a mechanistic nose-to-sphincter behavioral model.

CHAPTER 1

RESULTS

1.1 A novel cell type in Barrington's nucleus

Bar^{CRH} neurons were first described decades ago[45] and provide an obvious starting point for finding a specific premotor input that drives scent marking behavior and can be traced back to the nose. However, our initial tests and a previous study of Bar^{CRH} neural function showed modest effects on urination in awake animals[42], suggesting that these neurons are unlikely to facilitate voluntary urination. We therefore took a candidate approach to identify molecular markers for Bar neurons that may function to promote urinary sphincter relaxation, using previous literature and online databases[75]. We focused on estrogen receptor 1 (ESR1, ESRα), as it is expressed in a subset of Bar cells in both mice[44] and primates[76]. It is unknown if ESR1 marks a cell type distinct from Bar^{CRH} neurons. Immunostaining with αESR1 in CRH-Cre[77] x ROSA-LSL-tdTomato (CRH-tdT) individuals confirmed a small Bar subpopulation (~200 cells) expressing high amounts of ESR1 (Bar^{ESR1} neurons, Figure 2a-e). The majority of Bar^{ESR1} neurons (~3/4 of the Bar^{ESR1} population, Figure 2e) do not overlap with CRH-tdT, and the overlapping minority likely represents an upper bound on co-expression since tdT integrates CRH promoter activity over the lifetime of the animal. Bar^{ESR1} neurons are found in a dorsal cluster within the Nissl-defined ovoid Bar nucleus, whereas Bar^{CRH} neurons are more numerous (~500 cells[42]), ventrally biased, and extend further along the rostrocaudal axis beyond traditional, Nissl-defined Bar borders[78] (Figure 2c-d). Moreover, in ESR1-Cre mice[79], 96.8 % of Bar^{ESR1} neurons (N = 3 mice) overlap with reporter expression (Figure 3a), confirming that the CRH and ESR1 promoters are active in largely independent Bar populations.

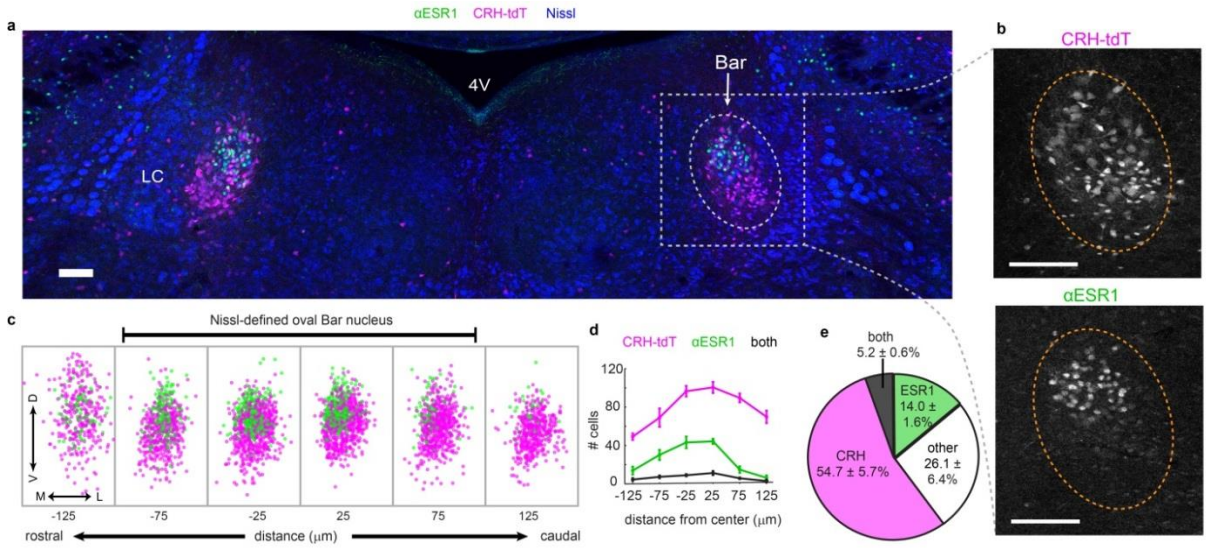

Figure 2. Bar^{ESR1} and Bar^{CRH} neurons are spatially distinct
a, ESR1-immunostaining in Bar (dotted oval) in CRH-tdT mouse. LC = locus coeruleus, 4V = 4th ventricle. **b,** Larger view of CRH-tdT (top) and αESR1 (bottom) channels from (a)**. c,** Rostrocaudal overlay of αESR1 cells (green) in Bar registered to centroid of CRH-tdT cells (magenta). **d,** Cell counts, and **e**, cell percentages in Bar (mean ± s.e.m., N = 6).

This separation of ESR1 and CRH in Bar subpopulations suggests that Bar^{ESR1} neurons could correspond to the glutamatergic, CRH-negative Bar population with unknown function and projections to urinary targets in the spinal cord[36]. We therefore evaluated αESR1 expression at the protein and mRNA levels, in conjunction with inhibitory and excitatory neuron markers VGAT and VGLUT2, to reveal that the majority of Bar^{ESR1} neurons express VGLUT2 (93.6 % reporter overlap, N = 3 mice) and not VGAT (2.2 % reporter overlap, N = 4 mice; Figure 3b-k). Bar^{ESR1} neurons are thus likely to use glutamate as a fast neurotransmitter to excite their synaptic targets.

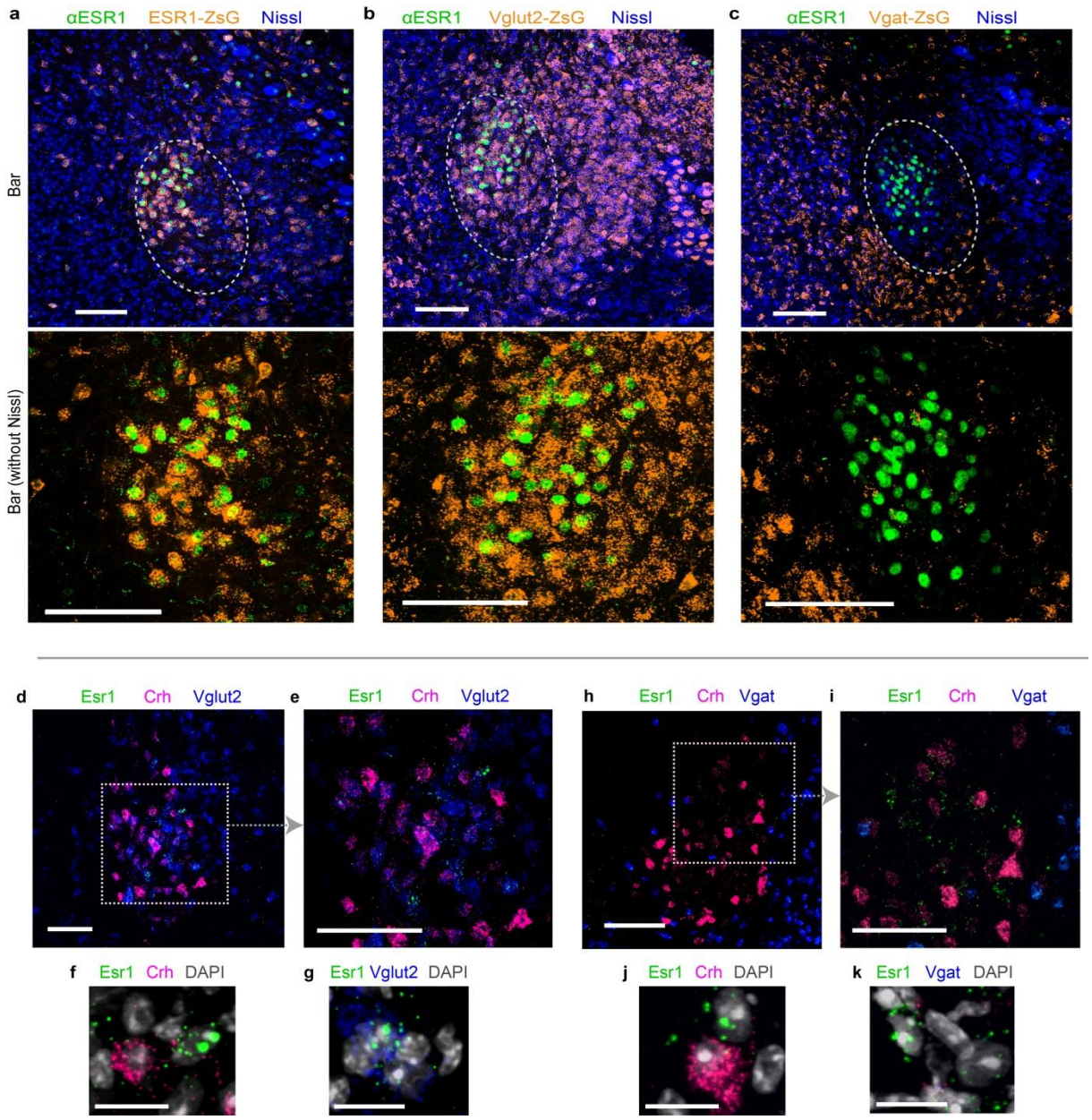

Figure 3. Neurotransmitter identity of Bar^{ESR1} neurons.
a, αESR1 overlap with ESR1-ZsGreen (Ai6) genetic reporter. Bottom is larger view without Nissl. **b,** αESR1 overlap with VGLUT2-ZsGreen genetic reporter. **c,** αESR1 overlap with VGAT-ZsGreen genetic reporter. **d,** RNAScope in-situ hybridization of Crh/Esr1/VGLUT2 mRNA in Bar region of a wild-type male mouse, 20X objective. **e,** Larger view of dotted area in (d), 40X objective. **f, g,** Close-up views of individual cells in (e), with DAPI counterstain. **h-k,** same as (d)-(g), but with VGAT mRNA probe. Scale bars = 100 μm, except panels f/g/j/k, scale bars = 20 μm.

Because ESR1 marks a superset of sexually dimorphic neurons in the brain, we also evaluated whether aromatase (ARO), which can convert testosterone to estrogen in males[80], is present in Bar. ARO expression in Bar neurons would imply that male mice can locally convert testosterone to estradiol for functional significance of ESR1 in Bar^{ESR1} neurons. However, using ARO-Cre mice[81] crossed to fluorescent reporter mice, we find very few ARO+ cells or axons in Bar (Figure 4a-b), suggesting that males do not convert testosterone to estradiol there, unless from an unknown mechanism such as hormonal ARO transfer.

Finally, we assessed the presence of the inhibitory neurotransmitter GABA itself in Bar of CRH-tdT mice, as recent studies have suggested excitatory and inhibitory heterogeneity amongst CRH-expressing neurons in other brain regions[82]. Although both Bar^{ESR1} and Bar^{CRH} neurons have little overlap with inhibitory markers such as VGAT and $GAD_{65/67}$[36,42], more exotic cell types with co-expression of excitatory and inhibitory markers are increasingly recognized[83]. We stained for GABA using an antibody conjugated to BSA with glutaraldehyde, coupled with glutaraldehyde fixation[84] (Figure 4c-e). Using this method, we found diffuse GABA staining in areas with mostly inhibitory neurons such as striatum, as well as punctate cell body staining in a minority of cortical neurons that always overlapped with CRH-tdT interneurons there (Figure 4d), but clearly did not stain cell bodies of all cortical inhibitory neurons. In Bar, we saw the same intense cell body labelling, but only in a subset of Bar^{CRH} neurons, particularly in the ventral part of the nucleus with few Bar^{ESR1} neurons. No GABA cell bodies were detected in Bar cells that do not express CRH (Figure 4e). Thus the expression of GABA in small subsets of Bar^{CRH} neurons is consistent with further heterogeneity within the total Bar population, in addition to the spatial separation of ESR1 and CRH populations.

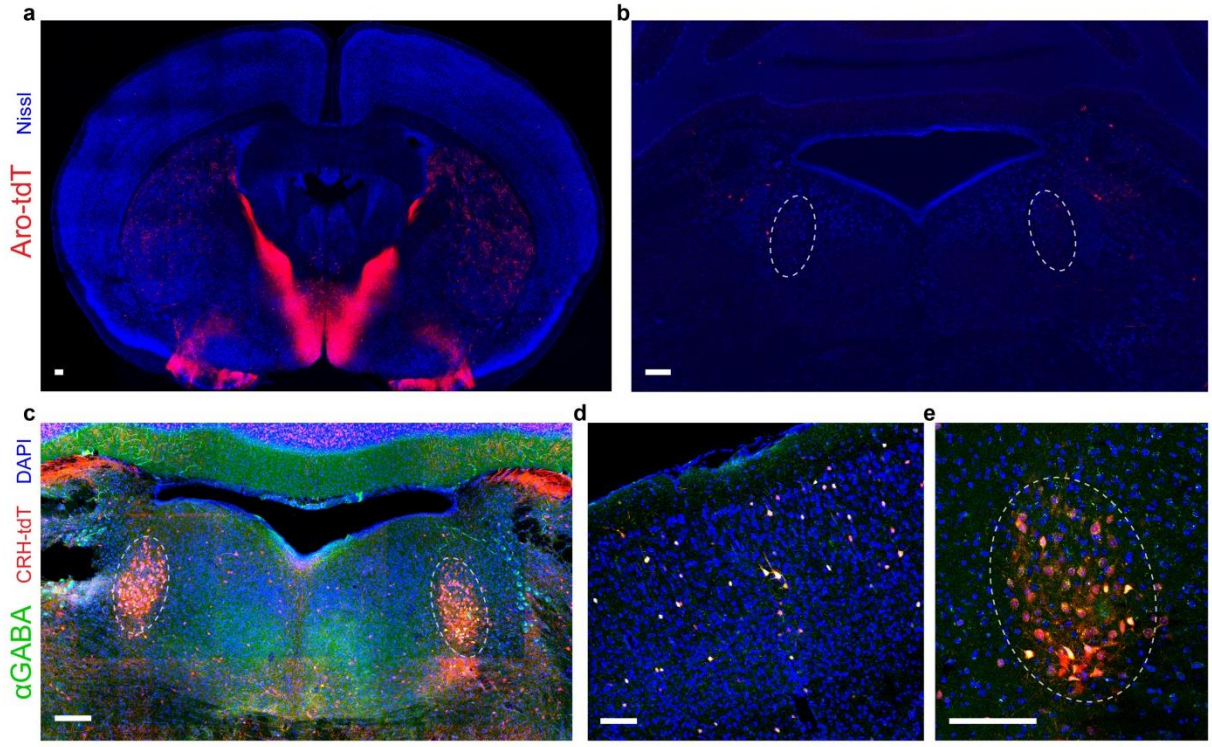

Figure 4. Aromatase and GABA in Bar.
a, Male ARO-tdT reporter mouse section at the level of the BNST shows intense aromatase expression there, as previously reported[71]. **b,** Bar section from the same mouse as (a), showing almost no ARO+ fibers or cell bodies. **c**, GABA immunostaining in Bar of a male mouse. **d**, Control cortical sections show sparse GABA+ cell bodies overlapping with CRH-tdT expression. **e**, Closer view of GABA+ / CRH-tdT cell bodies in Bar. Scale bars = 100 μm.

1.2 Outputs of Bar^{ESR1} neurons

To investigate the potential for Bar^{ESR1} neurons to relax the urethral sphincter, we first evaluated direct anatomical connections to the lumbosacral spinal cord that contains urinary interneurons and motoneurons. Injection of the retrograde tracer cholera toxin subunit b (CTB) centered at the S1 spinal cord resulted in co-expression with Bar^{ESR1} cells, indicating their direct projections to the general region of bladder and sphincter interneurons (Figure 5). To further investigate these projections, we unilaterally injected AAV expressing Cre-dependent GFP into the Bar of ESR1-Cre or CRH-Cre animals, and imaged the lower thoracic to sacral spinal cord (Figure 6a-c). The lumbosacral mediolateral column (ML) contains

preganglionic autonomic neurons that excite the bladder (along with intermingled interneurons)[58,85], and the lumbosacral dorsal grey commissure (DGC; aka. dorsal commissural nucleus, lamina X, central autonomic nucleus) contains interneurons that directly inhibit or relax sphincter motoneurons of the dorsolateral nucleus (DL, analogous to Onuf's nucleus in humans) via Bar input[57,86,58] (Figure 6a). Consistent with the known role of Bar^{CRH} neurons in bladder pressure regulation, Bar$^{CRH\text{-}GFP}$ axons showed a dense focal projection to the ML (Figure 6b-c, bottom) with only sparse fibers arching further medially or to thoracolumbar levels T13-L2 (Figure 6c,e, bottom). Bar$^{ESR1\text{-}GFP}$ axons projected similarly across the lumbosacral ML, with additional lighter fibers seen in the thoracolumbar ML (Figure 6c,e, top). Importantly, they also provided much denser innervation of the sphincter-inhibiting DGC, extending rostrally from the proposed L3-L4 burst generator[87] to mid-sacral levels (Figure 6c,e,f, top). Bilateral labeling of Bar^{ESR1} or Bar^{CRH} neurons with a second Cre-dependent virus (AAV-FLEX-ChR2) confirmed the same projection patterns (Figure 6d). Very few axons, in comparison, extended rostrally into the brain (Figure 7), suggesting that the main synaptic targets of both Bar^{ESR1} and Bar^{CRH} neurons are in the lumbosacral spinal cord. Overall, the cell body distribution, molecular expression, and efferents of Bar^{ESR1} neurons indicate that they constitute an uncharacterized cell type within Bar[36], distinct from Bar^{CRH} neurons.

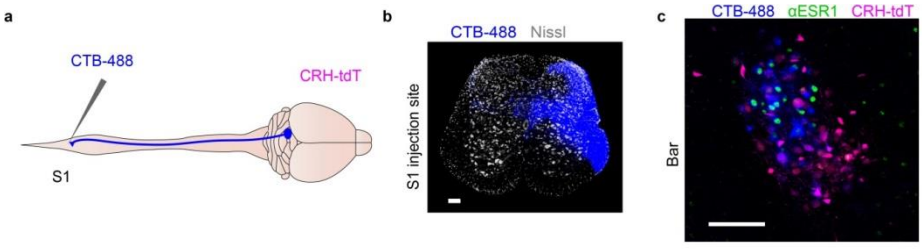

Figure 5. Direct spinal projections of Bar^{ESR1} neurons.
a, Schematic of CTB injection into S1 spinal cord. **b,** CTB injection site. **c,** Retrograde CTB labeling in Bar with αESR1 and CRH-tdT. Dotted ovals delineate Bar. Scale bars = 100 μm.

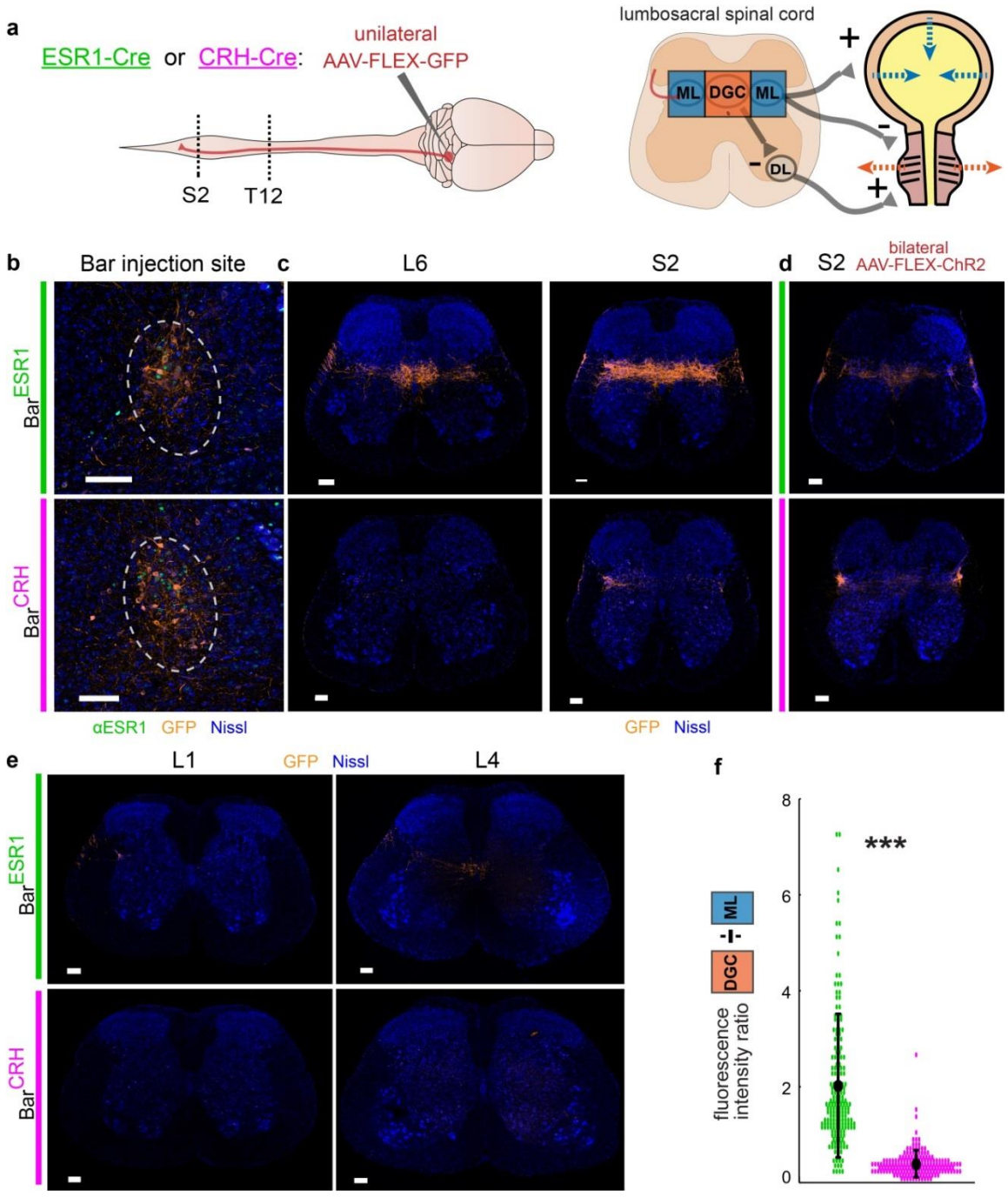

Figure 6. Bar^{ESR1} projections are biased to sphincter-inhibiting interneurons.
a, Schematic for identifying Bar cell type axonal projections to spinal cord and simplified urinary circuitry in the lumbosacral spinal cord. ML = mediolateral column, DGC = dorsal grey commissure, DL = dorsolateral nucleus. **b**, GFP expression at Bar injection site in ESR1-Cre (top) or CRH-Cre (bottom) individuals. **c**, Axonal projections in lumbosacral spinal cord (right L6, left S2) for injections in (b). **d**, Axonal projections in lumbosacral S2 spinal cord for injection sites in Figure 13b. **e**, Axonal projections in rostral lumbar spinal cord (right L1, left L4) for injections in (b). **f**, Quantification of Bar^{ESR1} and Bar^{CRH} axonal projections in lumbosacral spinal cord. Points are individual sections, thick black line is mean ± s.e.m for Bar^{CRH} (magenta, N = 10 mice), Bar^{ESR1} (green, N = 10 mice). Scale bars = 100 μm. ***p<0.001 (Mann-Whitney U test).

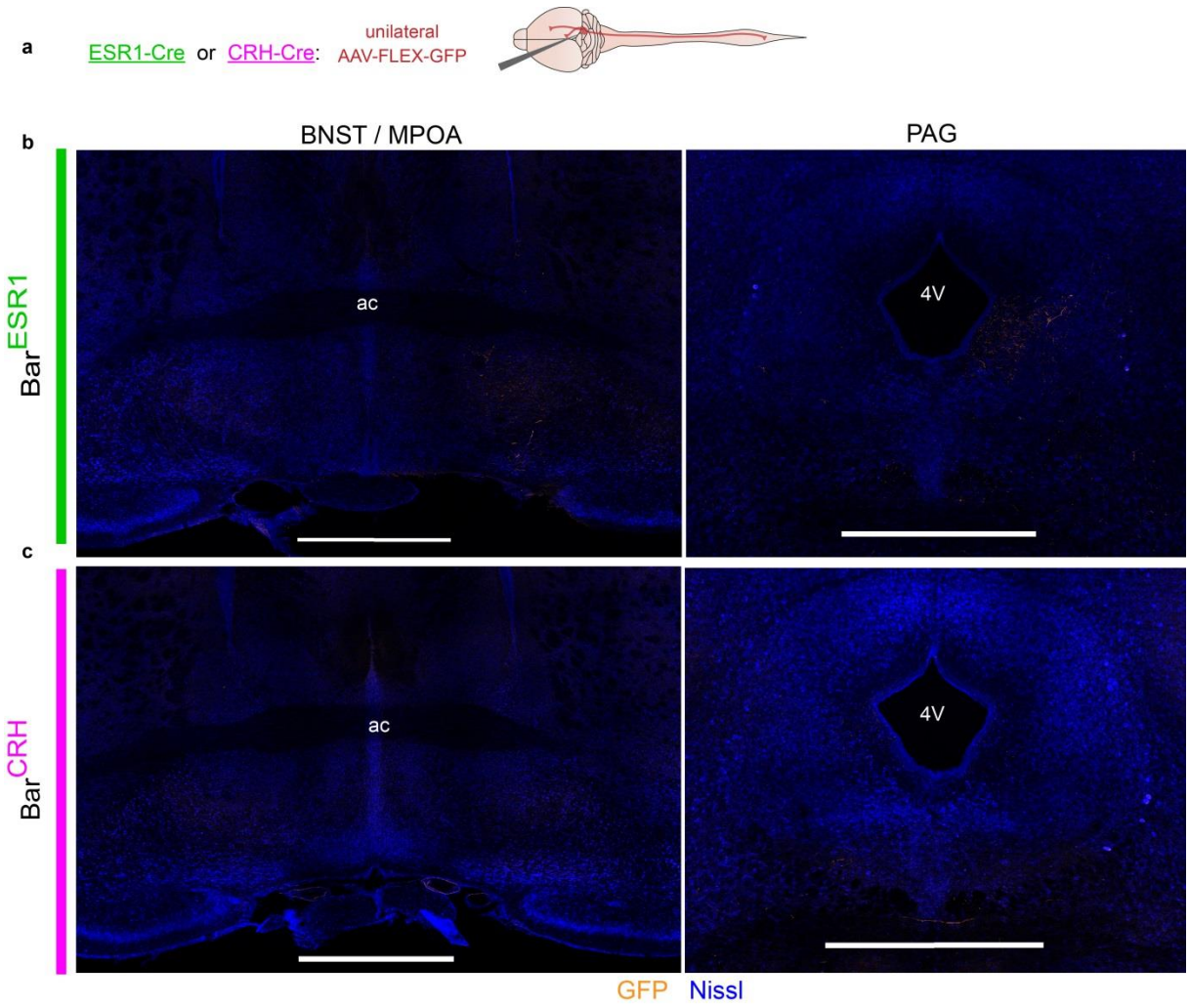

Figure 7. Few Bar^{ESR1} and Bar^{CRH} axons project rostrally.
a, Schematic for testing Bar cell type axonal projections to the same brain areas that provide its major inputs. **b,** Representative Bar^{ESR1} axon projections BNST and PAG, from same injection site as Figure 6b. **c,** Same as (b), but for Bar^{CRH} axon projections. Scale bars = 1 mm.

Although the results above imply that Bar^{ESR1} neurons and Bar^{CRH} neurons could be contributing to different pelvic targets, we further tested this idea using pseudorabies virus (PRV) tracing from potential autonomic and somatic targets in the periphery, using CRH-tdT mice with αESR1immunostaining in Bar. We first determined the optimal survival periods when Bar is first labelled after PRV injection into two autonomic targets (bladder and

preputial gland[88], Figure 8a,d) and two somatic striated muscle targets (EUS and bulbospongious muscle, Figure 8b,c). Although using these early timepoints cannot completely eliminate ambiguity in connections across multiple trans-synaptic jumps, it is expected to minimize additional synaptic spread of virus within Bar microcircuits. At these optimal survival periods, Bar neurons labelled from injections in *autonomic* targets showed overrepresentation of Bar^{CRH} neurons, but an underrepresentation of Bar^{ESR1} neurons (Figure 9b,d,e). Conversely, neurons labelled from injections in *somatic* targets showed overrepresentation of total Bar^{ESR1} neurons (Figure 9c,d,e). Both types of Bar neurons were labelled to some degree from all targets, and all injections showed both thoracolumbar and lumbosacral infection, confirming a shared network of spinal interneurons for the coordination of multiple targets[58,89,90]. Overall, both the anterograde tracing above and these retrograde PRV tracing experiments suggest that Bar^{ESR1} neurons have more direct control over striated pudendal nerve muscle targets, whereas Bar^{CRH} neurons contribute more focal output to autonomic targets of the pelvic ganglion.

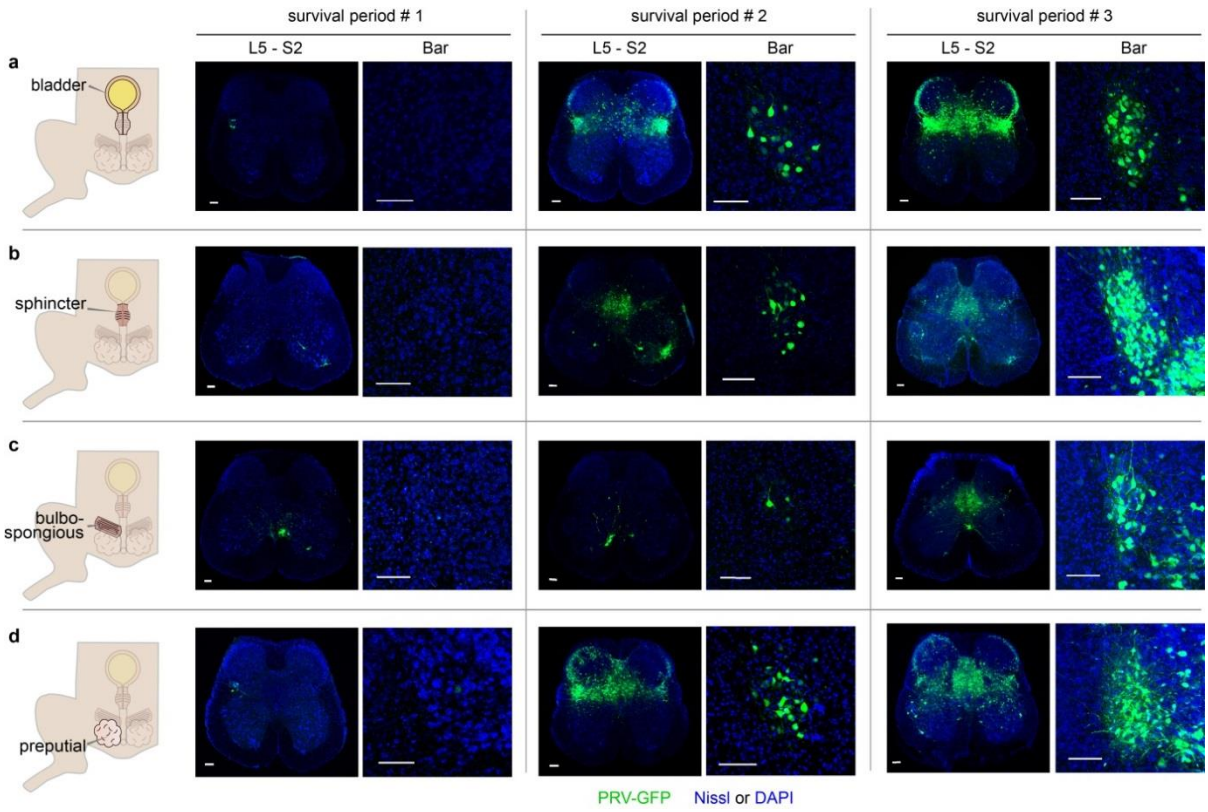

Figure 8. Timecourse of PRV infection from urination-related targets to lumbosacral spinal cord and Bar. Injection of pseudorabies virus (PRV-GFP) into four output targets involved in urination. PRV infection and GFP expression increases spinal cord and Bar with time, first in L5-S2 regions of the spinal cord and then in Bar. Survival periods: **a**, bladder: #1: 48 hr., #2: 60 hr., #3: 72 hr. **b**, sphincter: #1: 72 hr., #2: 84 hr., #3: 96 hr. **c**, bulbospongious muscle: #1: 72 hr., #2: 84 hr., #3: 108 hr. **d**, preputial gland: #1: 72 hr., #2: 84 hr., #3: 108 hr. Scale bars = 100 μm.

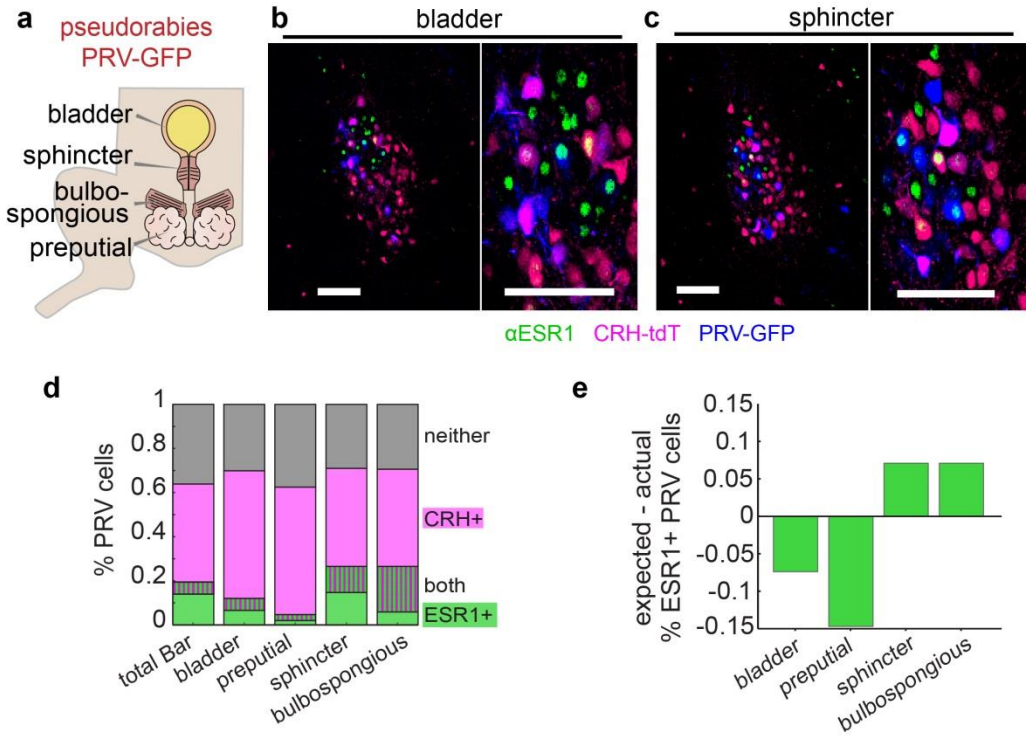

Figure 9. **Pseudorabies virus (PRV) injections into pelvic targets reveals a somatic bias for Bar^{ESR1} connectivity**.
a, Schematic for PRV injections into urine-related targets. **b, c,** Retrograde PRV-GFP expression with αESR1 and CRH-tdT after injection of (j) bladder or (k) sphincter. Right, larger views. **d,** Percentage of PRV-GFP labeled cells overlapping with CRH-tdT (magenta), αESR1 (green), both (hatched), or neither (grey) for the four starter targets: bladder (N = 3), sphincter (N = 3), preputial (N = 3), and bulbospongious (N = 2). Total Bar is distribution from Figure 2e. **e,** Deviation from the expected percentage of PRV cells overlapping with αESR1 for the four starter targets, same mice as (d). Scale bars = 100 μm.

1.3 Inputs to Bar^{ESR1} neurons

In addition to having different outputs, could cell types in Bar may have different inputs that provide clues to their function? Monosynaptic rabies tracing[91,92] is ideally suited to address this question, but this method relies on clean separation between cell types for conclusive anatomy. In Bar, however, there is a minority overlap between Bar^{ESR1} and Bar^{CRH} populations (Figure 2e), and orthogonal Flp-recombinase mouse lines do not exist to separate them using Cre-ON / Flp-OFF or similar approaches[93]. Furthermore, combinatorial labelling based on retrograde anatomy is difficult or impossible based on the proximity of the major

lumbosacral targets for these cell types. Thus, we used input-output tracing[94] of spinally-projecting Bar^{ESR1} neurons to provide the cleanest possible starter population for monosynaptic tracing (Figure 10a), and compared to previous results using standard rabies tracing from all CRH+ neurons in the Bar region[42]. Using this method, we could trace specific monosynaptic inputs from tens of Bar^{ESR1} starter cells (Figure 10b-d). Similar to the previously published Bar^{CRH} input data, we found that the major inputs come from two distinct areas: (1) the caudal ventrolateral periaqueductal grey (PAGvl), and (2) an ill-defined and sparse group of cells straddling the border between ventral bed nucleus of the stria terminalis and lateral preoptic area (BNSTv / LPOA; Larry Swanson, personal communication). These BNSTv / LPOA cells may correspond to magnocellular BNST cells found to focally project to Bar in the rat[95]. In addition, we find minor inputs to Bar^{ESR1} neurons from various other sources across the brain (Figure 10d), although these were significantly less than what was found for Bar^{CRH} neurons[42]. Our starter populations contained a few cells that appeared to be part of locus coeruleus (LC) and not Bar, so it is possible that these minor inputs may reflect connectivity to LC as well as Bar. Regardless of technical limitations and the existence of minor inputs, it is clear that Bar^{ESR1} neurons get the vast majority of their synaptic input from PAGvl and BNSTv/LPOA, and overall seem to have narrower inputs than Bar^{CRH} neurons, although matched comparison to spinally-projecting Bar^{CRH} neurons is needed to fully address the differences seen.

Of the major Bar^{ESR1} inputs identified, PAGvl has a clear role in initiating reflexive urination[96,1,5], although specific roles in regulating bladder or urethral targets or natural, voluntary urination remain unknown. There is no direct evidence that BNSTv/LPOA inputs participate in urinary function, although others have speculated for roles in sleep-urinary

interactions and sexual behavior, based on anatomy[95,97,98]. To further explore the inhibitory or excitatory nature of these inputs, we used standard retrograde tracing with fluorescently-labelled CTB in VGAT-reporter mice. After bilateral injection in Bar (Figure 10e), we waited for retrograde transport and then examined the overlap between VGAT+ cells and retrograde-labelled cells in PAGvl and BNSTv/LPOA (Figure 10f). We found that the majority of PAGvl cells are *not* likely to be inhibitory (30% overlap with Vgat-Ai6, N=2 mice), while the majority of BNSTv/LPOA cells are (85% overlap with Vgat-Ai6, N=2 mice). This nonspecific CTB tracing includes inputs from all neurons in Bar *and* surrounding area, plus VGAT expression is integrated over the lifetime of the animal in reporter mice, and glutamate and GABA can be co-expressed[83]. These technical caveats withstanding, the majority of excitatory input to Bar^{ESR1} neurons seems to come from PAGvl, as expected from previous anatomical and functional literature. However, further experiments confirming the sign of these inputs to Bar^{ESR1} neurons as well as their firing patterns in behaving animals are needed to determine the nature of Bar^{ESR1} activation during scent marking urination. For example, a simple model of excitation from PAGvl is parsimonious, but some degree of disinhibition is also likely based on previous experiments using inhibitory receptor antogonists[61,96], and this disinhibition may be cell-type-specific[99].

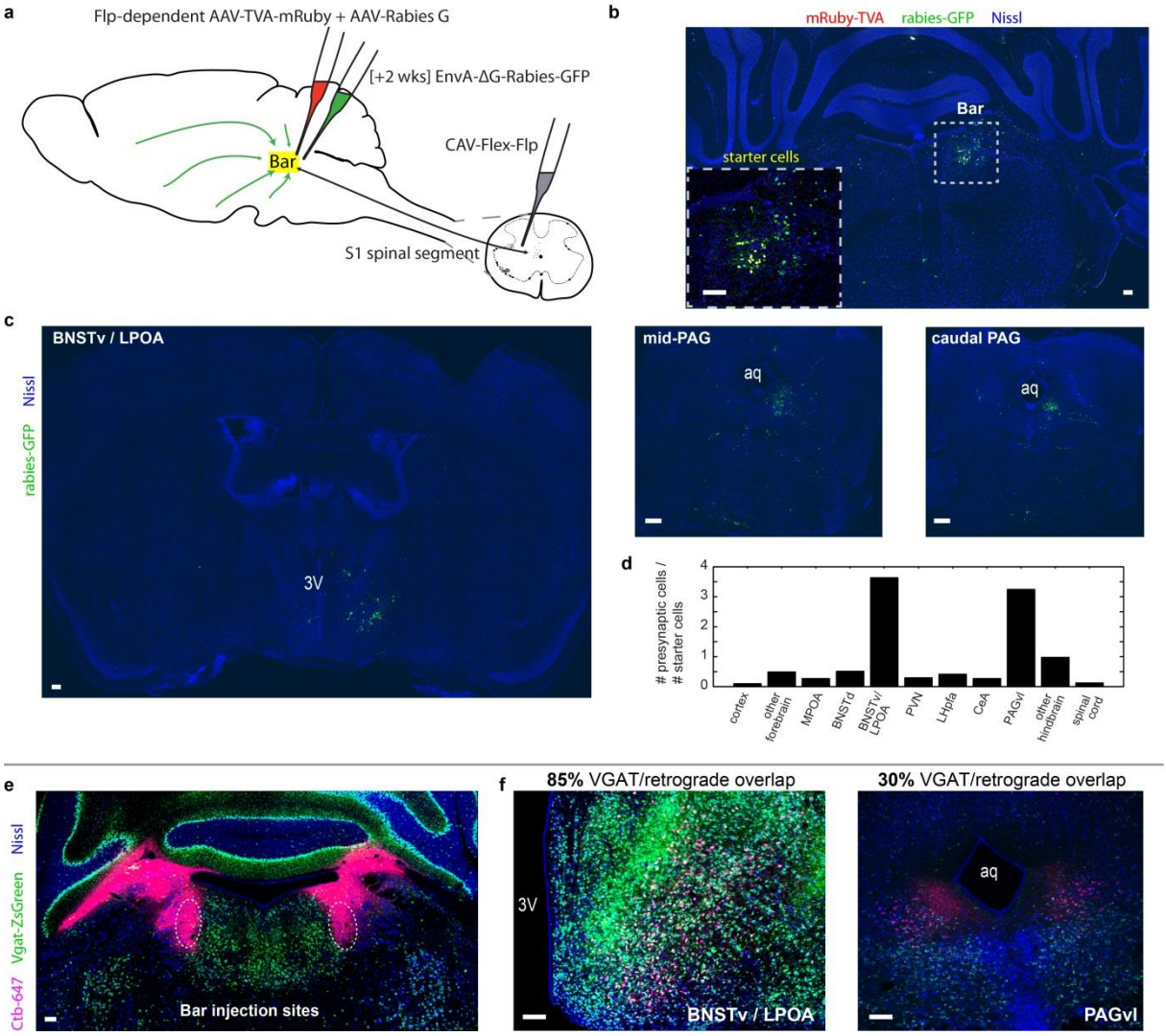

Figure 10. Inputs to Bar^{ESR1} neurons that project to lumbosacral spinal cord .
a, Schematic of viral strategy for input-output tracing. **b**, Injection site at Bar. Inset shows close-up of dotted box area. **c**, Examples of retrogradely-labelled cells in BNSTv / LPOA (left), mid-PAG (middle), and caudal PAG (right). **d**, Quantification of inputs across the brain and spinal cord (N = 2 mice). **e**, Example CTB injection sites at Bar (dotted ovals) in VGAT-ZsGreen mouse. **f**, Retrogradely-labelled cells in BNSTv / LPOA (left), and PAGvl (right) from injection site in (e), along with percentages of retrograde cells overlapping with VGAT-ZsGreen. 3V = 3rd ventricle, aq = cerebral aqueduct. Scale bars = 100 μm.

1.4 Activity of Bar^{ESR1} neurons during voluntary urination

Some Bar neurons increase spiking activity during reflexive urination, while others decrease activity[41]. How these neurons respond during natural, voluntary urination is unknown, although fMRI data in humans suggests at least some increased activity[100,7,56,2]. To determine the temporal activation of Bar^{ESR1} cells in relationship to natural urination behavior, we unilaterally injected Bar with AAV-FLEX-GCaMP6s in male ESR1-Cre mice and imaged population calcium activity with fiber photometry (Figure 11a). We promoted voluntary urination in GCaMP-infected subjects by adding female odor to an arena lined with absorbent paper and record the male's position from above at the same time as their urine output from below. This enables quantification of both the timing and abundance of voluntary urination events during freely moving behavior (Figure 12). We observed robust, discrete increases in GCaMP fluorescence that were highly correlated with detected urination events, compared to randomly chosen intervals (Figure 11b,d,e). The lags for maximal cross correlation between urine detection and GCaMP fluorescence transients revealed no significant difference between the timing of Bar^{ESR1} population activity and urine marks (GCaMP precedes by 0.37 ± 0.16 seconds, mean ± s.e.m., N = 76 urination events across 7 mice, p = 0.18, Wilcoxon signed rank test). Altogether, the anatomical and physiological evidence demonstrates that ESR1 defines a novel cell type in Bar with a direct role in urination.

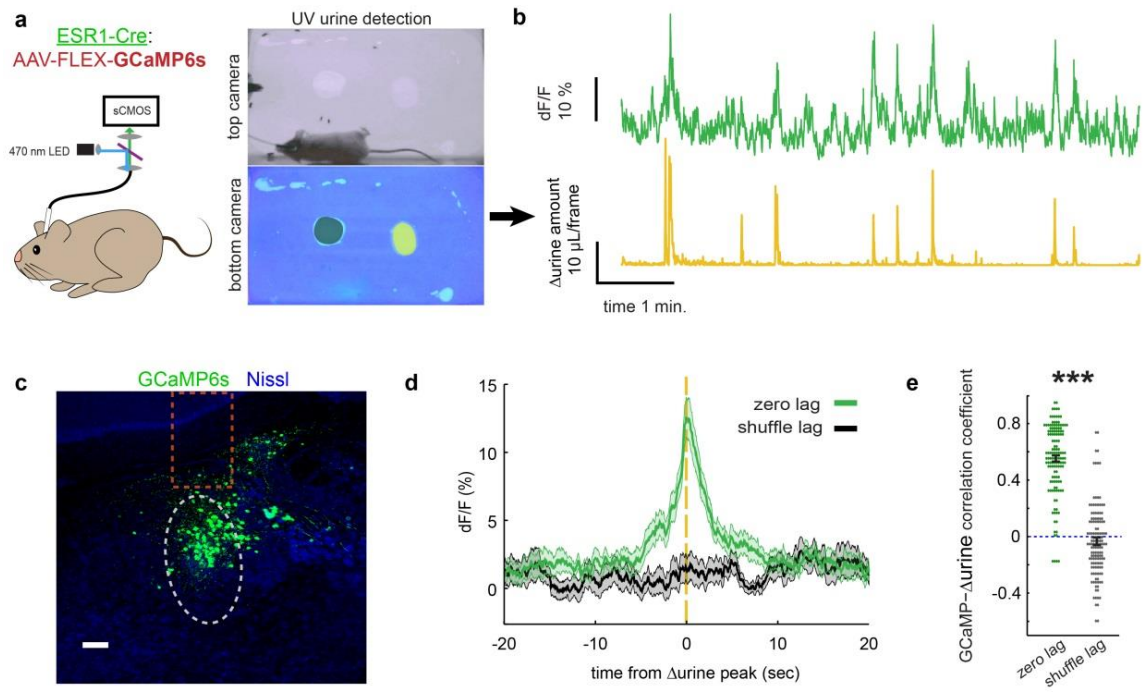

Figure 11. Bar^{ESR1} activity increases during urination events.
a, Schematic of fiber photometry experiment and example urine quantification with control odor (black shading) and female odor (yellow shading) on bottom camera view. **b**, Example Bar$^{ESR1\text{-}GCaMP6s}$ fluorescence (top) and derivative of urine detection (Δurine, bottom). **c**, Example GCaMP6s expression in Bar (grey dotted oval) of ESR1-Cre mouse. Dotted orange rectangle shows approximate fiber location. **d**, GCaMP6s fluorescence synchronized to Δurine peaks (green) or at shuffled times (black) for all mice (mean ± s.e.m, N = 76 urination events from 7 mice). **e**, Correlation coefficient between GCaMP6s and Δurine traces at zero lag (green) and random lag (grey) for all mice (mean ± s.e.m., same events as panel n). Scale bar = 100 μm. ***p<0.001 (Mann-Whitney U test)

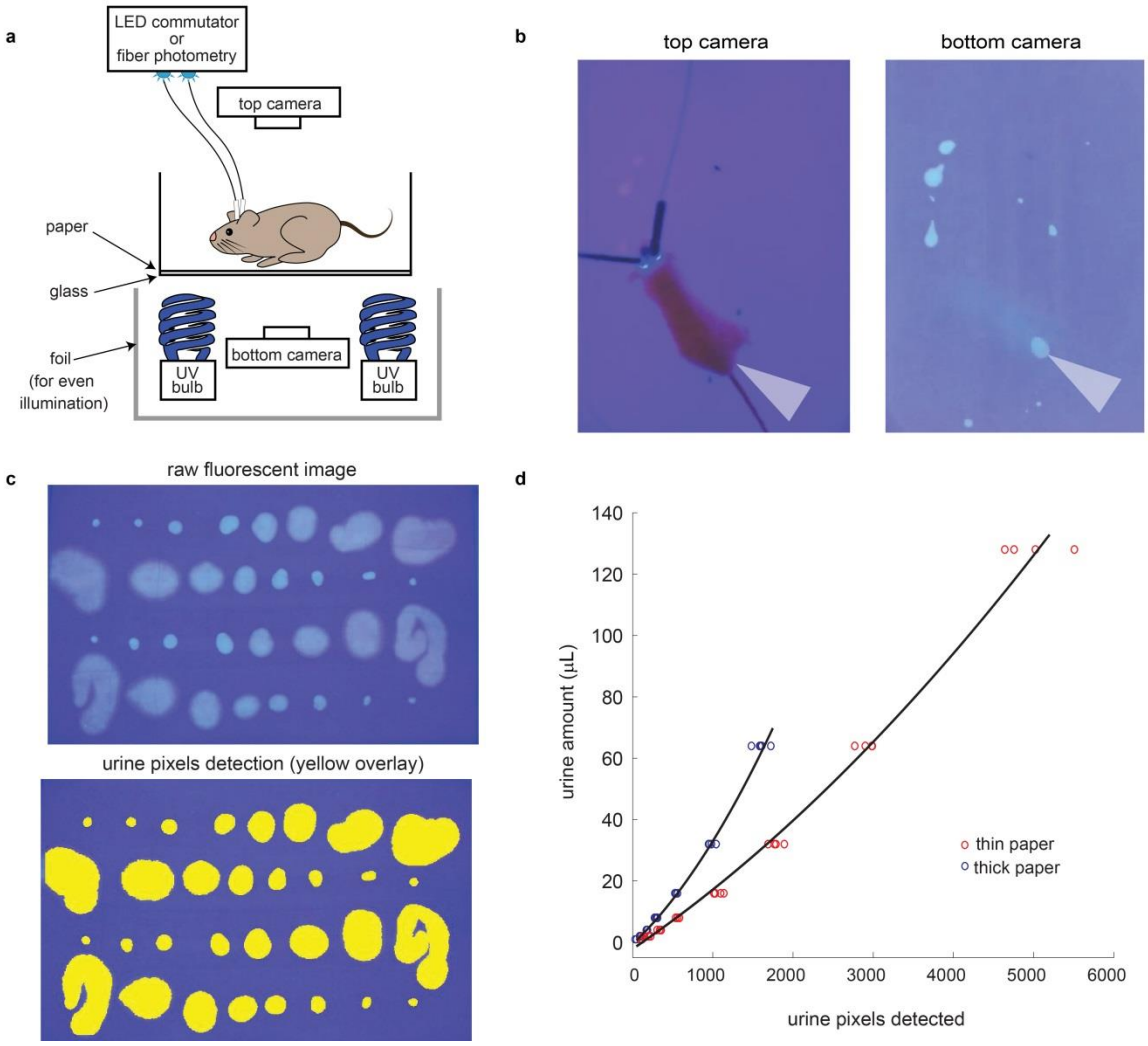

Figure 12. Visualizing and quantifying urination behavior.
a, Schematic of behavioral setup for simultaneous optogenetics / fiber photometry, video recording, and analysis of urine excretion of awake behaving mice. **b,** Left: top camera records mouse position, right: urine fluoresces under UV light enabling excretion to be visualized throughout assay. Grey carrot indicates position between synchronized images from top and bottom cameras. **c,** Example of automated urine pixel detection with calibration data consisting of 4 replicates of 8 different volumes of male mouse urine on thin chromatography paper. **d,** Second order polynomial fit to calibration data on thick and thin paper; coefficients from these were used to calculate all urine amounts reported in microliters.

1.5 Bar^{ESR1} neurons are sufficient to drive urination

If Bar neurons are excitatory and increase their firing rate during urination, then one might expect specific stimulation of some Bar subset to recapitulate induced urination results

from nonspecific electrical or pharmacological stimulation of the region. $Bar^{CRH\text{-}ChR2}$ photostimulation was previously shown to increase bladder pressure during urethane-anesthetized cystometry[42], but the sufficiency of these cells for urine release in awake animals has not been characterized. To determine if either Bar^{ESR1} or Bar^{CRH} neurons drive urination in behaving animals, we first bilaterally infected them with AAV-FLEX-ChR2 or -GFP ($Bar^{ESR1\text{-}ChR2}$, $Bar^{ESR1\text{-}GFP}$, or $Bar^{CRH\text{-}ChR2}$, Figure 13a-c) and performed slice recordings to confirm that both $Bar^{ESR1\text{-}ChR2}$ and $Bar^{CRH\text{-}ChR2}$ neurons reliably responded to photostimulation at frequencies previously used in electrical stimulation (Figure 14). We then quantified and compared the latency and amount of urine induced by photostimulation in awake, freely-moving individuals *without* urine-promoting odor cues. While photostimulation of GFP-infected individuals produced no effect on urine excretion, $Bar^{ESR1\text{-}ChR2}$ stimulation led to robust, frequency-dependent urine release, following light onset with a mean latency of 2.1 seconds (Figure 13d-h; Supplementary Video 1). Over 96% of $Bar^{ESR1\text{-}ChR2}$ stimulation trials at 10-50 Hz resulted in urination (Figure 13d,f). In comparison, photostimulation of $Bar^{CRH\text{-}ChR2}$ neurons during freely-moving behavior had a much smaller effect on urination despite generally higher ChR2 viral infection levels (Figure 13c-h; Supplementary Video 2). Less than 37% of $Bar^{CRH\text{-}ChR2}$ stimulation trials at 10-50 Hz resulted in the voiding of urine (Figure 13f). Of this subset, the latency and amount of urine produced differed from $Bar^{ESR1\text{-}ChR2}$ at all frequencies tested (Figure 13d-h). We additionally investigated the extent to which Bar^{ESR1} and Bar^{CRH} neural activity could initiate voiding without conscious sensory input. Photostimulation under isoflurane anesthesia, known to depress reflex urination[101–103], resulted in urine voiding in 43% of the $Bar^{ESR1\text{-}ChR2}$ trials, but only 6% of the $Bar^{CRH\text{-}ChR2}$ trials, with none of the $Bar^{CRH\text{-}ChR2}$ voids occurring during the photostimulus window (Figure

13i; Supplementary Video 3). This indicates that Bar^{ESR1} neuronal activity is sufficient to trigger rapid and efficient urination and hints at a distinct mechanism from neighboring Bar^{CRH} activity that is known to increase bladder pressure.

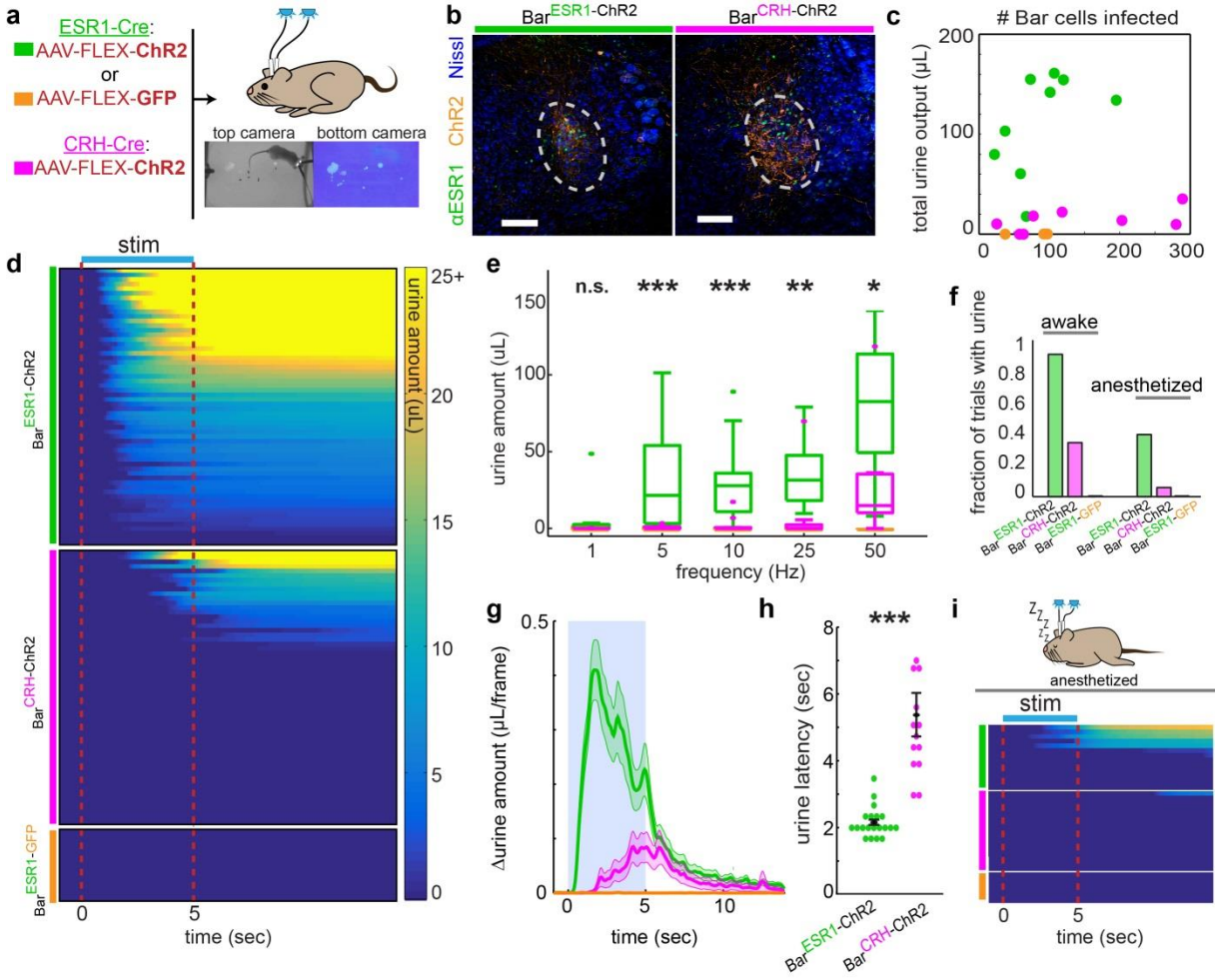

Figure 13. Photostimulation of Bar^{ESR1} neurons induces efficient urination in awake and anesthetized animals.

a, Schematic of optogenetic stimulation and example urine detection. **b,** Example ChR2 expression in ESR1-Cre (left) or CRH-Cre (right) individuals. **c,** Total urine output across all trials for each individual versus ChR2 expression. **d,** Heatmap of urine output following awake photostimulation for all trials >10Hz (N = 10 Bar$^{ESR1\text{-}ChR2}$, 10 Bar$^{CRH\text{-}ChR2}$, 3 Bar$^{ESR1\text{-}GFP}$ mice), sorted by decreasing total urine amount. **e,** Urine amounts at different photostimulation frequencies: boxplots show median, 25th/75th quartiles, ranges, and outliers (same mice as panel d). **f,** Fraction of trials with photostimulated urine detected in panels (d), awake, and (i), anesthetized. **g,** Δurine amount around 50 Hz photostimulation (blue shading; same mice as panel d; mean ± s.e.m, N = 20 trials from 10 mice each). **h,** Urination latency after 50 Hz photostimulation (same trials as panel g). **i,** Heatmap of urine output around anesthetized photostimulation for all trials (N = 7 Bar$^{ESR1\text{-}ChR2}$, 8 Bar$^{CRH\text{-}ChR2}$, 3 Bar$^{ESR1\text{-}GFP}$ mice). Scale bars = 100 µm. *p<0.05, **p<0.01, ***p<0.001, n.s. p>0.05 (Mann-Whitney U test for Bar$^{ESR1\text{-}ChR2}$ compared to Bar$^{CRH\text{-}ChR2}$). Colors for all panels: green = Bar$^{ESR1\text{-}ChR2}$, magenta = Bar$^{CRH\text{-}ChR2}$, orange = Bar$^{ESR1\text{-}GFP}$.

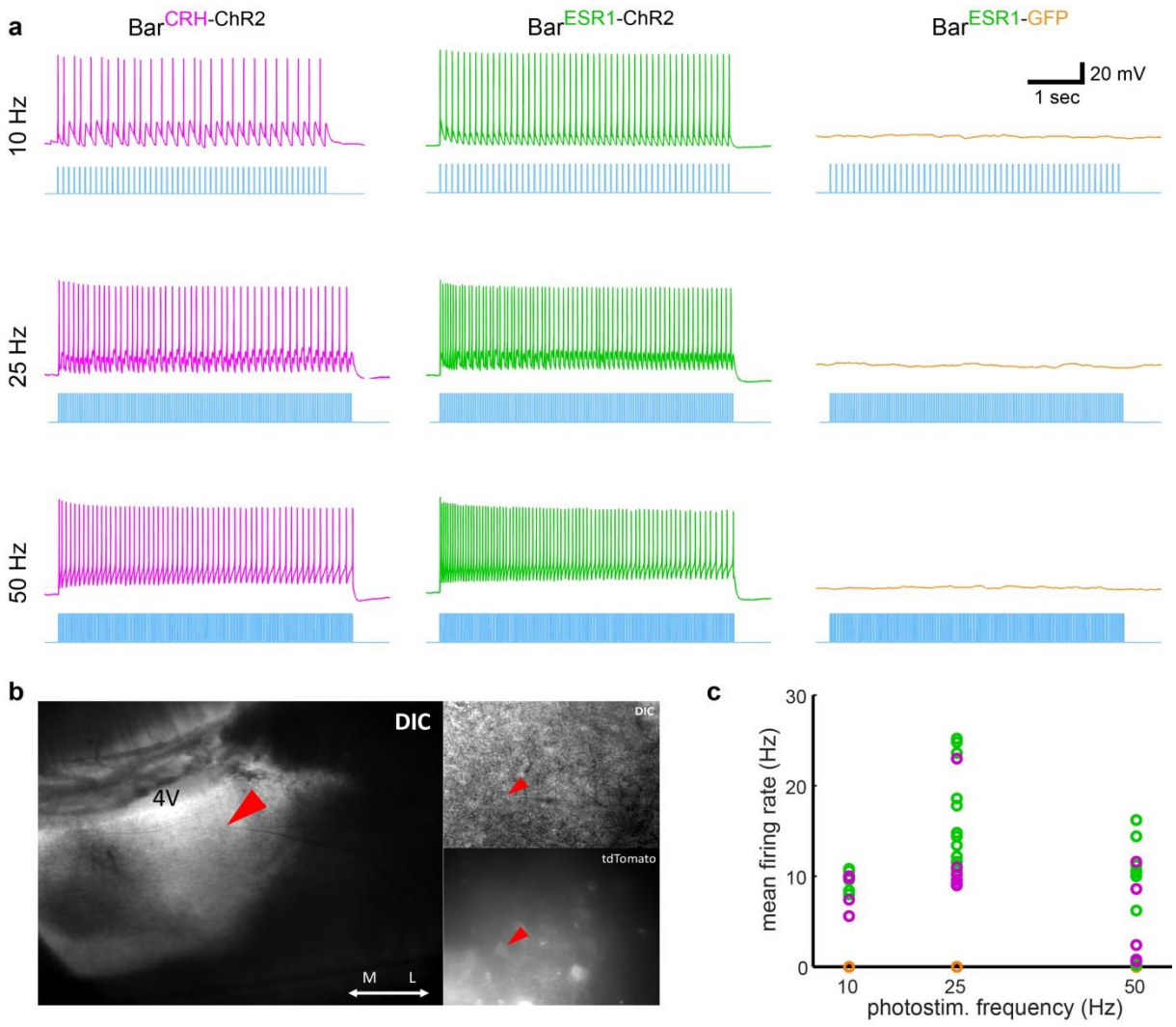

Figure 14. Whole-cell slice recordings of Bar$^{CRH\text{-}ChR2}$ and Bar$^{ESR1\text{-}ChR2}$ neurons during photostimulation. **a,** Example current clamp traces from representative Bar$^{CRH\text{-}ChR2}$ (magenta), Bar$^{ESR1\text{-}ChR2}$ (green), and Bar$^{ESR1\text{-}GFP}$ (orange) neurons during 5 sec photostimulation bouts at 10/25/50 Hz. **b,** Visualization of recording location of Bar$^{ESR1\text{-}ChR2}$ neuron in (a) showing ChR2-tdTomato expression. **c,** Summary of stimulated firing rate versus photostimulation frequency for all recorded Bar$^{CRH\text{-}ChR2}$ (magenta, N = 6), Bar$^{ESR1\text{-}ChR2}$ (green, N = 12), and Bar$^{ESR1\text{-}GFP}$ (orange, N = 4) neurons. Most neurons, particularly Bar$^{CRH\text{-}ChR2}$, are affected by depolarization block at 50Hz.

1.6 Urethral sphincter relaxation via Bar^{ESR1} neurons

To directly test the mechanistic effects of Bar^{ESR1} and Bar^{CRH} neurons on urinary muscle targets, we performed external urethral sphincter (EUS) electromyography (EMG) and cystometry (bladder filling and pressure recording) under isoflurane anesthesia (Figure 15a).

We perfused saline at a constant rate into the bladder to stimulate reflex voiding and observed natural cycles of bladder pressure increase and associated EUS bursting muscle patterns, which correlated with voiding and subsequent bladder pressure decrease (Figure 15b). As mentioned in the Introduction, these bursting contractions interspersed with periods of muscle relaxation are believed to enable efficient urine flow through the narrow rodent urethra[70,104]. Following observation of regular cystometry cycles, we stopped the saline pump when the bladder was "filled" or "empty" (75% or 10% of the volume observed to trigger reflex urination, respectively) and initiated 5 seconds of photostimulation (Figure 15b, blue arrows). We found that both $Bar^{ESR1\text{-}ChR2}$ and $Bar^{CRH\text{-}ChR2}$ photostimulation produced reliable, time-locked bladder pressure increases at similar latencies (Figure 15c-d). The initial latency and slope of the bladder pressure increase by stimulation of each cell type was indistinguishable by our analysis. However, both the peak pressure and ending pressure (25 seconds after stimulus onset) were significantly less for $Bar^{ESR1\text{-}ChR2}$ photostimulation. This difference occurs because only with the $Bar^{ESR1\text{-}ChR2}$ photostimulation did we observe abundant urine release, which results in a sharp pressure decrease below the starting value (Figure 15c-f; Supplementary Video 4). When $Bar^{CRH\text{-}ChR2}$ photostimulation ceased, the bladder usually returned to the same pressure level observed prior to $Bar^{CRH\text{-}ChR2}$ stimulation (Fig 15c-d,f), independently confirming our observations that significant urine release does not normally occur through activation of this cell population (Supplementary Video 5).

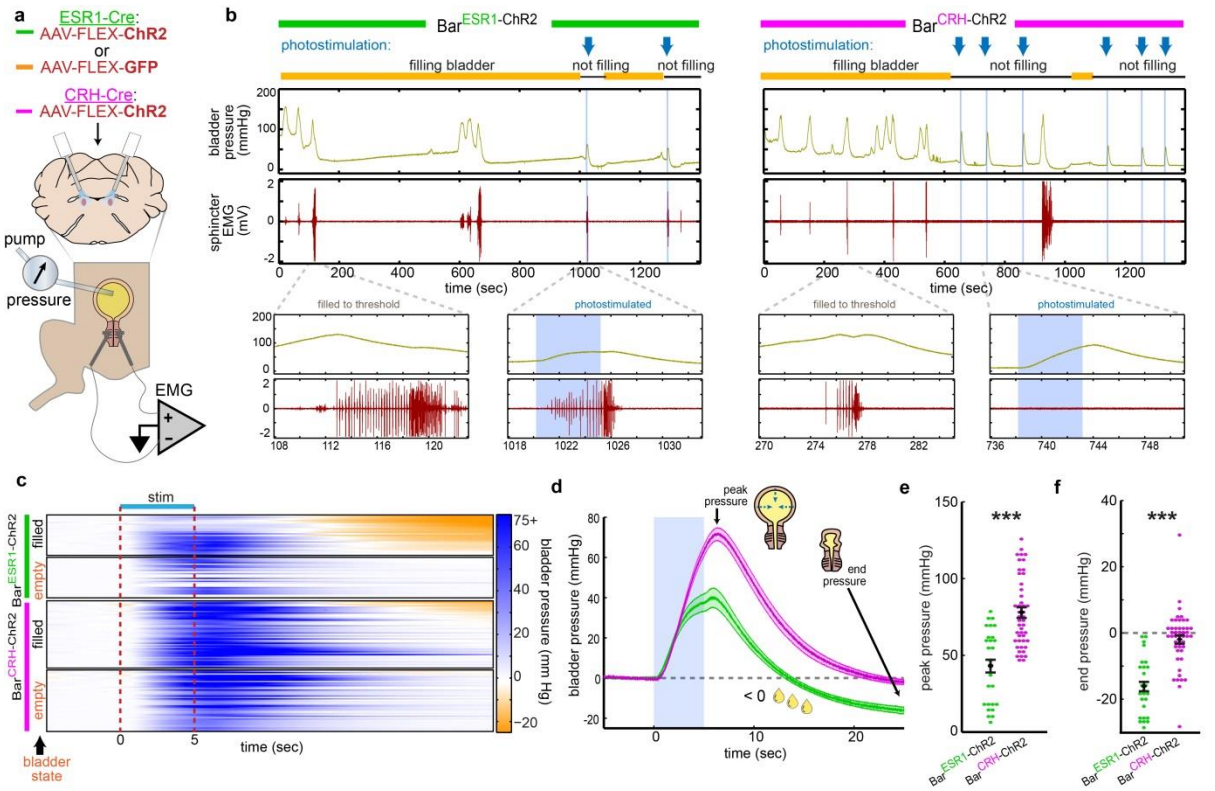

Figure 15. Bar^{ESR1} neurons facilitate urine release during cystometry.
a, Schematic for optogenetic Bar stimulation during cystometry. **b,** Representative raw bladder pressure and EUS EMG traces for Bar$^{ESR1\text{-}ChR2}$ (left) and Bar$^{CRH\text{-}ChR2}$ (right) individuals. Blue arrows and shading indicate photostimulation times, and yellow/black lines denote cystometry pump on/off. Top traces are 20 minutes; bottom traces show 15 second detail when the bladder is filled to threshold (no photostimulation) versus when Bar is photostimulated. **c,** Heatmap of bladder pressure, sorted by increasing end pressure (decreasing urine release), around photostimulation for both filled and empty bladder trials (N = 3 Bar$^{ESR1\text{-}ChR2}$, top, and 5 Bar$^{CRH\text{-}ChR2}$, bottom, mice). **d,** Bladder pressure for 'filled' bladder data in panel (c), showing peak and end pressure where negative pressure indicates urine release (mean ± s.e.m., green = Bar$^{ESR1\text{-}ChR2}$, magenta = Bar$^{CRH\text{-}ChR2}$). **e,** Peak and **f,** end bladder pressure from (d), mean ± s.e.m. ***p<0.001 (Mann-Whitney U test).

The reason for the observed differences in photostimulated urine release only becomes clear when examining the EUS EMG responses. The photostimulated urination in Bar$^{ESR1\text{-}ChR2}$ mice coincided with a reliable bursting pattern of sphincter activity, the extent of which was dependent on bladder fill level (Figure 16a-b). Pulsatile urination occurred during the bursting periods (Supplementary Video 4), consistent with previous observations of urine flow during the relaxation periods between bursts[70,104] and our calculations of relaxation time between

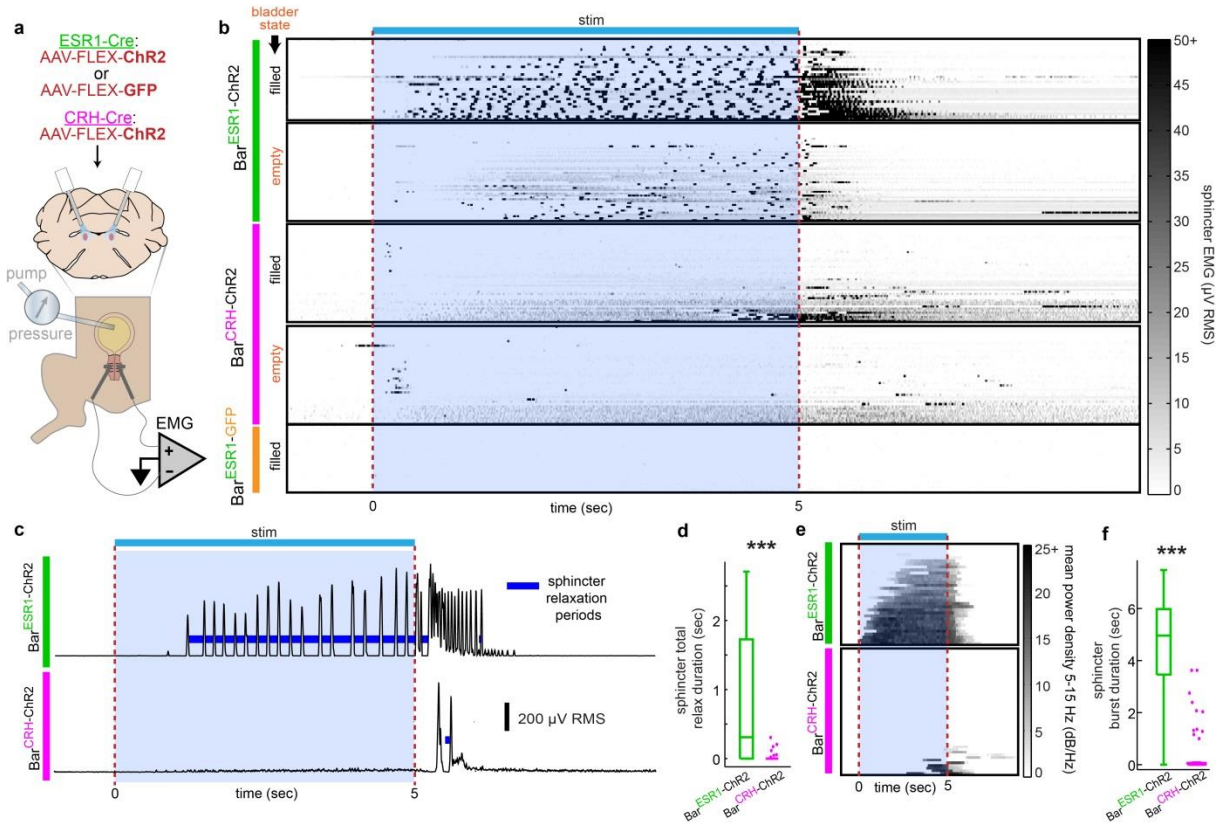

Figure 16. Bar^{ESR1} neurons relax the urethral sphincter by promoting bursting activity.
a, Schematic for optogenetic Bar stimulation during cystometry and urethral EMG recording. **b,** Heatmap of EUS EMG, sorted by increasing mean voltage, around photostimulation for both filled and empty bladder trials (N = 6 Bar$^{ESR1\text{-}ChR2}$, top, 5 Bar$^{CRH\text{-}ChR2}$, middle, and 3 Bar$^{ESR1\text{-}GFP}$, bottom, mice). **c**, Example RMS EMG traces from single 'filled' bladder trials in (b), showing calculated sphincter relaxation periods (dark blue) between bursts. **d,** Total sphincter relaxation time boxplot (median, 25th/75th quartiles, ranges, and outliers) for 'filled' bladder trials in (b). **e,** Heatmap of mean EMG power density at bursting frequencies (5-15 Hz) for 'filled' bladder trials in (b) (Bar$^{ESR1\text{-}ChR2}$, top, and Bar$^{CRH\text{-}ChR2}$, bottom). **f,** Sphincter burst duration boxplot for trials in (e). ***p<0.001 (Mann-Whitney U test).

burstlets (Figure 16c-d). Frequency analysis of the sphincter EMG signal also shows that 85% of the Bar$^{ESR1\text{-}ChR2}$ stimulations with a filled bladder resulted in sphincter relaxation/bursting and associated voiding (Figure 16e-f; Figure 18a-b). Additionally, we observed burst-like EMG responses in the absence of bladder contractions on a subset of empty bladder trials (Figure 17), such that the effect of Bar^{ESR1} neurons on the sphincter cannot be solely due to reflex activity from bladder afferents. In contrast, photostimulation of Bar$^{CRH\text{-}ChR2}$ neurons

produced either no detectible change in sphincter activity, tonic sphincter discharge (constriction), or rare irregular bursting (13% of trials), which was always preceded by tonic (constricting) activity and accompanied by bladder pressure increase (Figure 16b-e). This tonic activity increase was characteristic of a spinal guarding reflex mediated through bladder afferents to prevent urination during bladder distension.

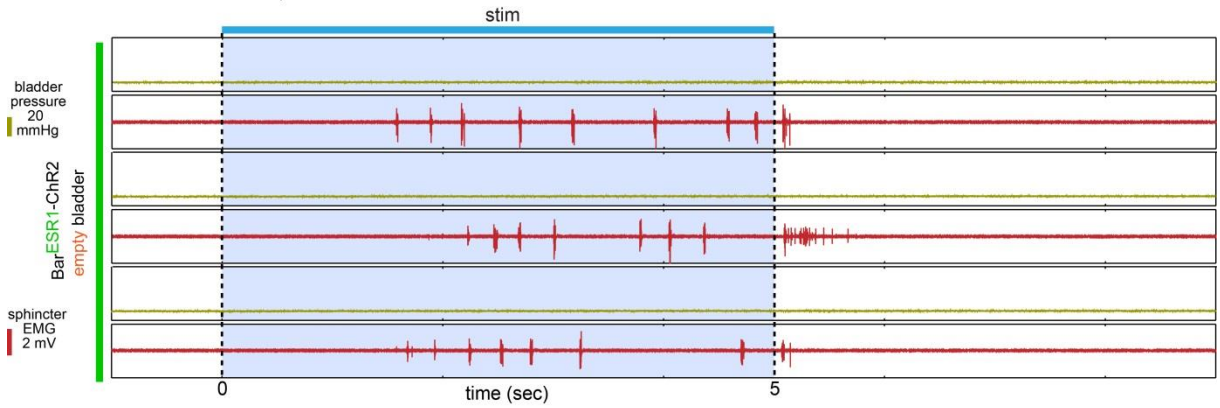

Figure 17. Bar$^{ESR1\text{-}ChR2}$ photostimulation can enable urethral sphincter relaxation without bladder contraction.
Three example Bar$^{ESR1\text{-}ChR2}$ photostimulation trials in the empty bladder condition (from heatmap in Figure 16b), in which burst-like EMG activity was observed in the absence of bladder response. Top/yellow traces are bladder pressure, bottom/red traces are raw EMG. Blue shading and dotted lines delineate photostimulation periods.

The extent to which urethral sphincter bursting occurs during natural, awake rodent behavior varies across sex and species and remains controversial[70,104,63,65]. Thus, to investigate natural sphincter activity, we surgically implanted a wireless pressure recorder into the corpus spongiosum that surrounds the urethra and can serve as a proxy for the urethral pressure[105] (Figure 18c-d). Upon recovery, we analyzed the urination behavior in response to odor cues and found urethral sphincter bursting patterns to occur during the awake behavior (Figure 18e-f). Notably, the duration and slope of the spectral power seen during the Bar$^{ESR1\text{-}ChR2}$ photostimulation bursts mimicked wirelessly recorded pressure during awake, natural scent-

marking urination (compare Figure 18b and 18f). Overall, these awake and anesthetized urinary recordings indicate that stimulation of both Bar populations equally increase bladder pressure, but only Bar^{ESR1} neurons relax the EUS via bursting to enable efficient urine flow as in natural, awake urination in male mice.

Figure 18. Frequency characteristics of urethral sphincter bursting during natural behavior and after Bar photostimulation.
a, Schematic for optogenetic Bar stimulation during EUS EMG recording. **b,** Example raw EUS EMG and corresponding spectral power in the 5-15 Hz band for photostimulated burst responses in $Bar^{CRH\text{-}ChR2}$ (top) and $Bar^{ESR1\text{-}ChR2}$ (bottom) mice. $Bar^{CRH\text{-}ChR2}$ burst is preceded by an increase in tonic activity during the photostimulation period, whereas $Bar^{ESR1\text{-}ChR2}$ burst occurs at low latency without preceding tonic activity, and displays decreasing frequency characteristic of natural bursts in (f). **c,** Example video frame from wireless corpus spongiosum pressure recording in the presence of female odor (yellow shading). **d,** Schematic of corpus spongiosum recording setup. **e,** Corpus spongiosum pressure recording after presentation of female odor. Top, raw pressure; bottom, spectral power in the 5-15 Hz band. Yellow arrows mark approximate start times for urination events. **f,** Shorter timescale recordings as in (c), for 5 urination events across 2 mice. Binary images on the left show relative sizes of thresholded urine marks corresponding to bursts on the right. Frequency typically decreases over a large burst lasting a few seconds, although shorter bursts were also observed (2^{nd} from top).

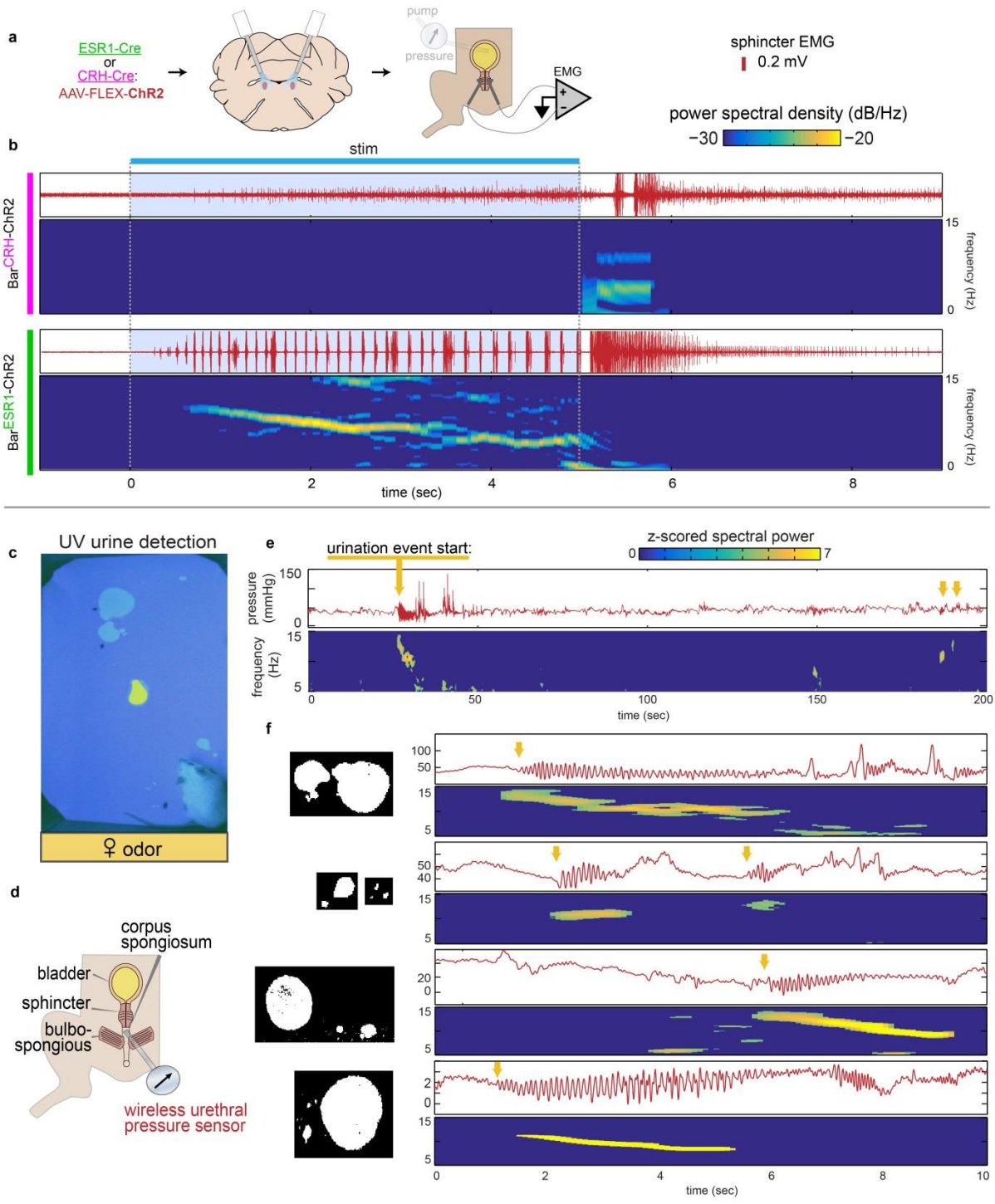
a
ESR1-Cre
or
CRH-Cre:
AAV-FLEX-ChR2
pump
pressure
EMG
sphincter EMG
0.2 mV
power spectral density (dB/Hz)
−30
−20
b
stim
BarCRH-ChR2
BarESR1-ChR2
frequency (Hz)
time (sec)
c
UV urine detection
♀ odor
d
corpus spongiosum
bladder
sphincter
bulbo-spongious
wireless urethral pressure sensor
e
urination event start:
z-scored spectral power
pressure (mmHg)
frequency (Hz)
time (sec)
f
time (sec)

1.7 Bar^{ESR1} neurons are necessary for voluntary scent marking urination

So far we have established that Bar contains separable spinal projections, with Bar^{ESR1} neurons correlating to scent marking urination and its bursting properties. To prove this link, one must specifically and reversibly inhibit these neurons during behavior. Lesions and pharmacological manipulation of Bar in rats and cats, as well as spinal injury patients and studies, have shown that the general Bar region is acutely necessary for reflexive and voluntary urination. However, it is not known if this necessity translates to any single cell type in Bar or to scent marking behavior. To investigate the extent to which Bar neurons participate in natural, motivated urination behavior, we first established a rapid behavioral assay that compares the voluntary baseline urination rate (two minutes in the presence of a control odor) to the rate during the subsequent two minutes, in the presence of motivating female urine odor (Figure 19; Supplementary Video 6). The reliable and rapid change in the amount of urine marks in response to female urine indicates that olfactory cues access circuits which relax the EUS and generate voluntary urination.

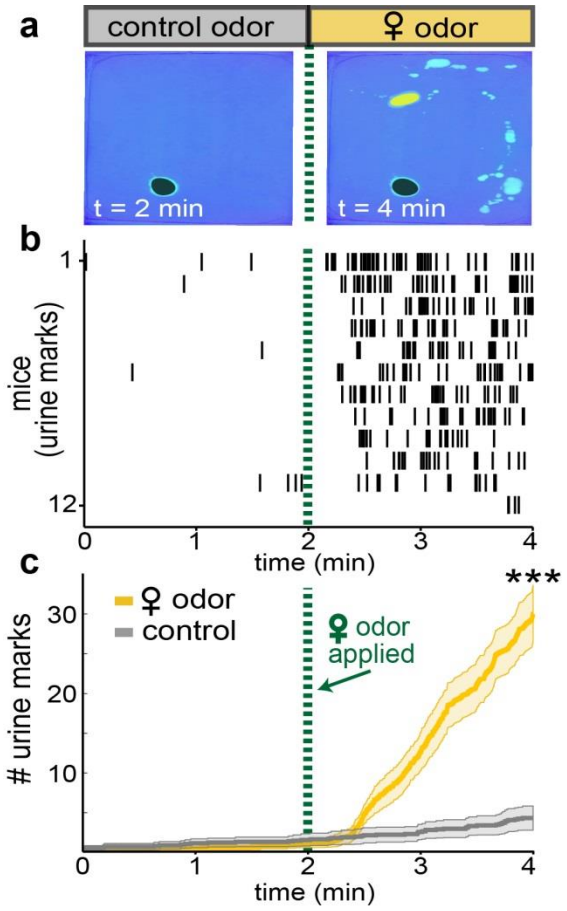

Figure 19. Naïve male mice rapidly and robustly scent mark to female odor cues.
a, Scent marking behavior in wild-type mice. Left: after 2 min. exposure to control odor (black shading), right: after additional 2 min. with female odor (yellow shading). **b,** Raster plot of urine marks detected. **c,** Urine marks during habituation with control odor only (grey) or with female odor (yellow) (mean ± s.e.m., N = 12 mice). ***p<0.001 (Wilcoxon signed rank) for number of urine marks at 2 min. and 4 min.

Next, we employed this assay to test if Bar^{ESR1} or Bar^{CRH} neurons are specifically necessary for scent marking. We bilaterally infected them with inhibitory DREADD hM4Di[106], using AAV-FLEX-hM4Di in ESR1-Cre or CRH-Cre mice ($Bar^{ESR1\text{-}hM4Di}$ or $Bar^{CRH\text{-}hM4Di}$; Figure 20a-c). After three weeks for recovery and hM4Di expression, individuals were then injected with either clozapine N-oxide (CNO, the exogenous hM4Di ligand) or saline on alternate days and assayed for their urination rate in the presence of female urine. Female-odor evoked urination was reversibly diminished following CNO

injections in Bar$^{ESR1\text{-}hM4Di}$ mice but not Bar$^{CRH\text{-}hM4Di}$ or wild-type control mice (Figure 20d-e), despite higher viral infection levels in CRH-Cre mice (Figure 20c), and without affecting locomotion or odor sampling (Figure 21a-b).

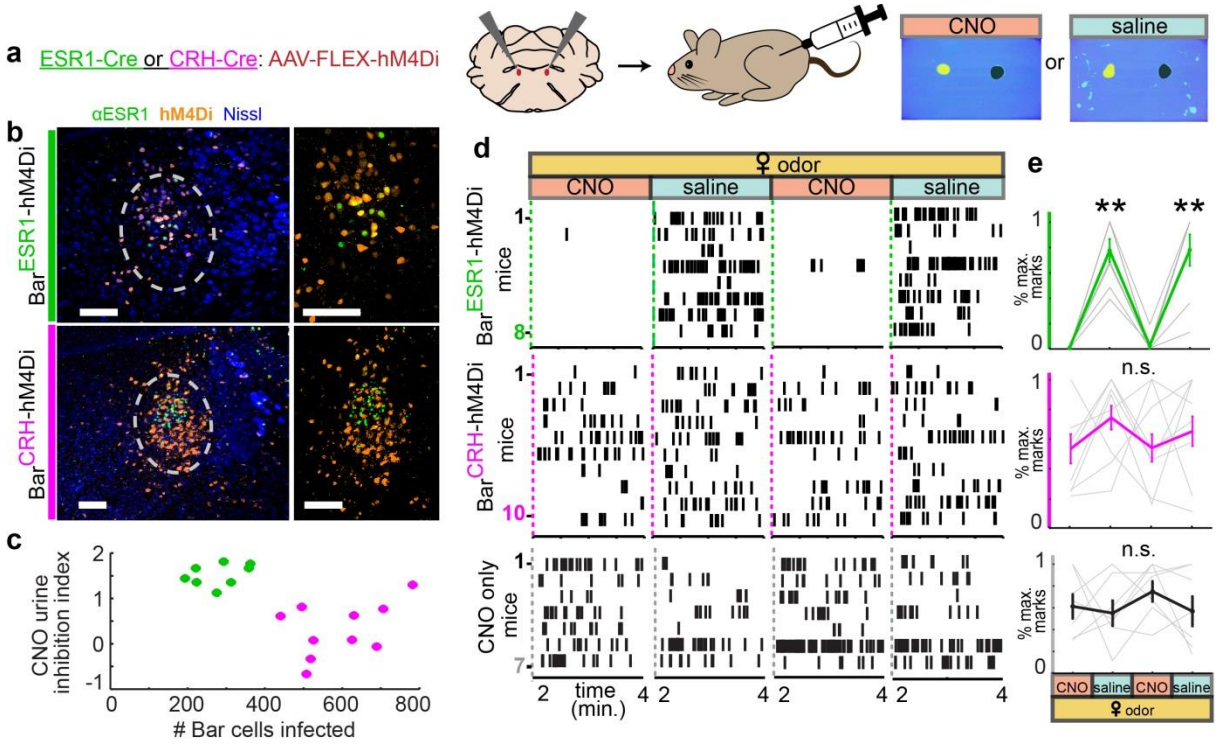

Figure 20. Chemogenetic inhibition of Bar^{ESR1} neurons impairs voluntary scent marking urination. **a,** Schematic of chemogenetic inhibition of Bar during scent marking urination. **b,** Example hM4Di expression in Bar of ESR1-Cre, top, and CRH-Cre, bottom, mice; larger views minus Nissl on the right**. c,** Number of Bar cells infected with hM4Di virus versus CNO urine inhibition index (see Methods) for all mice (green for ESR1-Cre, magenta for CRH-Cre). **d,** Raster plots of urine marks on consecutive days with either CNO or saline (Bar$^{ESR1\text{-}hM4Di}$, top, Bar$^{CRH\text{-}hM4Di}$, middle, CNO-only control, bottom). **e,** Percentage of maximum urine marks across all CNO or saline days for, top, Bar$^{ESR1\text{-}hM4Di}$ (N = 8), middle, Bar$^{CRH\text{-}hM4Di}$ (N = 10) and, bottom, CNO control (N = 7) mice (thin lines individual mice, thick lines mean ± s.e.m.). **p=0.01, n.s. p>0.05 (Friedman's with Dunn-Sidak posthoc) for differences between saline and CNO days. **f,** Schematic of optogenetic inhibition of Bar^{ESR1} during scent marking urination. **g,** Δurine amount around 2 min. photoinhibition period. Female odor presented within 15 seconds of light on, and subsequent sniff periods shown in blue. N = 9 trials from 3 mice. **h,** Δurine amount ± 5 sec. from end of photoinhibition for control odor and female odor (mean ± s.e.m., N = 9 total trials from 3 mice) .**i,** Urine amount, and, **j**, female odor sniff time during 2 min. photoinhibition period and 2 min. immediately following (mean ± s.e.m., same trials as h). **p<0.01, n.s. p>0.05 (Wilcoxon signed rank). Green shading denotes photoinhibition periods.

A previous study[42] found a subtle effect on urination from Bar$^{CRH\text{-}hM4Di}$ inhibition at a much longer 2-hour timescale, which we replicated here (Figure 21c) and is consistent with a

modulatory role for either Bar^{CRH} neurons or the population of overlapping Bar$^{CRH+ESR1}$ neurons that would be expected to be inhibited with both drivers.

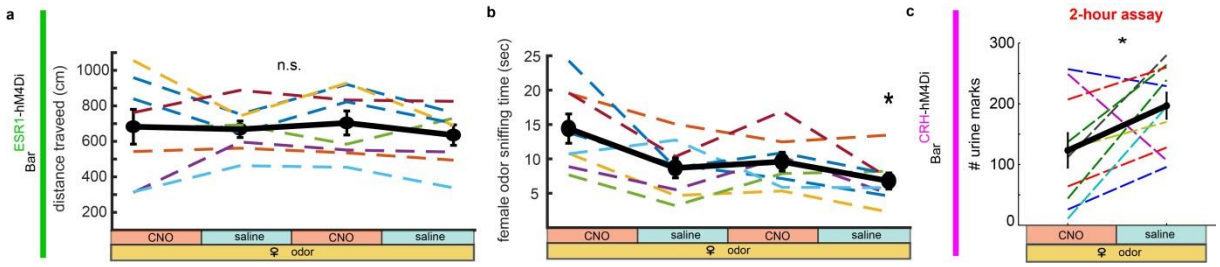

Figure 21. Behavioral controls for Bar$^{ESR1\text{-}hM4Di}$ and Bar$^{CRH\text{-}hM4Di}$ chemogenetic inhibition.
a, Total distance traveled during the assay shown in Figure 7a-e for Bar$^{ESR1\text{-}hM4Di}$ mice (N = 8). Thin dotted lines are individuals, thick black line is mean ± s.e.m. **b,** Same as (b), but for total female urine odor sniffing time. **c,** Analysis of Bar$^{CRH\text{-}hM4Di}$ mice (N = 10) injected with either saline or CNO on consecutive days prior to a 2-hour urination assay, similar to that previously published[42] and which is not limited to odor-evoked, voluntary urination. n.s. $p>0.05$, *$p<0.05$ (Friedman's with Dunn-Sidak posthoc in panels a & b, Mann-Whitney U test in panel (c) for difference between CNO and saline treatment days).

We additionally assayed for necessity of Bar^{ESR1} neurons at faster timescales by bilaterally injecting them with AAV encoding the inhibitory opsin ArchT (AAV-FLEX-ArchT, Bar$^{ESR1\text{-}ArchT}$ mice; Figure 22a; Figure 23a). We compared urination during 2 minutes of photoinhibition with female odor present to an additional 2 minutes immediately after photoinhibition ceased (Figure 22b). Sniffing of the female odor did not differ during and after photoinhibition, but urination was largely inhibited during the photoinhibition window (Figure 22d-e; Supplementary Video 7). Most trials with female odor, but not with control odor, resulted in urination within seconds of light termination. This suggests that the post-inhibitory urine release resulted from priming by odor cues rather than trivial rebound activity upon the cessation of light delivery (Figure 22c; Figure 23c). Finally, photoinhibition during anesthetized cystometry revealed that ongoing Bar^{ESR1} activity is necessary to maintain sphincter bursting, since initiating brief photoinhibition during a reflexive urination event

terminated EUS bursting activity and urine release within milliseconds (Figure 23d-e). Together, our experiments indicate that Bar^{ESR1} neurons are essential for urethral inhibition (relaxation) and scent marking behavior promoted by olfactory cues in male mice, and suggest an updated model of Bar function with parallel projections to the spinal cord having different roles in voluntary urination (Figure 24).

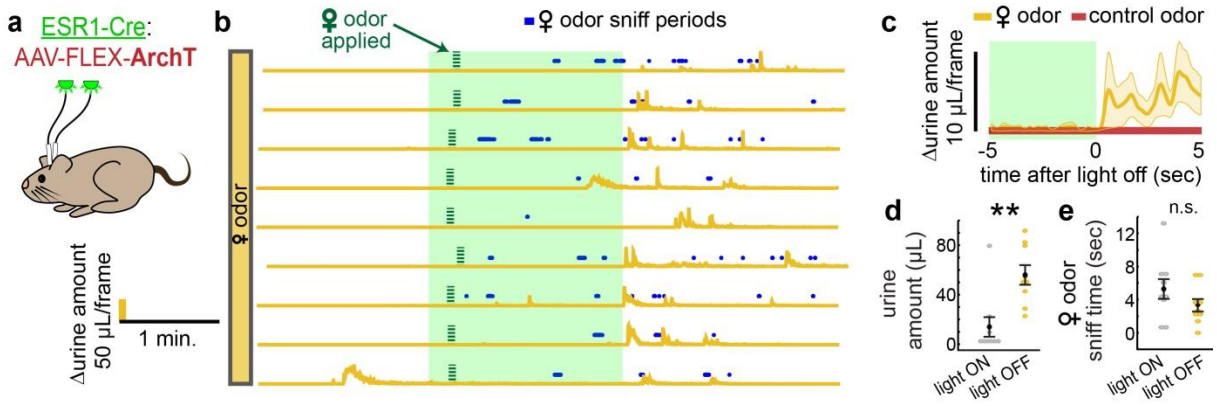

Figure 22. Optogenetic inhibition of Bar^{ESR1} neurons also impairs scent marking urination.
a, Schematic of optogenetic inhibition of Bar^{ESR1} during scent marking urination. **b,** Δurine amount around 2 min. photoinhibition period. Female odor presented within 15 seconds of light on, and subsequent sniff periods shown in blue. N = 9 trials from 3 mice. **c,** Δurine amount ± 5 sec. from end of photoinhibition for control odor and female odor (mean ± s.e.m., N = 9 total trials from 3 mice) .**d,** Urine amount, and, **e**, female odor sniff time during 2 min. photoinhibition period and 2 min. immediately following (mean ± s.e.m., same trials as h). **p<0.01, n.s. p>0.05 (Wilcoxon signed rank). Green shading denotes photoinhibition periods.

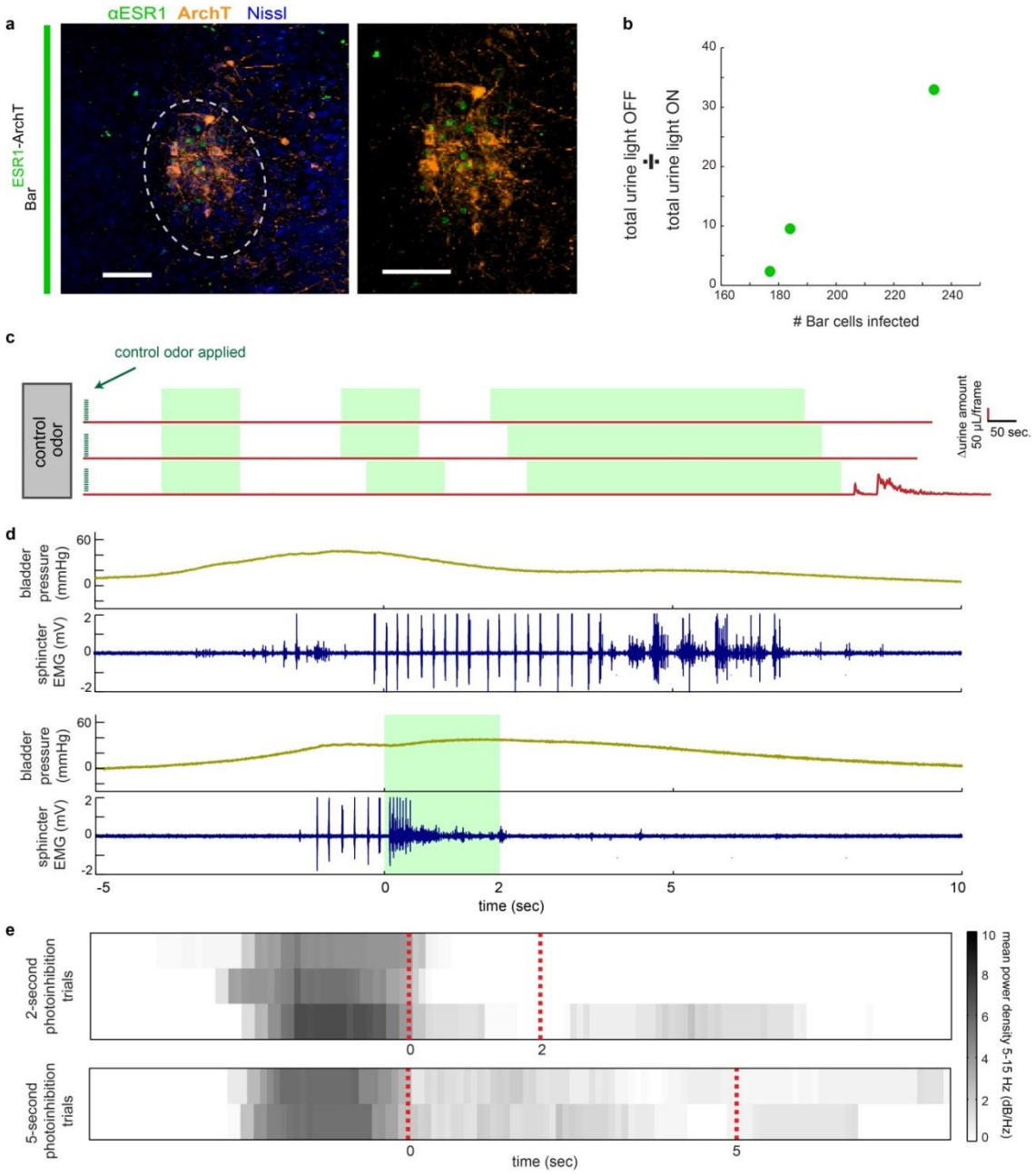

Figure 23. Bar$^{ESR1\text{-}ArchT}$ photoinhibition terminates sphincter bursting during cystometry and does not result in rebound urination in awake mice.

a, Example ArchT-GFP expression in Bar of ESR1-Cre mouse; right, larger views minus Nissl. **b,** Number of Bar cells infected with ArchT virus versus total urine with light OFF (not inhibited) divided by that with light on (while inhibited) for all mice (N = 3). **c,** Δurine amount around two 30 second photoinhibition periods followed by one 2 minute photoinhibition period, during which only control odor was present. N = 9 total photoinhibition bouts from 3 mice. **d,** Bladder pressure and sphincter EMG during cystometry, top, with natural unimpeded cycling, and bottom, in which 2 seconds of Bar$^{ESR1\text{-}ArchT}$ photoinhibition was triggered as soon as a bladder-filling-evoked burst was detected, which terminates bursting within ~100ms. **e,** Heatmap of mean EMG power density at bursting frequencies (5-15 Hz) during Bar$^{ESR1\text{-}ArchT}$ photoinhibition as in bottom of panel (d) (top: 2 second inhibition trials; bottom: 5 second inhibition trials; N = 2 mice). Green shading or red dotted lines mark photoinhibition periods. Scale bars = 100 µm.

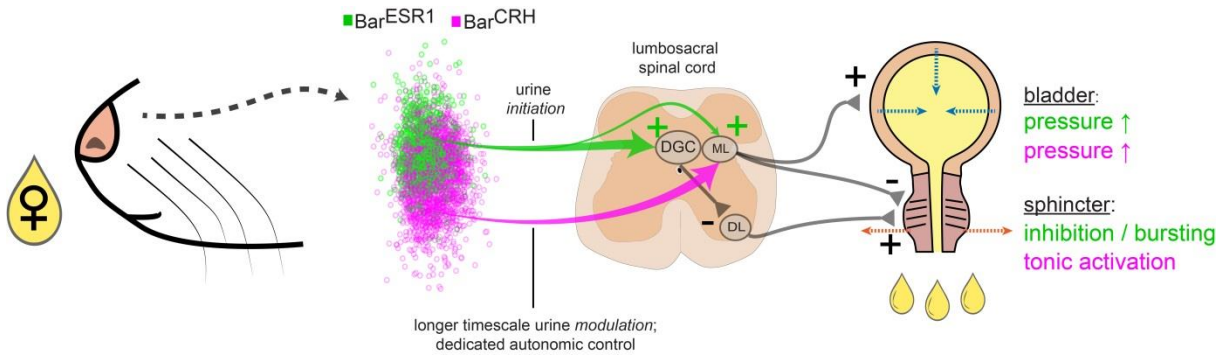

Figure 24. Simplified summary of Bar neuron function for scent marking behavior in male mice. Bar^{ESR1} (green) and Bar^{CRH} (magenta) neurons are intermingled (cell overlay from Figure 2c), and the minority Bar^{ESR1} population projects to both the mediolateral column (ML) and heavier to the dorsal grey commissure (DGC), which directly inhibits sphincter motoneurons in the dorsolateral nucleus (DL). Activation of Bar^{ESR1} neurons increases bladder pressure and simultaneously inhibits the sphincter via bursting, thus driving efficient urine excretion, whereas activation of Bar^{CRH} neurons produces a focal increase in bladder pressure and tonic excitation or no effect at the sphincter. Thoracolumbar projections of Bar^{ESR1} neurons are not shown, as well as afferent feedback connections from bladder and urethra.

1.8 Nose-to-sphincter circuit interactions

Our model underscores the main advantage of scent marking behavior as a systems neuroscience model, in that it has relatively simple input and output, and thus allows for more rigorous study of the entire "nose-to-sphincter" circuit in between. To completely realize this circuit, we must first identify the important components of female urine and the male mouse olfactory pathways that process them. Many molecules in female urine[107] are known to be processed through both the main and accessory olfactory systems in male mice[108,109]. The ultimate goal of understanding the transformation from nose to sphincter during scent marking behavior requires decoding of the relative contributions of these systems and how they ultimately influence Bar^{ESR1} neurons. We used broad deletion of the TrpC2 channel expressed in vomeronasal (VNO) sensory neurons to test if constitutive knockout of the accessory olfactory system affects scent marking behavior in male mice. Here we find that scent

marking behavior in these TrpC2$^{-/-}$ mice is variable and not significantly increased after the introduction of female urine, implying a significant role for the accessory olfactory system (Figure 25). However, these constitutive TrpC2$^{-/-}$ knockout mice show many deficits and behavioral changes[110], and it remains to be determined how *acute* manipulations of MOE and VNO can affect scent marking. In our assay, mice normally sample involatile odors by directly sniffing the female odor for several seconds, before responding with their own countermarks (Figure 19; Figure 21). They are only able to find the source of the nonvolatile odor components quickly by using volatile odor trails processed by the main olfactory epithelium (MOE).

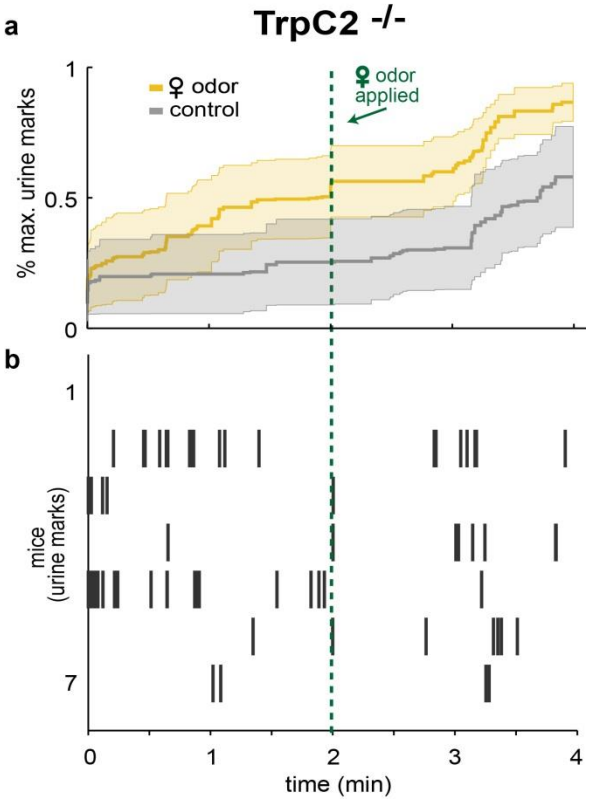

Figure 25. **TrpC2 KO mice scent mark indiscriminately**.
a, Urine marks during habituation with control odor only (grey) or with female odor (yellow) (mean ± s.e.m., N = 7 mice). **b,** Raster plot of urine marks detected.

Based on these behavioral observations, it seems likely that both the VNO and MOE are necessary for our rapid scent marking assay. Further work is needed to determine how these pathways converge[111] and which specific components of female urine[112,107] and olfactory receptors are important. Recent developments are making rapid progress for deorphanizing such receptors and ligands[109,113–115], and a complete nose-to sphincter circuit is attainable at the cellular and synaptic levels (Figure 26).

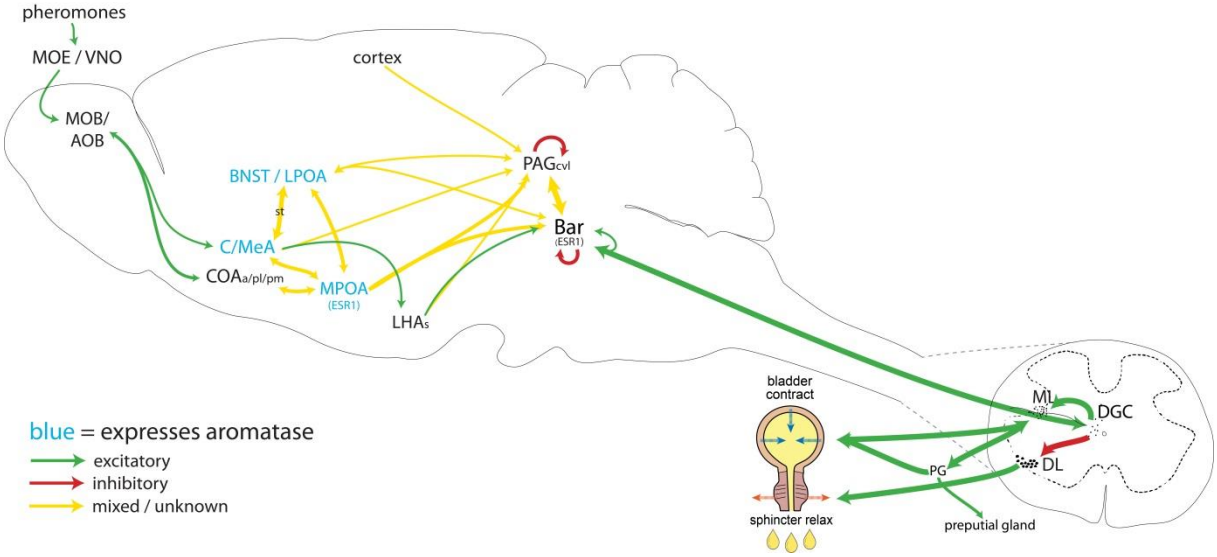

Figure 26. A hypothetical minimal nose-to-sphincter circuit.
Pheromones in female urine are detected by the MOE and VNO, and lead to increased activity in the MOB and AOB, respectively. This information is then passed to a network of downstream brain areas that are highly connected, and almost all pathways are bidirectional. Because the behavior is sexually dimorphic and likely masculinized via aromatase[71], we can surmise that olfactory information is gated by one of the few areas in the brain with aromatase expression (blue text). Many neurotransmitters and neuromodulators are involved in these pathways (yellow arrows), and Bar^{ESR1} neurons provide the premotor gate that leads to urethral sphincter and bladder activity. A minimum of 7 synapses must be traversed for information transmission from olfactory epithelium to EUS muscle, and each synapse provides an opportunity for convergence and divergence with other ongoing brain activity. Note that this is a very simplified hypothetical circuit model and many connections are left out for clarity, but may play roles in scent marking behavior. Abbreviations: AOB = accessory olfactory bulb, Bar = Barrington's nucleus, BNST / LPOA = bed nucleus of stria terminalis / lateral preoptic area, C/MeA = central/medial amygdala, COA = cortical amygdala, DGC = dorsal grey commissure, DL = dorsolateral nucleus, ML = mediolateral columns (lumbosacral), MOE = main olfactory epithelium, MPOA = medial preoptic area, PAGcvl = periaqueductal grey (caudal ventrolateral part), PG = pelvic ganglia, VNO = vomeronasal organ.

However reductionist we consider it, the nose-to-sphincter circuit does not operate in a vacuum. It is embedded in the context of ongoing activity throughout the nervous system, and the bursting EUS motor output co-occurs with three other well-known outputs: increased exploratory behavior, luteinizing hormone (LH) secretion leading to testosterone production[116], and ultrasonic vocalizations[117–119] (USVs). Increased exploration takes the form of the previously mentioned odor sampling interspersed with movements and rearing (Supplementary Video 6), and is important for spreading urine output around the environment in separate spots or marks to attract females[14,17]. Here we track broad movement parameters during scent marking behavior (Figure 21), but much work remains to fully understand how these motor patterns are coordinated. LH secretion occurs rapidly after encountering female urine and leads to increased testosterone levels within minutes[116,30], likely via hypothalamic processes involving kisspeptin and gonadotrophin releasing hormone[120]. We do not track this output but it also may play a role in preparing the mouse for impending sexual encounters or guiding learning to increase the probability of related behaviors in the future. USVs occur rapidly after female urine is encountered (Figure 27a), often before involatile odors are sampled. Nevertheless, this motor output is less robust than scent marking urination, as only 54% (93/185) of mice vocalized in prescreening trials for all experiments reported here, in contrast to 79% (141/185) producing low-latency increases in urination output. Recent work suggests that because both behaviors are influenced by body cavity pressures, they may be directly coupled[121], but direct analysis of correlations between USVs and urine marks *within* animals versus shuffled controls *across* animals shows that these behavioral outputs are not directly coupled (Figure 27b). Urine marks frequently occur without USVs, and vice versa, although they both tend to occur rapidly after female urine is introduced. It remains to be seen

whether all of these various responses of male mice to female urine are processed in completely separate pathways or how they interact and influence each other within the nervous system. Such interactions could provide clues and insight into the anatomy and synaptic mechanisms underlying the minimal nose-to-sphincter circuit.

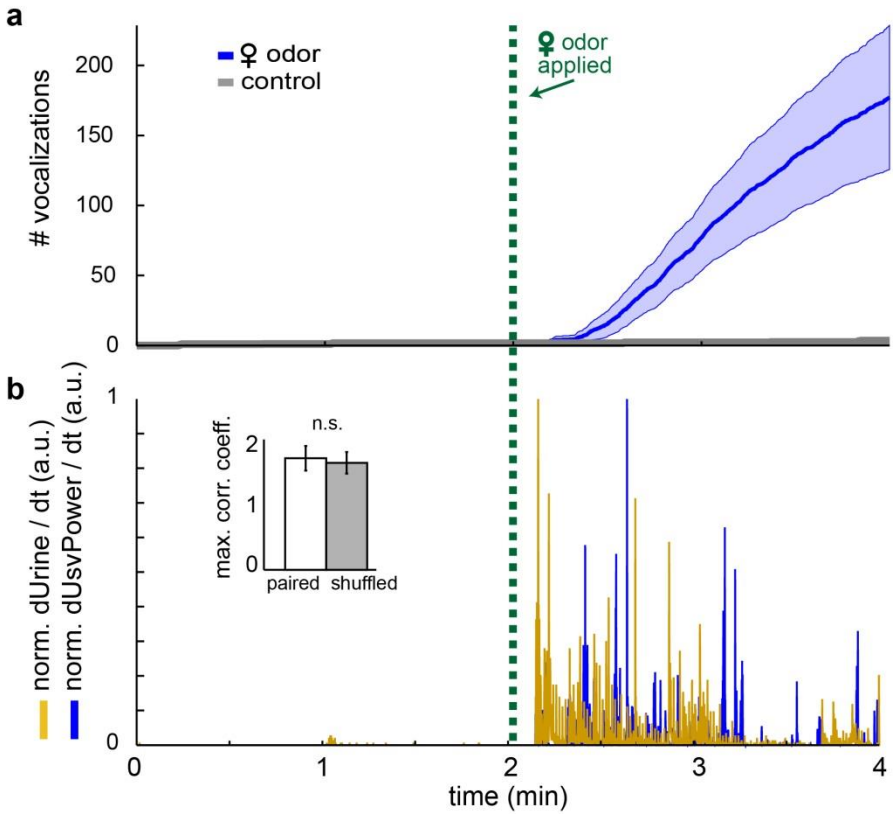

Figure 27. **Ultrasonic vocalizations are weakly correlated to scent marking urination**.
a, Number of vocalizations with control odor only (grey) or with female odor (blue) (mean ± s.e.m., N = 12 mice). **b,** Example trace for one trial showing normalized changes in urine pixels and USV power. Inset shows maximum correlation coefficients for these signals in paired trials in the same mouse versus shuffled trials where USV and urine traces are randomly correlated across different mice. n.s., p>0.05 (Wilcoxon signed rank).

One final hint regarding the nature of the nose-to-sphincter circuit is its plasticity. We find that scent marking behavior in mice can show single trial learning. After the first two-minute exposure to female odor, a mouse can process and abstract all of the cues representing

the odor-predicting environment, and then funnel their synaptic weights onto ~200 Bar^{ESR1} neurons, such that those environmental cues, rather than the female odor, can subsequently drive the urination response (Figure 28). This suggests that the circuit is not only part of a larger system that is wired to produce urination, vocalization, exploration, and testosterone; it is also preconfigured for rapid plasticity likely to involve cortical, hippocampal, and striatal interactions.

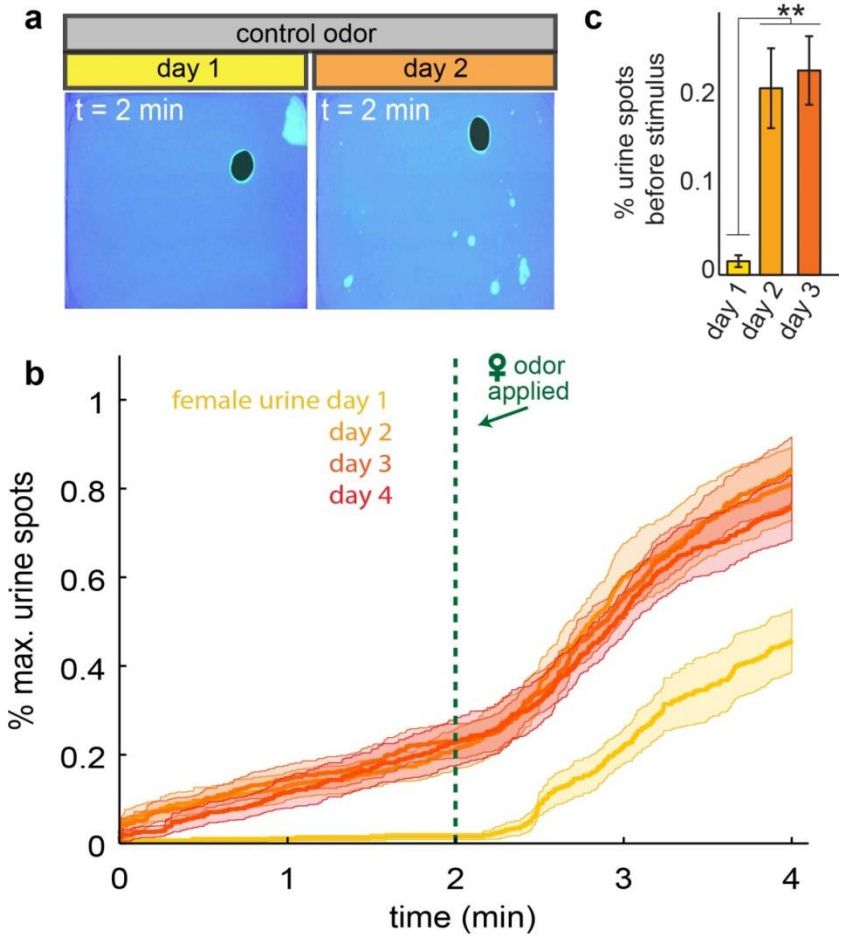

Figure 28. Single-trial conditioning of scent marking response to cues predicting female odor.
a, Example change in scent marking during the first two minutes of the assay (control odor period), before female urine odor is applied, from day 1 (left) to day 2 (right). **b,** Urine marks during four consecutive days with female odor presented (mean ± s.e.m., N = 12 mice). **c,** Percentage of urine marks during the control odor period from day 1 to day 3. **p<0.01 (Friedman's with Dunn-Sidak posthoc).

The Results, in part, are a reprint of material as it appears in bioRxiv, available at: https://doi.org/10.1101/270801. This material, in part, has also been submitted for publication in Nature Neuroscience, 2018. Keller JA, Chen J, Simpson S, Wang E, Lilascharoen V, George O, Lim B, Stowers L, 2018. The dissertation author was the primary investigator and author of these papers.

CHAPTER 2

DISCUSSION

Bar is well established as a key conserved brainstem node to coordinate the switch from urine storage to elimination, and is currently modeled as a single, divergent projection for bladder and urethral control[1]. Here we establish the existence of molecularly and functionally distinct Bar projections to the lumbosacral spinal cord for urinary control. Surprisingly, the minority Bar^{ESR1} neurons are the most potent drivers of urination via unique access to the urethral sphincter in mice. The fact that previous broad electrical stimulation in rodent Bar did not produce urethral inhibition or bursting[59], in contrast to optogenetic stimulation of Bar^{ESR1} neurons here, implies interactions between nearby cell types. Our data therefore suggests an updated model in which no single cell type confers absolute or dedicated control of urination, but rather all Bar cells work together for optimal control of bladder and urethra according to varying environmental demands over a range of timescales (Figure 24).

2.1 Urinary cell types in Bar

While Bar^{ESR1} neurons can clearly initiate urination, a role for the majority Bar^{CRH} neurons beyond focal bladder contraction remains less certain. Previously, Bar neurons have been categorized based on their electrophysiological correlations with reflexive bladder contractions in anesthetized[122–126,50,39,40] or awake[127] rodents and cats: (a) *direct* neurons with sustained increased activity (~20% of total), (b) *inverse* neurons with decreased activity (~50% of total), and (c) *on/off* neurons with transient activity just before or after contraction (~5% of total). Bar^{CRH} neurons have been proposed to map onto direct neurons based on

population fiber photometry[42], and some have suggested a role for these in prolonging bladder contraction and maintaining appropriate pressure rather than initiating urination[40,41,85]. *Independent* neurons (~25% of total recorded) that do not correlate with bladder activity are also reported, but Bar neurons that accompany sphincter relaxation or natural voluntary urination events have not been described. Our results suggest that physiological cell types in Bar should contain a urethral inhibition dimension, as well as a target dimension based on unique spinal interneuron connections[90,99]. Although it is tempting to speculate that molecularly-defined Bar neuron subsets map onto physiological types, a more complete and dynamic catalog of Bar neuron gene expression and spiking activity during a variety of conditions will likely be needed to fully classify their roles.

2.1.1 Anatomical and morphological differences in Bar cell types

A recent study used retrograde fluorescent beads injected in thoracolumbar and lumbosacral spinal cord to show little overlap between neurons in Bar projecting to these regions in adult rats. Although labelling fibers of passage at thoracolumbar levels could not be ruled out[99], whole cell slice recordings from each retrogradely-defined population revealed differences in many cell properties. For example, thoracolumbar-projecting Bar neurons had higher spontaneous firing rates and were inhibited, rather than excited, by glutamate antagonists. The anatomical data presented in this thesis suggests that Bar^{ESR1} neurons provide heavier projections than Bar^{CRH} neurons to thoracolumbar levels (albeit still light compared to lumbosacral projections; Figure 6), and thus could have unique cellular properties to permit a role in inhibition of sympathetic reflexes during urination, which is known to come from Bar[52]. Another study also showed differences in whole cell recording parameters in molecularly-defined cell types in Bar of juvenile mice[42]. In contrast to the adult rat study, they

report significant differences in Bar^{CRH+} and Bar^{CRH-} cells in resting cell membrane resistance and capacitance, but not spontaneous firing rate. The Bar^{CRH-} cells by themselves did separate according to firing rate, though, and our data suggests that these two groups could correspond to Bar^{ESR1} neurons and local inhibitory interneurons[1,42]. The lower capacitance and higher resistance of putative Bar^{ESR1} neurons indicates that these neurons are generally smaller than Bar^{CRH} neurons and, along with a bias towards reflexive rather than voluntary urination, may have contributed to undersampling in previous single unit studies. Additionally, smaller size suggests that Bar^{ESR1} neurons could be recruited first by size principle[128], given equal excitatory input to all cell types in Bar, consistent with a role in *initiation* of urination or pulsed scent marking that can occur regardless of bladder fill level. More extensive Bar input, in turn, could recruit all Bar projection neurons for complete bladder emptying. Furthermore, a single brain projection to intermingled populations in Bar would be able to effectively inhibit all urination when it is unsafe or inappropriate.

The existence of Bar^{CRH} axon terminals in DGC was previously reported by Hou et al.[42] and Verstegen et al.[36] and both of these studies suggest that such axons could allow Bar^{CRH} neurons to relax the urethral sphincter. The current study shows that while these Bar^{CRH} projections to DGC can be found, they are rare compared to the ML projections except in a few sections (Figure 6). Although different mouse strains were used across studies, this is unlikely to explain any discrepancies since mixed backgrounds were used in the current data. Also, the Verstegen et al. data included only female animals, so it is possible that the Bar^{CRH}→DGC projection is stronger in females. Finally, the Hou et al. study used much larger viral injection volumes with very high titers of the AAV9 serotype that can induce immune responses in the rodent brain, particularly at longer incubation times[129]. Although the

Verstegen et al. study does not report viral titer, it does use much longer incubation times with AAV9. Thus it is possible that the stress-sensitive CRH promoter is turned on in cells that do not normally express CRH (i.e. some Bar^{ESR1}→DGC neurons) under these conditions. Using smaller injection volumes and shorter incubation times, the current data shows much fewer Bar^{CRH}→DGC axons, as well as the corresponding function expected: focal excitation of autonomic pelvic targets.

Additional rostral projections of Bar^{CRH} neurons have been reported using classical dye tracers[47], but we find little evidence for these using cell-type-specific viral tracing techniques here (Figure 7). Since the borders between Bar and neighboring regions can be vague using pan-neuronal markers, the previously reported projections could have included axons from locus coeruleus or laterodorsal tegmentum. Regardless, it is clear that much work is needed to fully understand the details of synaptic partners for all Bar cell types, particularly with regard to intermingled urinary spinal interneurons[58,130] and related brainstem outputs such as the dorsal motor nucleus of the vagus nerve (colon control for defecation), nucleus ambiguous (abdominal cavity pressure control), and the "pontine storage center" (aka. L-region; directly contracts EUS to stop urination) that is known to exist in cats but not rodents[5,1]. It is possible that Bar cell types have different influences on these neurons that are not revealed by mesoscopic neuroanatomy, or alternatively that intermingled neurons provide differential feedback from bladder and urethral stretch receptors to Bar^{ESR1} and Bar^{CRH} neurons. Using mice for urinary studies should allow a thorough characterization of these connections akin to mouse locomotion, with precisely-defined cell types in brainstem and spinal cord[131,132] and detailed models of their interactions[133].

2.1.2 Different urinary timescales

While we found no evidence that Bar^{CRH} neurons initiate rapid, odor-induced voluntary urination, we did replicate an earlier study showing a modest inhibition during a much longer two hour assay[42], and Bar^{CRH} cells have been reported to play a role in urination patterns regulated by long-term social status changes[3,42]. CRH itself has negative effect on urination at longer timescales[134,49] and according to dominance status[3,42]. Thus, it is possible that Bar neuron subtypes can also be divided based on the timescale of urinary effects. These effects could be mediated by slower changes in hormone responses or gene expression, although more complete transcriptome analyses of Bar cell types across multiple states will likely be necessary to understand such functions.

2.2 Potential non-urinary functions of Bar

Beyond its well-known role in urination, Bar is implicated in a wider range of pelvic functions and has recently been termed the "pelvic organ stimulating center"[5,37] by anatomical and correlational evidence for roles in behaviors requiring varying levels of pelvic floor and autonomic coordination[1,3,135–137]. This multifunctional view of Bar (implying that the term "pontine micturition center" is a misnomer[36]) perhaps provides the most parsimonious explanation for molecular, cellular, and physiological heterogeneity in this relatively small nucleus. For example, ejaculation necessitates striated urethral muscles for expulsion, but simultaneous bladder inhibition and backflow prevention[1,138]. Urethral sphincter and bulbospongious bursting is the defining muscular feature of the expulsion phase of ejaculation[138–143] and likely uses the same burst generator in the L3-L4 DGC that is active during urination in rodents[87]. The current data shows that Bar^{ESR1} neurons provide input to the

DGC at these rostral lumbar levels as well as more caudally (Figure 6), and that they can powerfully initiate urethral sphincter bursting, even without affecting the bladder (Figure 16 and 17). One could speculate that during ejaculation, the bladder is inhibited by ensuring a subset of Bar^{CRH} neurons remain silent, whilst urethral sphincter bursting is promoted by increased activity of Bar^{ESR1} neurons. This type of control could be enacted by a single input into Bar and differential expression of neuromodulatory receptors or responses among cell types[144], or by more complicated control consisting of specific targeting of excitatory and inhibitory transmission[99]. Differential targeting of particular muscle fiber types or contraction mechanisms is also possible, such as purinergic and cholinergic bladder contractions, nitric oxide relaxation of urethral smooth muscle versus striated cholinergic control, and proximal to distal topography plus different muscle fiber types in the urethra[51,145,146]. Pharmacological manipulations during cell-type-specific Bar photostimulation could be used to discern these possibilities of pelvic target decoupling at the brainstem level.

Similar autonomic and somatic pelvic dissociation is required during other behaviors that rely on both voluntary and involuntary action such as defecation[135] and childbirth[147]. Bar neurons are known to respond to colonic distension[50] and are involved in defecation responses to stress[3,135]. They are additionally among the first in the brain labelled after PRV injection into not only bladder[89,148–153] and urethra[90,149,151,152,154], but also uterus and cervix[155–157], kidney and spleen[158], ischiocavernosus / bulbospongious / levator ani muscles[159–161], distal colon[162], prostate gland[160], and preputial glands (Figure 9). Thus Bar as a whole is well situated to control the various functions of the entire peripheral pelvic ganglion[163–167] as well as various striated pelvic floor muscles[52,5,37,168–173,147].

Furthermore, the idea of regulation at different timescales or for temporal sequencing could extend to other pelvic autonomic functions such as pheromone release from the preputial gland, which is also known to be regulated by social status[174], or other slower functions attributed to the pelvic ganglia. The preputial gland is a known potent source of female attractant pheromones[175,176], and our PRV tracing (Figure 9) suggests that it is almost exclusively controlled by Bar^{CRH} neurons. Dedicated control of this gland, separate from initiation of voiding by Bar^{ESR1} neurons, could ensure that pheromones are released into the urine stream when appropriate (i.e. only after a urine stream starts). Other, similar functions of the pelvic ganglia, but for which little is known in the central nervous system[163], include sperm production and transport, prostate gland secretions, and other reproductive secretions that vary by species[177,178]. Thus, while the role of Bar^{ESR1} neurons in voluntary urination is clear, our demonstration of functional heterogeneity across Bar invites further study into potential roles for all its neurons in regulating various other pelvic functions.

2.3 Potential roles of ESR1 and CRH in Bar

Other clues for the reasons behind heterogeneity in Bar come from differential gene expression and the functions of separated genes. What are the potential functions of ESR1 and CRH in Bar? Due to the complexity outlined above, it is clear that the answer to this question will likely require a more complete understanding of Bar neuron subtypes, including their specific synaptic connections, their endogenous activity during a variety of behaviors, and how those are affected by specific gene manipulations. Several clues can guide future experiments. The observation that ESR1 and CRH are overlapping in a minority of cells in Bar at both the protein and mRNA levels suggests that their functions are not completely

orthogonal. The function of CRH has received the most attention in Bar, with its proposed role being a co-transmitter in Bar^{CRH} neurons that inhibits urination and is upregulated by social stress[3]. Other than that data point, very little is known about the dynamics of gene expression and cell type in Bar. However, the CRH promoter has an estrogen response element[179], and CRH also has an inhibitory effect on atrial natriuretic peptide[180], which is also expressed in Bar[43] and is the most well-known diuretic hormone[181,182]. CRH is also known to inhibit sperm production and ovulation at the hypothalamic level[120].

Much less is known about the role of estrogen in Bar^{ESR1} neurons, although it has been speculated to play a role in sexual function and childbirth[44,76]. Removal of estrogen in female rats has been shown to decrease the sphincter bursting silent periods that we demonstrate can be driven by $Bar^{ESR1\text{-}ChR2}$ photostimulation[183]. Estradiol (E2) is unlikely to have a direct effect on Bar^{ESR1} neurons in males, since this most potent estrogen does not circulate in meaningful levels in males[184], and ARO is not expressed there to convert testosterone to E2 (Figure 4). Bulk manipulations of neurons expressing ARO or "masculinization" of female circuits by injecting pulses of estrogen in neonatal mice both affect urination parameters over long periods of time in the open field, without female cues[71,81], suggesting that the locus of sexual dimorphism in scent marking behavior is upstream of Bar. However, the roles of estrogens in males remain obscure, and one study has reported that the less potent estrogen, estrone (E1) supports normal urination in male mice[185]. Thus it is possible that ESR1 plays a pro-urination, trophic, vascular[186], and/or protective[187] role in male Bar^{ESR1} neurons.

2.3.1 ESR1 and CRH functions in female Bar

Alternatively, high ESR1 levels in Bar neurons may have evolved in females for a variety of reasons, and considered vestigial remnants in males[188]. For example, both E2 and

CRH are reproductive hormones and their levels increase dramatically in the first stage of labor[189,190]. Accordingly, the roles of ESR1 and CRH in Bar may be related to changes in pelvic function that occur during pregnancy and childbirth, such as relaxing pelvic floor muscles[147,137], inhibiting bladder muscle, or contracting uterine muscle. Alternatively, ESR1 and CRH expression could indirectly relate to these processes by compensating for stretching and damage caused therein, which is a major determinant of urinary dysfunction in women[191]. Finally, female rodent scent marking has been reported to be dependent on estrous state[17,192–194], although other studies have contradicted this claim[195–197] and there are likely subtle differences across species, strain, environment, and age. There are many sites for sex steroid interactions in any hypothetical nose-to-sphincter pathway, and one must be careful to interpret any global hormone manipulations until a full view of the scent marking circuit is clear. Future studies manipulating the ESR1 and CRH genes specifically in Bar^{ESR1} neurons can clarify these possible functions.

2.4 Clinical relevance

Urinary disorders and incontinence directly or indirectly affects nearly everyone at some point in their life[11,1], yet we still have relatively little understanding of how the brain functions or fails to function during this process. Common disruptions to urinary function include childbirth (e.g. rectal prolapse after pudendal nerve damage[191]), stress urinary incontinence (SUI) and associated depression, detrusor-sphincter dyssynergia (DSD) in paraplegics or after spinal cord injury[198], Fowler's syndrome (inability to voluntarily relax the EUS in women[199]), Hinman's Syndrome (behaviorally-induced sphincter dysfunction in children[200]), paruresis (inability to urinate in public[201]), overactive bladder (OAB^2), and

nocturnal enuresis (bedwetting[3]). These are only a few examples for which better models of CNS control of urination are needed in order to adequately address them. Bar^{ESR1} neurons can now be used as a valuable tool to study these problems, as well as a potential target for more specific and effective therapies. The ability to control voluntary urination in male mice on a timescale of seconds using female odor also opens up new avenues to record and manipulate neural activity during natural urination that is not driven by bladder distension.

2.4.1 Human versus rodent and cat urinary models

Barrington used ether-anesthetized cats in his initial studies of brainstem control of urination[34,35], and since then reflexive urination in anesthetized cats and rats has dominated the literature, with a few studies using mice as well[66]. However, important differences in urinary function exist between humans, cats, and rodents, including PET evidence for laterality in Bar for human urination[100] and ejaculation[136] but not in fMRI evidence for anesthetized rat urination[202]. The most notable species difference, however, is the existence of EUS bursting, which occurs naturally in rodents but *not* humans and cats, and is believed necessary for urine flow to overcome surface tension with a smaller urethra[63]. There is some evidence that EUS bursting can occur in anesthetized female primates[203], and exogenous bursting increases voiding efficiency in cats[204], but even the prevalence of urethral bursting for normal, voluntary urination in rodents is controversial.

Very few studies have examined urethral responses during natural, unrestrained urination in rodents, particularly in males. A recent study suggested that bursting plays a smaller role in mice than rats, but all recordings were done in restrained female rats and mice with bladder filling catheters. Thus, bursting may be less important for urine release in female mice, particularly when the bladder is exogenously filled to capacity. A subset of female

cystometry recordings for the current thesis (data not shown) also revealed fewer and shorter, more variable bursts than in males, consistent with widespread sexual dimorphism in pelvic organs and related peripheral and spinal circuits[205,206,164]. Another pair of studies in female rats without bladder catheters provide similar evidence that urethral sphincter bursting is not a completely reliable predictor of urine output[64,63]. However, a much stronger correlation between burst length and urine output is provided in paucity of data in males, including a previous study measuring corpus spongiosum pressure in male rats[67] as well as the current data (Figure 16; Figure 18; Supplemental Video 4). Thus the contribution of bursting seems to be greater in males, although more direct comparisons are needed[207]. The data are further complicated by the fact that the sphincter muscle is widely differentiated on the proximal to distal axis[51], and the strength of both tonic and bursting urethral EMG activity depends on electrode placement and type[104,208]. More work is needed to identify the specific mechanisms of EUS burst generation in the spinal cord in rodents, and how differences from cats and humans relate to incontinence issues. Using photostimulation of $Bar^{ESR1\text{-}ChR2}$ neurons in male mice to generate robust EUS bursting should greatly accelerate progress in this direction.

2.4.2 Isoflurane and optogenetics in male mice as a new urinary model

The experimental power of the mouse as a model system has not been fully leveraged in urinary studies because of their small size and reduced tolerance to urethane anesthesia compared to rats[209]. Urethane is by far the most common anesthetic used in cystometry recordings in other species because it preserves pelvic functions, despite a host of potentially confounding side effects[210]. Also, females animals are almost exclusively used for urinary incontinence studies because of the increased risk of urinary dysfunction in women, and EUS

recordings are particularly problematic in *female* rodents because of their smaller urethral muscles[66].

Our finding of photostimulated urination and EUS bursting in $Bar^{ESR1\text{-}ChR2}$ mice anesthetized with isoflurane is surprising, given several studies showing reduced responses in cystometry recordings using isoflurane in rats[101,102] and mice[103]. Previous results using electrical stimulation of Bar in rats were also unsuccessful in generating bursting responses (William de Groat, personal communication). In these studies[38,59,211], urethane anesthesia may have a depressing effect on Bar^{ESR1}→lumbosacral synapses, although normal bursting cycles during bladder filling argue against this possibility. Another difference from the current study, apart from nonspecific electrical rather than optogenetic stimulation, is that 50 Hz stimulation was always used for electrical stimulation. The present data suggests that depolarization block can occur at >25 Hz stimulation, particularly in Bar^{CRH} neurons, but also some Bar^{ESR1} neurons (Figure 14). When interpreting any experiment with exogenous activation of neurons, it is important to know how those neurons fire during behavior and what other neurons they project to and influence. The stimulation frequencies we use here for $Bar^{ESR1\text{-}ChR2}$ photostimulation are consistent with the only behaving recordings there in rodents[127], as well as those in anesthetized animals[41]. The increase in urine output from 25 Hz to 50 Hz photostimulation reported here in awake mice likely results from complex summation of currents experienced at varying light intensities and variable levels of viral expression in individual cells. Targeted single unit recordings of Bar neuron types during a variety of behaviors will be needed to fully understand their functions and to guide more realistic and natural stimulation patterns. Regardless, the current results demonstrate that bursting and efficient urination can be elicited by Bar^{ESR1} firing at less than 10 Hz, and suggest that local

interactions or depolarization block can suppress this effect during nonspecific electrical stimulation at 50 Hz.

The anatomical connections of Bar^{ESR1} neurons to the lumbosacral spinal cord are suggestive of a direct effect mediated through DGC inhibition of EUS motoneurons in the dorsolateral nucleus (DL), but we cannot rule out the possibility of a role for other projections. However, previous studies and observed anatomy argue against this possibility. We find very few axons projecting rostrally from Bar^{ESR1} or Bar^{CRH} neurons (Figure 7), and these pale in comparison to the DGC projections (Figure 6c). Furthermore, lesions or brain cuts rostral to Bar have been shown to have no effect on reflexive urination[212] or urination stimulated from broad pharmacological stimulation of Bar[61]. A previous study in rats has also shown that cutting the pelvic nerve (from lumbosacral cord) but not hypogastric nerve (from thoracolumbar cord) disrupts scent marking behavior[213]. Thus the most parsimonious route for the effects of $Bar^{ESR1\text{-}ChR2}$ photostimulation reported here is directly through the lumbosacral spinal cord, and this urinary model can capitalize on the plethora of tools available to dissect neural mechanisms in the mouse.

2.5 The nose-to-sphincter circuit

The control of scent marking behavior by Bar^{ESR1} neurons provides a solid handle for completing the circuit back to the nose (Figure 26). The reliability of this behavior in untrained animals suggests a strong genetic component and high selection pressure for correct circuit assembly. In some sense, this is not surprising as males that scent mark abundantly gain a direct advantage in attracting female sexual partners, and can even terminate pregnancies of competitor males via the Bruce effect[214]. However, as mentioned previously,

over-abundance of urine marks can attract unwanted predator attention and waste metabolic resources. In this sense, it does seem amazing that the numerous synapses needed for this behavior to occur can be so robustly constructed by the genome and early life experiences, particularly in light of the multifarious nature of the brain.

Liquid waste elimination is a fundamental animal need, but it must compete with many other potential priorities in a complicated world. Behaviorists since at least Tinbergen have surmised how such arbitration can occur in the nervous system[215]. These behavioral interactions could explain the need for heterogeneous urination control at the brainstem level, which forms the main advance set forth in this thesis. For example, scent marking to conspecific odor cues is highly sexually dimorphic, but all adult mice additionally urinate under extreme stress[216,3], analogous to stress incontinence in humans[1]. Mice will also mark more in novel environments[19,217,218], which is the main reason why a habituation procedure is used for the scent marking assay in this thesis. There is also some evidence that the brain can provide centrifugal control of bladder tension without urination[103,219,201], and it is well known that ascending signals alert the brain to find a safe and appropriate occasion when the bladder reaches capacity[127]. Urination is also modulated by circadian rhythms and sleep[4], fluid homeostasis and thirst[220–222], and even abdominal pressure increases such as sneezing[223]. Finally, control of urination is under complex developmental regulation in rodents, whereby maternal anogenital licking is required in early postnatal life to induce reflex urination and defecation, but this response is later replaced by supraspinal reflexes and even later by voluntary control[1,72,224]. All of these complications are likely to manifest at one or more levels of the nose-to-sphincter circuit (Figure 26), and the decoupling of bladder and urethra in Bar

can allow the brain more options for complex control of urination behavior relative to brain state and environment.

One of the main motivations behind this thesis is exemplified by the words of William James in the Epigraph. Over a century ago he categorized the various types of "decision making" that can occur in humans, each with varying degrees of deliberation and influence from innate biases versus that from logical discourse based on previous interactions with the environment. For the type analogous to the mouse's decision to inhibit the urethra and allow urine flow, he aptly invokes the metaphor of a flood breaking unexpectedly through a dam. Understanding the tradeoff and balance of innate and learned influences is a fundamental goal in neuroscience, but there are relatively few paradigms in which to rigorously study the neural mechanisms at hand in mammals. Here we find that scent marking behavior in mice shows single trial learning responses (Figure 28), which is a rare and powerful model for the type of learning that can influence rash decisions in humans[225–227]. However, little is known about how the nervous system can somehow figure out which patterns of activity were predictive of positive or rewarding experiences, and specifically assign those patterns credit by increasing their synaptic strength[228]. Learning during scent marking behavior suggests a tractable way to tackle this "credit assignment" problem[229], using established retrograde circuit manipulation techniques to discern causal roles for learning in neurons upstream of Bar^{ESR1} neurons. The relative simplicity of scent marking behavior can thus be leveraged for a greater understanding of how behavior in general can be biased on evolutionary timescales but modulated by environmental interactions over a lifetime.

CHAPTER 3

MATERIALS AND METHODS

3.1 Animals

All animal procedures were conducted in accordance with institutional guidelines and protocols approved by the Institutional Animal Care and Use Committee at The Scripps Research Institute. BALB/cByJ male mice were group housed at weaning, single housed at 8 weeks old for at least 1 week before any testing, and maintained on a 12/12hr light/dark cycle with food and water available ad libitum. All mouse lines are available at The Jackson Laboratory: CRH-Cre[77] (stock #: 012704), ESR1-Cre[79] (stock #: 017911), VGAT-Cre (stock #: 016962), VGLUT2-Cre (stock #: 016963), ARO-Cre[81] (stock #: 027038), TrpC2 KO (stock #: 021208), ROSA-LSL-tdTomato (Ai9, stock #: 007909), and ROSA-LSL-ZsGreen (Ai6, stock #: 007906). CRH-Cre and ESR1-Cre mice were backcrossed into the BALB/cByJ background for at least three generations.

3.2 General surgical procedures

Mice were anesthetized with isoflurane (5% induction, 1-2% maintenance, Kent Scientific SomnoSuite) and placed in a stereotaxic frame (David Kopf Instruments Model 962). Ophthalmic ointment (Puralube) was applied, buprenorphine (Buprenex, 0.15mg/kg) was administered intramuscularly at the beginning of the procedure, and 500uL sterile saline containing carprofen (Rimadyl, 5mg/kg) and enrofloxacin (Baytril, 5mg/kg) was administered subcutaneously at the end of the procedure. Mice were monitored daily and given at least 14 days for recovery and viral expression before subsequent behavioral testing.

3.3 AAV viral vectors

For photostimulation, AAV9-CAG-FLEX-ChR2-tdTomato (UPenn AV-9-18917P) was injected bilaterally at $1.4x10^{12}$ GC/mL in both ESR1-Cre and CRH-Cre animals. For CRH-Cre animals only, we also included AAV1-EF1α-FLEX-hChR2-eYFP (1:1 mix with above, UPenn AV-1-20298P) since this virus infected more Bar^{CRH} neurons in preliminary experiments. For photostimulation controls, AAV9-CAG-FLEX-GFP (UNC AV5220) was injected bilaterally at $3.2x10^{13}$ GC/mL in ESR1-Cre mice. For ESR1-Cre DREADD inhibition[106], AAVdj-CAG-FLEX-hM4Di-GFP[230] (Addgene plasmid # 52536, a gift from Scott Sternson) was produced by the Salk Institute Gene Transfer Targeting and Therapeutics Core (GT3) and injected bilaterally at $8x10^{12}$ GC/mL. We did not see efficient expression using this virus in CRH-Cre animals, so for CRH-Cre DREADD inhibition, AAVdj/1-EF1α-FLEX-hM4Di-mCherry (Addgene plasmid # 50461, a gift from Bryan Roth) was produced by Virovek and injected bilaterally at $4x10^{12}$ GC/mL. For photoinhibition, AAV9-CAG-FLEX-ArchT-GFP (UNC AV6222) was injected bilaterally at $2.2x10^{12}$ GC/mL in ESR1-Cre animals, and the same virus and titer were used for anatomical axon tracing unilaterally in both ESR1-Cre and CRH-Cre animals. For fiber photometry, AAV-CAG-FLEX-GCaMP6s[231] (UPenn AV-9-PV2818) was unilaterally injected at $3.2x10^{12}$ GC/mL in ESR1-Cre animals. For input-output tracing, AAVdj-EF1a-fFLEX-mRuby-2a-TVA and AAVdj-EF1a-fFLEX-RvG vectors were produced by Varoth Lilascharoen, mixed 1:1, and injected at ~$1x10^{12}$ GC/mL titers.

3.4 Pseudorabies (PRV) viral vector

PRV-152 (encoding CMV-GFP) was produced by the NIH Center for Neuroanatomy with Neurotropic Viruses (grant no. P40RR018604) and handled according to published

protocol[232]. Titer was $2x10^9$ pfu/mL, and 0.01% Fast Green was mixed in immediately before injection for visualization.

3.5 Canine adenovirus vector (CAV)

For input-output tracing, CAV2-FLEX-Flp[94] (IGMM, France) was unilaterally injected in S1 spinal cord, as described below for CTB injections, at $5.2x10^{12}$ pp/mL, immediately prior to AAV helper virus injections in Bar.

3.6 Rabies viral vector

EnvA-ΔG-Rabies-eGFP[91] was produced by GT3 and injected at $3.7x10^8$ pp/mL, 14 days after CAV and helper AAV injections. Survival time was 5 days.

3.7 Viral injection and fiber optic implantation

Injections were made using pulled glass pipettes (tips broken for ID = 10-20μm) and a Picospritzer at 25 – 75 nL/min. For Bar injections, the overlying muscle was removed and a medial-lateral angle of 33° was used to avoid the 4th ventricle. The pipette entry coordinate relative to bregma was 5.3mm caudal, 2.5mm lateral, and 3.2mm diagonally below the dura. The surrounding skull area was thinned for visualization with a diamond drill bit and the rostral-caudal coordinate was adjusted if necessary to coincide with the junction of the inferior colliculus and cerebellum, and to avoid hitting the transverse sinus. AAVs were injected 30-150nL per side, and the pipette was left in place for 5 min after injection, before slowly retracting. CAV was injected and 100nl per site, and ΔG-Rabies at 250nL per site. Fiber optic implants (4 mm length, Plexon 230 μm diameter for ChR2/ArchT and Doric 400 μm diameter for GCaMP) were inserted along the pipette track as above, 300 μm above the injection site for ChR2/ArchT, and 50μm for GCaMP. Additionally, two anchor screws (Antrin Miniature

Specialties M1 X .060") were attached over frontal cortex for animals with implants. After injection/implantation, the skull was covered with superglue and dental cement to seal the craniotomy and hold the implants in place.

3.8 CTB injections

For all injections, 150nL CTB-488 or CTB-647 (ThermoFisher, 0.5% in PBS) was slowly pressure injected using a Picospritzer, and the pipette was left in place for 5 min. before slowly retracting. Survival time was 5 days.

3.8.1 S1 spinal cord

A 1-2 cm incision was made over lumbar segments, and the connective tissue and muscle overlying the vertebrae was minimally dissected[233] to expose L1 and L2 vertebrae[234]. Vertebrae and underlying spinal segments were located by spinous process tendon attachments and spinous process shape, and confirmed by pilot injections of DiD dye. A spinal adapter[233] for the stereotaxic frame (Stoelting 51690) was used to clamp L2 transverse processes, and a beveled glass pipette was lowered into the space between L1 and L2 vertebrae, 400μm lateral to the spinous process midline and 600μm below dura, to target the S1 sacral mediolateral column and dorsal grey commissure. After injection, the site was covered with gelfoam and the overlying skin was sutured.

3.8.2 Barrington's nucleus

Bar was bilaterally targeted with CTB exactly as described for viral injections above.

3.9 Pseudorabies (PRV) injections

For all injections, beveled glass pipettes were used with a Picospritzer to inject 2 uL total volume at ~500nL/min, keeping the pipette in place for at least 1 min. before retracting.

The injection site was washed with saline before the incision was closed with sutures. For each different target muscle or gland, an initial timecourse experiment was conducted with at least 2 animals at 3 different survival times based on previous literature in rats[89,90,235,157,161] (Figure 8). The earliest survival time at which labelling was seen in Bar (at least 10 Bar cells in each animal) was used for subsequent experiments.

3.9.1 Bladder detrusor muscle

The bladder was exposed via ~1cm midline abdominal incision of skin and abdominal muscle layers, and PRV was injected into the ventral bladder detrusor muscle. Survival period for early Bar infection was 60 hours.

3.9.2 Preputial gland

The preputial glands are located subcutaneously, just rostral to the prepuce, and were exposed via ~1cm midline abdominal incision. The left gland was gently separated from connective tissue and held upright with forceps as PRV was injected from above. Care was taken to avoid injecting directly into large fluid compartments of the gland (visualized with Fast Green). Survival period for early Bar infection was 84 hours.

3.9.3 External urethral sphincter (EUS) muscle

The EUS (aka. urethral rhabdosphincter)[51,52] was exposed via ~1cm midline abdominal incision of skin and abdominal muscle layers. The bladder neck was gently held with forceps to expose the EUS and provide counter-pressure. The EUS was injected just proximal to the pubic symphysis, with Fast Green appearance in muscle striations used for visual confirmation. Survival period for early Bar infection was 84 hours.

3.9.4 Bulbospongious (BS) muscle

The dorsal BS muscle (also known as the sexually dimorphic levator ani) was exposed via ~1cm midline scrotum incision. Connective tissue was gently retracted and Fast Green appearance in muscle striations were used for visual confirmation. Survival period for early Bar infection was 84 hours.

3.10 Odor-motivated urination assay

Sexually naïve male mice were briefly prescreened for urination responses to 100uL female urine (>1 second odor sampling period with >3 urine marks within 1 minute) before any further testing or manipulation, which excluded 21% of all mice tested. The remaining 79% had surgical procedures and recovery or a 2 week waiting period before starting habituation. Mice were habituated in the behavior room for 3 consecutive days, for 16/8/4 minute durations on days 1/2/3. On day 3, control stimuli (100uL tonic water, which fluoresces under UV illumination) were pipetted from above at 0 min. and 2 min. and the baseline response was recorded. On subsequent test days, a 4 min. assay was used, with 100uL tonic water delivered at 0 minutes and 100uL female urine delivered at 2 min. All behavior was conducted during light hours under dim red light, and 70% ethanol was used to clean equipment between trials. The recording box consisted of a UV-opaque acrylic homecage with the bottom cut out, placed on top of 0.35mm chromatography paper (Fisher Scientific 05-714-4) resting on clear glass (Figure 11). Two wide angle cameras (Logitech C930e), one above on a modified cage top, and one below the bottom glass, streamed video to a laptop computer at 15 frames per second, 640x360 pixel resolution. An analog pulse controlled LEDs in each camera field of view in order to synchronize cameras. Two UV fluorescent tube lights (American DJ Black-24BLB) surrounded by foil walls were used to

evenly illuminate the chromatography paper from below. Videos were cut using Adobe After Effects and subsequently analyzed for urine marks using custom MATLAB software. The red and green channels of the RGB camera frames were used for urine detection, and the blue channel for mouse tracking. An output video with urine detection overlay was generated to manually verify automatic spot detection. Noldus Ethovision XT was used to automatically track mice and determine distance traveled and odor sniffing periods, defined as when the nosepoint occluded the female urine stimulus.

3.11 Ultrasonic vocalizations (USVs)

USVs were recorded during the odor-motivated urination assay using a microphone (Dodotronic Ultramic250K) mounted on the custom cage top, next to the top video camera. Data was acquired at 196 kHz using SeaWave software and synchronized to video streams with a 4.1 kHz tone (RadioShack Piezo Buzzer, 273-0074) driven by the same analog pulse used for video synchronization LEDs. Analysis was performed in MATLAB using modified versions of previously described scripts[118]. USV power was calculated as acoustic power in the 35–85 kHz band, above a preset noise threshold.

3.12 Female urine collection

Adult (8-16 weeks) C57BL/6N female mice were housed 5 per cage, soiled male bedding was introduced into the cage 24 hours before the first collection night to induce estrous, and urine was pooled from 4 cages (20 mice total) over 4 days such that the stimulus consisted of a mix from all stages of the estrous cycle[236]. The mice were placed in metabolic cage for 12-16 hours at a time overnight, and urine was collected directly into a sterile tube on dry ice and temporarily stored at -20°C in the morning. After 4 consecutive nights of

collection, urine was thawed on ice, rapidly passed through a 0.22um filter (Millipore Steriflip SCGP00525) before aliquoting and storing at -80°C. Two different batches of urine were collected for all experiments, and each was used with both control and experimental groups.

3.13 Chemogenetic inhibition

After hM4Di viral injection, mice were allowed at least 21 days for recovery and expression, and then intraperitoneally injected 45-55 minutes before testing with either control saline plus 0.5% DMSO, or Clozapine N-oxide (CNO, 5mg/kg, Enzo Life Sciences BML-NS105-0025) in saline plus 0.5% DMSO. Control saline injections were performed on the 3 habituation days before female urine was given. Then on days 4/5/6/7, mice received CNO/saline/CNO/saline before the female urine countermarking assay described above. CRH-Cre mice were tested for 2 additional days (CNO, then saline) using the same assay but with 2-hour duration. Mice with less than 3 marks within 2 minutes after stimulus on both saline control days were excluded from analysis (8 of 34 mice), as well as mice that did not have bilateral hM4Di expression that spanned at least ±100μm from the Bar rostral-caudal center, defined by ovoid Nissl clustering medial to locus coeruleus (7 of 34 mice). The "CNO Urine Inhibition Index" (CUI) was calculated as [(fraction of max. urine marks on saline days) - (fraction of max. urine marks on CNO days)], such that CUI = 2 represents complete inhibition by CNO relative to saline, while CUI = 0 represents no difference between saline and CNO days.

3.14 Optogenetic stimulation

For photostimulation experiments, fiber-implanted mice were briefly anesthetized with 5% isoflurane before connecting and disconnecting patch cables (Plexon 0.5 m, 230 um

diameter). An LED current source (Mightex BLS-SA02-US) driving two 465 nm PlexBright Compact LED Modules (Plexon) through a Dual LED Commutator (Plexon) provided 10±1 mW exiting the fiber tips. Optical power was measured (ThorLabs PM20A) before and after each session. Mice were placed in the same recording box described above for behavior, but with thinner 0.19 mm chromatography paper (Fisher Scientific 05-714-1). Initial experiments with different pulse widths determined 15 msec to be more effective than 5 msec or 1 msec at driving urination responses. All photostimulation bouts occurred for 5 sec duration using 15 msec pulses at five different frequencies: 1, 5, 10, 25, and 50Hz. These frequencies were stimulated in increasing order on the first day, and then repeated in decreasing order on the second day. At least 1 min elapsed between different photostimulation bouts, with additional delays occasionally necessary to allow the mouse to move to a clean section of paper. Videos were cut using Adobe After Effects and subsequently analyzed for urine marks using custom MATLAB software. Urine amount was calculated from urinated pixels detected using second-order polynomial coefficients determined with MATLAB *polyfit* on male urine calibration data (Figure 12). Response latency was calculated as the earliest point when the normalized Δurine derivative reached 10% of maximum during the 15 sec response period. For a subset of mice, we repeated photostimulation on a third day under 1.5% maintenance isoflurane anesthesia. Four anesthetized 50 Hz/15 msec/5 sec photostimulation bouts separated by 1 min/1 min/1 min/5 min were conducted, then the isoflurane was removed and the mouse was allowed to recover to walking before waiting 5 min and following with two awake 50 Hz/15 msec/5 sec bouts separated by 1 min/5 min to confirm that awake urination was intact. After all experiments, mice were perfused and checked for viral expression and fiber placement as described for immunohistochemistry. Mice that did not have at least unilateral ChR2

expression that spanned ±100μm from the Bar rostral-caudal center were excluded from analysis (9 of 29 mice).

3.15 Optogenetic inhibition

For photoinhibition, all procedures were same as for photostimulation described above except for the following changes: fiber implanted mice were not anesthetized before connecting patch cables, but were habituated to the procedure for at least 3 days before testing. On the final habituation day, control odor was presented and 3 different photoinhibition periods were applied (2x 30 sec., 1x 2 min., separated by at least 30 seconds) to test the baseline effects of ArchT inhibition on urine output. Plexon 550 nm PlexBright Compact LED Modules were used, providing provided 6±1 mW exiting the fiber tips. During the odor-motivated urination assay (on day 4, as described above), 2 min. of constant photoinhibition was applied 105 seconds after control odor, and 10-15 seconds before female urine. Urine marking behavior continued for 2 min. after photoinhibition ceased. Mice that did not have bilateral ArchT expression that spanned ±100μm from the Bar rostral-caudal center were excluded from analysis (7 of 10 mice).

3.16 Fiber photometry

Bulk GCaMP fluorescence was collected at 20 Hz using a similar setup to that previously described[237]. ΔF/F was calculated as (F – median(F) / median(F)) for each trial. An analog pulse controlled LEDs in each camera field of view as well as an Arduino sending triggers to the sCMOS camera (Hamamatsu ORCA-Flash4), in order to synchronize video and GCaMP data streams. Mice were recorded for 8 min. during each trial (4 min. control odor only, then 4 min. with female urine stimulus). Δurine peaks were calculated from bottom

video (MATLAB *findpeaks* function) with a minimum peak of 0.18 µL/frame, and GCaMP traces were analyzed around these peaks (zero lag) or at randomly selected times within the same assay (shuffle lag) as a control. The MATLAB *corrcoef* function was used to calculate correlation between GCaMP and Δurine traces.

3.17 Electromyography and cystometry

Fiber-implanted mice were anesthetized with isoflurane (5% induction, 2% maintenance) and the bladder and external urethral sphincter (EUS, or urethral rhabdosphincter)[51,52] were exposed via ~1cm midline abdominal incision. Flanged PE20 tubing connected to a syringe pump and pressure sensor (Biopac Systems DA100C/TSD104A) using a 25G needle was inserted and sutured into the bladder dome. Two tungsten wires (A-M Systems 795500) were stripped of insulation 1-2mm at the ends and inserted bilaterally (~2mm separation) into the EUS just proximal to the pubic symphysis, using a 30G needle. A third ground wire was stripped 3-4mm at the end and placed subcutaneously. The abdominal incision was sutured, allowing the tubing and wires to exit and connect to a differential amplifier (Biopac Systems EMG100C: gain = 5000, sample rate = 10kHz, low pass filter = 5kHz, 60Hz notch filter and 100Hz high pass filter). A digital input was simultaneously acquired at 10kHz, which was controlled by a TTL switch that also triggered optogenetic stimulation. After suturing, isoflurane was reduced to 1.0-1.8% (minimal to eliminate movement artifacts) and the bladder was filled at 10-20uL/min for at least 45 min. before starting photostimulation. Once a regular rhythm of urination cycles was established, the volume threshold was calculated as the mean volume of 3 cycles, and “filled” and “empty” states were defined as 75% and 10% of this mean value. Only mice with natural bursting cycles were analyzed for photostimulated or photoinhibited responses.

Photostimulation consisted of 50 Hz/15 msec/5 sec photostimulation bouts separated by > 1 min. Photoinhibition consisted of constant illumination for 2 or 5 seconds, manually triggered at the beginning of a burst event. Root-mean-square (RMS) EMG traces were calculated using a 300 msec Gaussian filter and subtraction of the mean across 5 seconds prior to photostimulation. Sphincter relaxation periods were defined using RMS EMG data as periods between peaks >0.1mV (MATLAB *findpeaks* function) with amplitude less than the mean value prior to photostimulation. Frequency content of RMS EMG traces was calculated by first downsampling to 200 Hz, and then taking the FFT in overlapping 2 sec. rectangular windows. The spectrogram was thresholded at -40dB and burst duration was calculated as the time in which mean power in the 5-15Hz band is above this threshold.

3.18 Wireless corpus spongiosum recording

Wireless pressure sensors (Data Sciences International, DSI PA-C10) were sterilized and implanted in the bulb of the corpus spongiosum that surrounds the urethra as previously described[105,67,238], with the transmitter placed subcutaneously in the lateral abdominal area. After 1 week recovery, mice were recorded in the odor-motivated urine assay as described above, but with a single camera and UV illumination from above and the DSI RPC-1 receiver below the test cage. Pressure data was logged at 500 Hz and synchronized to urine imaging video. Frequency content of pressure traces was calculated by taking the FFT in overlapping 2 second hamming windows.

3.19 Slice electrophysiology

Mice were deeply anesthetized with isoflurane, and acute 300µm coronal brain sections were prepared after intracardial perfusion of ice-cold choline-based slicing solution

containing (in mM): 25 $NaHCO_3$, 1.25 NaH_2PO_4, 2.5 KCl, 7 $MgCl_2$, 25 glucose, 0.5 $CaCl_2$, 110 choline chloride, 11.6 sodium ascorbate, 3.1 sodium pyruvate). Brains were quickly transferred and sliced in the same solution with a vibratome (LeicaVT1200). Sections were transferred to a recovery chamber and incubated for 15-20 min at 35°C in recovery solution consisting of (in mM): 118 NaCl, 2.6 $NaHCO_3$, 11 glucose, 15 HEPES, 2.5 KCl, 1.25 NaH_2PO_4, 2 sodium pyruvate, 0.4 sodium ascorbate, 2 $CaCl_2$, 1 $MgCl_2$. Slices were maintained at room temperature for at least 30 min until transferred to bath for recording. Cutting solution, recovery solution, and ACSF were constantly bubbled with 95% O_2 / 5% CO_2. Slices were transferred to a recording chamber on an upright fluorescent microscope continuously perfused with oxygenated ACSF (in mM):125 NaCl, 25 $NaHCO_3$, 2.5 KCl, 1.25 NaH_2PO_4, 11 glucose, 1.3 $MgCl_2$ and 2.5 $CaCl_2$ at 28-31°C using a feedback temperature controller. Neurons labeled by fluorescent markers were visualized with a 40X water-immersion objective with epifluorescence and infrared differential interference contrast video microscopy. Recording pipettes were pulled from borosilicate glass (G150TF-4; Warner Instruments) with 3-5 MΩ resistance. The internal solution for current-clamp recording consisted of the following (in mM): 125 potassium D-gluconate, 4 NaCl, 10 HEPES, 0.5 EGTA, 20 KCl, 4 Mg_2-ATP, 0.3 Na_3-GTP, and 10 phosphocreatine. Recordings were made using a MultiClamp700B amplifier and pClamp software (Molecular Devices). The signal was low-pass filtered at 1 kHz and digitized at 10 kHz with a digitizer (Molecular Devices). For photostimulation of ChR2, 15 msec / 5 sec duration blue light pulses were emitted from a collimated light-emitting diode (473 nm; Thorlabs) driven by a T-Cube LED Driver (ThorLabs) under the control of a Digidata 1440A Data Acquisition System and pClamp software. Light was delivered through the reflected light fluorescence illuminator port and the

40X objective (light power at max setting measured at 13.45 mW). Analysis was performed in either Clampfit (Molecular Devices) or OriginPro 2016 (Origin Lab).

3.20 Immunostaining

Animals were perfused with cold PBS followed by 4% PFA, and the brain / spinal cord (SC) was dissected and postfixed in 4% PFA at 4°C for 24-48 hours. Spinal cords were dissected by hydraulic extrusion[239]. The brain/SC was then washed in PBS and embedded in 1% low melting point agarose and cut on a vibratome at 50μm for ESR1 and/or NeuN staining or 100μm for Nissl-only staining. Spinal cords were cut transversely across the entire thoracolumbar and lumbosacral regions and matched to segments using Nissl landmarks. For ESR1 immunostaining, free-floating sections were blocked in 1% BSA (Sigma A3059) in 1% PBST (PBS plus Triton X-100) for 3 hours, followed by primary incubation with anti-ESR1 antibody[76] (antigen is mouse C-terminus fragment; Santa Cruz sc-542 or Lifespan C47042, rabbit polyclonal, 100μg/mL diluted 1:500 in 1% BSA / 0.3% PBST) overnight at room temperature. Sections were washed 3X with 0.1% PBST and blocked again at room temperature for 1 hour, before incubating in secondary antibody (ThermoFisher Alexa-Fluor 488 or 647 anti-rabbit IgG H+L diluted 1:2000 in 1% BSA / 0.3% PBST) at room temperature for 3 hours. Nissl stain (ThermoFisher NeuroTrace Blue or Deep Red diluted 1:200) was also included here if necessary, or incubated for 2 hours in 0.3% PBST if used alone. Sections were washed 2X in 0.1% PBST followed by 2X PBS, then mounted with ProLong Diamond (ThermoFisher). NeuN staining followed the same protocol as above but with NeuN primary antibody (EMD Millipore MAB377) diluted at 1:1000. For GABA staining only[84], animals were perfused cold PBS followed by 4% PFA and 0.2% glutaraldehyde (EMS 16000), and the brains were postfixed in the same solution for 4 hours at 4°C. Other steps were same as above,

but using anti-GABA/BSA (Sigma A2052) diluted at 1:1000 and blocking solution was 10% normal goat serum with 0.2% gelatin in 0.3% PBST.

3.21 Fluorescent in situ hybridization

Mice were anesthetized with isoflurane before rapid brain extraction, embedding in OCT, and freezing on dry ice. Coronal sections were cut at 20μm and stored at -80°C until processing according to the protocol provided in the RNAscope Multiplex Fluorescent v2 kit (Advanced Cell Diagnostics). Sections were fixed in 4% PFA, dehydrated, and hybridized with mixed probes: CRH (Mm-crh, Cat. 316091), ESR1 (Mm-Esr1-O2-C2, a custom 16ZZ probe targeting 1308-2125 of NM_007956.5.), VGAT (Mm-Slc32a1, Cat. 319191), and VGLUT2 (Mm-Slc17a6-C2, Cat. 319171) for 2 h at 40°C and followed by amplification. Signal in each channel is developed using TSA Cyanine 3, fluorescein, and Cyanine 5 (PerkinElmer) individually. Sections were counterstained with DAPI and mounted with ProLong Diamond.

3.22 Confocal Microscopy

Images were captured with Nikon A1 Confocal Microscope with a 10x air, 20x air or 40x oil objective. Nikon Elements software settings were optimized for each experiment to maximize signal range, and z-stack maximum projections were used for representative images and axonal projections while single optical slices were used for quantification of cell body overlap. For RNAScope, z-stacks were collected in 1 um increments throughout the z-axis.

3.23 Anatomical quantification

The rostrocaudal center of Bar was defined as two consecutive 50μm section with greatest ESR1 and CRH-tdT labelling whenever possible, or by distinctive ovoid Nissl or

NeuN boundaries. Custom MATLAB scripts were used to draw ROIs around Bar and semi-automatically count cells with clear cell body staining. Cells with high expression of ESR1 were distinguished from background labeling by thresholding in the ESR1 color channel just below the mean intensity level of nearby parabrachial neurons with established strong ESR1 expression[76,240]. Cartesian coordinates for cell locations were saved and the centroid of CRH-tdT cells was used to register different sections to generate the overlay plot in Figures 2 and 24. For calculation of fluorescence intensity ratio (Figure 6f) in the lumbosacral mediolateral column (ML) and dorsal grey commissure (DGC), all intact L5-S2 sections with visible axons were used. A rectangular ROI was drawn using the Nissl color channel to encapsulate the MLs and area in between. This ROI was then equally divided into medial-lateral thirds and the Bar axon color channel was used to calculate the sum of pixel intensity across each third. The ratio was calculated as this total pixel intensity in the middle DGC third divided by that of the 2 ML thirds averaged together.

3.24 Statistics and code

Nonparametric tests were used for all experiments. The Wilcoxon signed rank test (MATLAB *signrank*) was used for comparison of 2 paired groups, and the Mann-Whitney U test (aka. Wilcoxon rank sum test; MATLAB *ranksum*) for 2 unpaired groups. Friedman's test (MATLAB *friedman*) was used to compare across CNO and saline treatments for 4-day DREADD experiments, followed by Dunn-Sidak posthoc tests (MATLAB *multcompare*). Points with error bars represent mean ± s.e.m.

REFERENCES

1. de Groat, W. C., Griffiths, D. & Yoshimura, N. Neural Control of the Lower Urinary Tract. in *Comprehensive Physiology* (ed. Terjung, R.) 327–396 (John Wiley & Sons, Inc., 2014).

2. Griffiths, D. Neural control of micturition in humans: a working model. *Nat. Rev. Urol.* **12,** 695–705 (2015).

3. Valentino, R. J., Wood, S. K., Wein, A. J. & Zderic, S. A. The bladder–brain connection: putative role of corticotropin-releasing factor. *Nat. Rev. Urol.* **8,** 19–28 (2011).

4. Holstege, G. Micturition and the soul. *J. Comp. Neurol.* **493,** 15–20 (2005).

5. Holstege, G. The emotional motor system and micturition control. *Neurourol. Urodyn.* **29,** 42–48 (2010).

6. Griffiths, D. J. & Fowler, C. J. The micturition switch and its forebrain influences. *Acta Physiol.* **207,** 93–109 (2013).

7. Fowler, C. J. & Griffiths, D. J. A decade of functional brain imaging applied to bladder control. *Neurourol. Urodyn.* **29,** 49–55 (2010).

8. Birder, L., de Groat, W., Mills, I., Morrison, J., Thor, K. & Drake, M. Neural control of the lower urinary tract: Peripheral and spinal mechanisms. *Neurourol. Urodyn.* **29,** 128–139 (2010).

9. Drake, M. J., Fowler, C. J., Griffiths, D., Mayer, E., Paton, J. F. R. & Birder, L. Neural control of the lower urinary and gastrointestinal tracts: Supraspinal CNS mechanisms. *Neurourol. Urodyn.* **29,** 119–127 (2010).

10. Fowler, C. J., Griffiths, D. & de Groat, W. C. The neural control of micturition. *Nat. Rev. Neurosci.* **9,** 453–466 (2008).

11. Minassian, V. A., Drutz, H. P. & Al-Badr, A. Urinary incontinence as a worldwide problem. *Int. J. Gynecol. Obstet.* **82,** 327–338 (2003).

12. Bayani, D.-M., Taborsky, M. & Frommen, J. G. To pee or not to pee: urine signals mediate aggressive interactions in the cooperatively breeding cichlid Neolamprologus pulcher. *Behav. Ecol. Sociobiol.* **71,** (2017).

13. Yabuki, Y., Koide, T., Miyasaka, N., Wakisaka, N., Masuda, M., Ohkura, M., Nakai, J., Tsuge, K., Tsuchiya, S., Sugimoto, Y. & Yoshihara, Y. Olfactory receptor for prostaglandin F2α mediates male fish courtship behavior. *Nat. Neurosci.* **19,** 897–904 (2016).

14. Reynolds, E. Urination as a Social Response in Mice. *Nature* **234,** 481–483 (1971).

15. Hurst, J. L. The functions of urine marking in a free-living population of house mice, Mus domesticus Rutty. *Anim. Behav.* **35,** 1433–1442 (1987).

16. Hurst, J. L. The complex network of olfactory communication in populations of wild house mice Mus domesticus Rutty: urine marking and investigation within family groups. *Anim. Behav.* **37,** 705–725 (1989).

17. Hurst, J. L. Urine marking in populations of wild house mice Mus domesticus Rutty. III. Communication between the sexes. *Anim. Behav.* **40,** 233–243 (1990).

18. Hurst, J. L. & Beynon, R. J. Scent wars: the chemobiology of competitive signalling in mice. *BioEssays* **26,** 1288–1298 (2004).

19. Maruniak, J., Owen, K., Bronson, F. & Desjardins, C. Urinary Marking in Male House Mice: Responses to Novel Environmental and Social Stimuli. *Physiol. Behav.* **12,** 1035–1039 (1974).

20. Manzo, J., Garcia, L. I., Hernandez, M. E., Carrillo, P. & Pacheco, P. Neuroendocrine control of urine-marking behavior in male rats. *Physiol. Behav.* **75,** 25–32 (2002).

21. Arakawa, H., Blanchard, D. C., Arakawa, K., Dunlap, C. & Blanchard, R. J. Scent marking behavior as an odorant communication in mice. *Neurosci. Biobehav. Rev.* **32,** 1236–1248 (2008).

22. Lehmann, M. L., Geddes, C. E., Lee, J. L. & Herkenham, M. Urine Scent Marking (USM): A Novel Test for Depressive-Like Behavior and a Predictor of Stress Resiliency in Mice. *PLoS ONE* **8,** e69822 (2013).

23. Borelli, K. G., Blanchard, D. C., Javier, L. K., Defensor, E. B., Brandão, M. L. & Blanchard, R. J. Neural correlates of scent marking behavior in C57BL/6J mice: detection and recognition of a social stimulus. *Neuroscience* **162,** 914–923 (2009).

24. Kaur, A. W., Ackels, T., Kuo, T.-H., Cichy, A., Dey, S., Hays, C., Kateri, M., Logan, D. W., Marton, T. F., Spehr, M. & Stowers, L. Murine Pheromone Proteins Constitute a Context-Dependent Combinatorial Code Governing Multiple Social Behaviors. *Cell* **157,** 676–688 (2014).

25. Heymann, E. W. Scent marking strategies of new world primates. *Am. J. Primatol.* **68,** 650–661 (2006).

26. Drickamer, L. C. Rates of urine excretion by the house mouse (Mus domesticus): Differences by age, sex, social status, and reproductive condition. *J. Chem. Ecol.* **21,** 1481–1493 (1995).

27. Gosling, L. M., Roberts, S. C., Thornton, E. A. & Andrew, M. J. Life history costs of olfactory status signalling in mice. *Behav. Ecol. Sociobiol.* **48,** 328–332 (2000).

28. Desjardins, C., Maruniak, J. A. & Bronson, F. H. Social Rank in House Mice: Differentiation Revealed by Ultraviolet Visualization of Urinary Marking Patterns. *Science* **182,** 939–941 (1973).

29. Viitala, J., Korplmäki, E., Palokangas, P. & Koivula, M. Attraction of kestrels to vole scent marks visible in ultraviolet light. *Nature* **373,** 425–427 (1995).

30. Kavaliers, M., Choleris, E. & Colwell, D. D. Brief Exposure to Female Odors "Emboldens" Male Mice by Reducing Predator-Induced Behavioral and Hormonal Responses. *Horm. Behav.* **40,** 497–509 (2001).

31. Roberts, S. C., Gosling, L. M., Thornton, E. A. & McClung, J. Scent-marking by male mice under the risk of predation. *Behav. Ecol.* **12,** 698–705 (2001).

32. Curtis, A. L., Leiser, S. C., Snyder, K. & Valentino, R. J. Predator stress engages corticotropin-releasing factor and opioid systems to alter the operating mode of locus coeruleus norepinephrine neurons. *Neuropharmacology* **62,** 1737–1745 (2012).

33. Arakawa, H., Blanchard, D. C., Arakawa, K., Dunlap, C. & Blanchard, R. J. Scent marking behavior as an odorant communication in mice. *Neurosci. Biobehav. Rev.* **32,** 1236–1248 (2008).

34. Barrington, F. J. F. The relation of the hind-brain to micturition. *Brain* **44,** 23–53 (1921).

35. Barrington, F. J. F. The effect of lesions of the hind- and mid-brain on micturition in the cat. *Q. J. Exp. Physiol.* **15,** 81–102 (1925).

36. Verstegen, A. M. J., Vanderhorst, V., Gray, P. A., Zeidel, M. L. & Geerling, J. C. Barrington's nucleus: Neuroanatomic landscape of the mouse "pontine micturition center". *J. Comp. Neurol.* **525,** 2287–2309 (2017).

37. Holstege, G. How the Emotional Motor System Controls the Pelvic Organs. *Sex. Med. Rev.* **4,** 303–328 (2016).

38. Yamao, Y., Koyama, Y., Akihiro, K., Yukihiko, K. & Tsuneharu, M. Discrete regions in the laterodorsal tegmental area of the rat regulating the urinary bladder and external urethral sphincter. *Brain Res.* **912,** 162–170 (2001).

39. Tanaka, Y., Koyama, Y., Kayama, Y., Kawauchi, A., Ukimura, O. & Miki, T. Firing of micturition center neurons in the rat mesopontine tegmentum during urinary bladder contraction. *Brain Res.* **965,** 146–154 (2003).

40. Sasaki, M. Feed-forward and feedback regulation of bladder contractility by Barrington's nucleus in cats. *J. Physiol.* **557,** 287–305 (2004).

41. Sasaki, M. Role of Barrington's nucleus in micturition. *J. Comp. Neurol.* **493,** 21–26 (2005).

42. Hou, X. H., Hyun, M., Taranda, J., Huang, K. W., Todd, E., Feng, D., Atwater, E., Croney, D., Zeidel, M. L., Osten, P. & Sabatini, B. L. Central Control Circuit for Context-Dependent Micturition. *Cell* **167,** 73-86.e12 (2016).

43. Sutin, E. L. & Jacobowitz, D. M. Immunocytochemical localization of peptides and other neurochemicals in the rat laterodorsal tegmental nucleus and adjacent area. *J. Comp. Neurol.* **270,** 243–270 (1988).

44. VanderHorst, V. G. J. M., Gustafsson, J.-Å. & Ulfhake, B. Estrogen receptor-α and -β immunoreactive neurons in the brainstem and spinal cord of male and female mice: Relationships to monoaminergic, cholinergic, and spinal projection systems. *J. Comp. Neurol.* **488,** 152–179 (2005).

45. Vincent, S. R. & Satoh, K. Corticotropin-releasing factor (CRF) immunoreactivity in the dorsolateral pontine tegmentum: further studies on the micturition reflex system. *Brain Res.* **308,** 387–391 (1984).

46. Valentino, R. J., Page, M. E., Luppi, P. H., Zhu, Y., Van Bockstaele, E. & Aston-Jones, G. Evidence for widespread afferents to Barrington's nucleus, a brainstem region rich in corticotropin-releasing hormone neurons. *Neuroscience* **62,** 125–143 (1994).

47. Valentino, R. J., Pavcovich, L. A. & Hirata, H. Evidence for corticotropin-releasing hormone projections from Barrington's nucleus to the periaqueductal gray and dorsal motor nucleus of the vagus in the rat. *J. Comp. Neurol.* **363,** 402–422 (1995).

48. Sved, A. F., Cano, G., Passerin, A. M. & Rabin, B. S. The locus coeruleus, Barrington's nucleus, and neural circuits of stress. *Physiol. Behav.* **77,** 737–742 (2002).

49. McFadden, K., Griffin, T. A., Levy, V., Wolfe, J. H. & Valentino, R. J. Overexpression of corticotropin-releasing factor in Barrington's nucleus neurons by adeno-associated viral transduction: effects on bladder function and behavior. *Eur. J. Neurosci.* **36,** 3356–3364 (2012).

50. Rouzade-Dominguez, M.-L., Pernar, L., Beck, S. & Valentino, R. J. Convergent responses of Barrington's nucleus neurons to pelvic visceral stimuli in the rat: a juxtacellular labelling study. *Eur. J. Neurosci.* **18,** 3325–3334 (2003).

51. Lehtoranta, M., Streng, T., Yatkin, E., Paranko, J., Kolts, I., Talo, A. & Santti, R. Division of the male rat rhabdosphincter into structurally and functionally differentiated parts. *Anat. Rec. A. Discov. Mol. Cell. Evol. Biol.* **288A,** 536–542 (2006).

52. Thor, K. B. & de Groat, W. C. Neural control of the female urethral and anal rhabdosphincters and pelvic floor muscles. *AJP Regul. Integr. Comp. Physiol.* **299,** R416–R438 (2010).

53. Tanagho, E. A. & Miller, E. R. Initiation of voiding. *Br. J. Urol.* **42,** 175–183 (1970).

54. Yalla, S. V. & Resnick, N. M. Initiation of Voiding in Humans: The Nature and Temporal Relationship of Urethral Sphincter Responses. *J. Urol.* **157,** 590–595 (1997).

55. Karsenty, G., Reitz, A., Wefer, B., Boy, S. & Schurch, B. Understanding detrusor sphincter dyssynergia - significance of chronology. *Urology* **66,** 763–768 (2005).

56. Shy, M., Fung, S., Boone, T. B., Karmonik, C., Fletcher, S. G. & Khavari, R. Functional Magnetic Resonance Imaging during Urodynamic Testing Identifies Brain Structures Initiating Micturition. *J. Urol.* **192,** 1149–1154 (2014).

57. Blok, B. F., van Maarseveen, J. T. & Holstege, G. Electrical stimulation of the sacral dorsal gray commissure evokes relaxation of the external urethral sphincter in the cat. *Neurosci. Lett.* **249,** 68–70 (1998).

58. Shefchyk, S. J. Sacral spinal interneurones and the control of urinary bladder and urethral striated sphincter muscle function. *J. Physiol.* **533,** 57–63 (2001).

59. Kruse, M. N., Noto, H., Roppolo, J. R. & de Groat, W. C. Pontine control of the urinary bladder and external urethral sphincter in the rat. *Brain Res.* **532,** 182–190 (1990).

60. Kruse, M. N., Mallory, B. S., Noto, H., Roppolo, J. R. & de Groat, W. C. Properties of the descending limb of the spinobulbospinal micturition reflex pathway in the cat. *Brain Res.* **556,** 6–12 (1991).

61. Mallory, B. S., Roppolo, J. R. & de Groat, W. C. Pharmacological modulation of the pontine micturition center. *Brain Res.* **546,** 310–320 (1991).

62. Maggi, C. A., Giuliani, S., Santicioli, P. & Meli, A. Analysis of factors involved in determining urinary bladder voiding cycle in urethan-anesthetized rats. *Am. J. Physiol.-Regul. Integr. Comp. Physiol.* **251,** R250–R257 (1986).

63. LaPallo, B. K., Wolpaw, J. R., Chen, X. Y. & Carp, J. S. Contribution of the external urethral sphincter to urinary void size in unanesthetized unrestrained rats. *Neurourol. Urodyn.* (2015).

64. LaPallo, B. K., Wolpaw, J. R., Chen, X. Y. & Carp, J. S. Long-term recording of external urethral sphincter EMG activity in unanesthetized, unrestrained rats. *Am. J. Physiol.-Ren. Physiol.* **307,** F485–F497 (2014).

65. Kadekawa, K., Yoshimura, N., Majima, T., Wada, N., Shimizu, T., Birder, L. A., Kanai, A. J., de Groat, W. C., Sugaya, K. & Yoshiyama, M. Characterization of bladder and external urethral activity in mice with or without spinal cord injury - a comparison study with rats. *Am. J. Physiol. - Regul. Integr. Comp. Physiol.* **310,** R752–R758 (2016).

66. Andersson, K.-E., Soler, R. & Füllhase, C. Rodent models for urodynamic investigation. *Neurourol. Urodyn.* **30,** 636–646 (2011).

67. Nout, Y. S., Bresnahan, J. C., Culp, E., Tovar, C. A., Beattie, M. S. & Schmidt, M. H. Novel technique for monitoring micturition and sexual function in male rats using telemetry. *Am. J. Physiol.-Regul. Integr. Comp. Physiol.* **292,** R1359–R1367 (2007).

68. Streng, T., Santti, R., Andersson, K.-E. & Talo, A. The role of the rhabdosphincter in female rat voiding. *BJU Int.* **94,** 138–142 (2004).

69. Yang, P. J., Pham, J., Choo, J. & Hu, D. L. Duration of urination does not change with body size. *Proc. Natl. Acad. Sci.* **111,** 11932–11937 (2014).

70. le Feber, J. & van Asselt, E. Pudendal nerve stimulation induces urethral contraction and relaxation. *Am. J. Physiol.-Regul. Integr. Comp. Physiol.* **277,** R1368–R1375 (1999).

71. Wu, M. V., Manoli, D. S., Fraser, E. J., Coats, J. K., Tollkuhn, J., Honda, S.-I., Harada, N. & Shah, N. M. Estrogen Masculinizes Neural Pathways and Sex-Specific Behaviors. *Cell* **139,** 61–72 (2009).

72. Moore, C. L. The Role of Maternal Stimulation in the Development of Sexual Behavior and Its Neural Basis. *Ann. N. Y. Acad. Sci.* **662,** 160–177 (1992).

73. Fellini, L. & Morellini, F. Mice Create What-Where-When Hippocampus-Dependent Memories of Unique Experiences. *J. Neurosci.* **33,** 1038–1043 (2013).

74. Boehm, U. The vomeronasal system in mice: From the nose to the hypothalamus - and back! *Semin. Cell Dev. Biol.* **17,** 471–479 (2006).

75. Lein, E. S., Hawrylycz, M. J., Ao, N., Ayres, M., Bensinger, A., Bernard, A., Boe, A. F., Boguski, M. S., Brockway, K. S., Byrnes, E. J., Chen, L., Chen, L., Chen, T.-M., Chi Chin, M., Chong, J., Crook, B. E., Czaplinska, A., Dang, C. N., Datta, S., Dee, N. R., Desaki, A. L., Desta, T., Diep, E., Dolbeare, T. A., Donelan, M. J., Dong, H.-W., Dougherty, J. G., Duncan, B. J., Ebbert, A. J., Eichele, G., Estin, L. K., Faber, C., Facer, B. A., Fields, R., Fischer, S. R., Fliss, T. P., Frensley, C., Gates, S. N., Glattfelder, K. J., Halverson, K. R., Hart, M. R., Hohmann, J. G., Howell, M. P., Jeung, D. P., Johnson, R. A., Karr, P. T., Kawal, R., Kidney, J. M., Knapik, R. H., Kuan, C. L., Lake, J. H., Laramee, A. R., Larsen, K. D., Lau, C., Lemon, T. A., Liang, A. J., Liu, Y., Luong, L. T., Michaels, J., Morgan, J. J., Morgan, R. J., Mortrud, M. T., Mosqueda, N. F., Ng, L. L., Ng, R., Orta, G. J., Overly, C. C., Pak, T. H., Parry, S. E., Pathak, S. D., Pearson, O. C., Puchalski, R. B., Riley, Z. L., Rockett, H. R., Rowland, S. A., Royall, J. J., Ruiz, M. J., Sarno, N. R., Schaffnit, K., Shapovalova, N. V., Sivisay, T., Slaughterbeck, C. R., Smith, S. C., Smith, K. A., Smith, B. I., Sodt, A. J., Stewart, N. N., Stumpf, K.-R., Sunkin, S. M., Sutram, M., Tam, A., Teemer, C. D., Thaller, C., Thompson, C. L., Varnam, L. R., Visel, A., Whitlock, R. M., Wohnoutka, P. E., Wolkey, C. K., Wong, V. Y., Wood, M., Yaylaoglu, M. B., Young, R. C., Youngstrom, B. L., Feng Yuan, X., Zhang, B., Zwingman, T. A. & Jones, A. R. Genome-wide atlas of gene expression in the adult mouse brain. *Nature* **445,** 168 (2006).

76. VanderHorst, V. G. J. M., Terasawa, E. & Ralston, H. J. Estrogen receptor-α immunoreactive neurons in the brainstem and spinal cord of the female rhesus monkey: Species-specific characteristics. *Neuroscience* **158,** 798–810 (2009).

77. Taniguchi, H., He, M., Wu, P., Kim, S., Paik, R., Sugino, K., Kvitsani, D., Fu, Y., Lu, J., Lin, Y., Miyoshi, G., Shima, Y., Fishell, G., Nelson, S. B. & Huang, Z. J. A Resource of Cre Driver Lines for Genetic Targeting of GABAergic Neurons in Cerebral Cortex. *Neuron* **71,** 995–1013 (2011).

78. Kono, J., Konno, K., Talukder, A. H., Fuse, T., Abe, M., Uchida, K., Horio, S., Sakimura, K., Watanabe, M. & Itoi, K. Distribution of corticotropin-releasing factor neurons in the mouse brain: a study using corticotropin-releasing factor-modified yellow fluorescent protein knock-in mouse. *Brain Struct. Funct.* **222,** 1705–1732 (2017).

79. Lee, H., Kim, D.-W., Remedios, R., Anthony, T. E., Chang, A., Madisen, L., Zeng, H. & Anderson, D. J. Scalable control of mounting and attack by Esr1+ neurons in the ventromedial hypothalamus. *Nature* **509,** 627–632 (2014).

80. Yang, C. F. & Shah, N. M. Representing Sex in the Brain, One Module at a Time. *Neuron* **82,** 261–278 (2014).

81. Unger, E. K., Burke, K. J., Yang, C. F., Bender, K. J., Fuller, P. M. & Shah, N. M. Medial Amygdalar Aromatase Neurons Regulate Aggression in Both Sexes. *Cell Rep.* **10,** 453–462 (2015).

82. Nguyen, A. Q., Dela Cruz, J. A. D., Sun, Y., Holmes, T. C. & Xu, X. Genetic cell targeting uncovers specific neuronal types and distinct subregions in the bed nucleus of the stria terminalis. *J. Comp. Neurol.* **524,** 2379–2399 (2016).

83. Wallace, M. L., Saunders, A., Huang, K. W., Philson, A. C., Goldman, M., Macosko, E. Z., McCarroll, S. A. & Sabatini, B. L. Genetically Distinct Parallel Pathways in the Entopeduncular Nucleus for Limbic and Sensorimotor Output of the Basal Ganglia. *Neuron* **94,** 138-152.e5 (2017).

84. Brown, K. N., Chen, S., Han, Z., Lu, C.-H., Tan, X., Zhang, X.-J., Ding, L., Lopez-Cruz, A., Saur, D., Anderson, S. A., Huang, K. & Shi, S.-H. Clonal Production and Organization of Inhibitory Interneurons in the Neocortex. *Science* **334,** 480 (2011).

85. Sasaki, M. & Sato, H. Polysynaptic connections between Barrington's nucleus and sacral preganglionic neurons. *Neurosci. Res.* **75,** 150–156 (2013).

86. Grill, W. M., Bhadra, N. & Wang, B. Bladder and urethral pressures evoked by microstimulation of the sacral spinal cord in cats. *Brain Res.* **836,** 19–30 (1999).

87. Chang, H.-Y., Cheng, C.-L., Chen, J.-J. J. & de Groat, W. C. Serotonergic drugs and spinal cord transections indicate that different spinal circuits are involved in external urethral sphincter activity in rats. *AJP Ren. Physiol.* **292,** F1044–F1053 (2006).

88. Ambadkar, P. M. & Vyas, D. M. Innervation of the rat preputial gland. *Acta Anat. (Basel)* **110,** 98–102 (1981).

89. Nadelhaft, I. & Vera, P. L. Central nervous system neurons infected by pseudorabies virus injected into the rat urinary bladder following unilateral transection of the pelvic nerve. *J. Comp. Neurol.* **359,** 443–456 (1995).

90. Vizzard, M. A., Erickson, V. L., Card, J. P., Roppolo, J. R. & de Groat, W. C. Transneuronal labeling of neurons in the adult rat brainstem and spinal cord after injection of pseudorabies virus into the urethra. *J. Comp. Neurol.* **355,** 629–640 (1995).

91. Wickersham, I. R., Lyon, D. C., Barnard, R. J. O., Mori, T., Finke, S., Conzelmann, K.-K., Young, J. A. T. & Callaway, E. M. Monosynaptic Restriction of Transsynaptic Tracing from Single, Genetically Targeted Neurons. *Neuron* **53,** 639–647 (2007).

92. Wall, N. R., Wickersham, I. R., Cetin, A., De La Parra, M. & Callaway, E. M. Monosynaptic circuit tracing in vivo through Cre-dependent targeting and complementation of modified rabies virus. *Proc. Natl. Acad. Sci. U. S. A.* **107,** 21848–21853 (2010).

93. Fenno, L. E., Mattis, J., Ramakrishnan, C., Hyun, M., Lee, S. Y., He, M., Tucciarone, J., Selimbeyoglu, A., Berndt, A., Grosenick, L., Zalocusky, K. A., Bernstein, H., Swanson, H., Perry, C., Diester, I., Boyce,

F. M., Bass, C. E., Neve, R., Huang, Z. J. & Deisseroth, K. Targeting cells with single vectors using multiple-feature Boolean logic. *Nat. Methods* **11,** 763–772 (2014).

94. Schwarz, L. A., Miyamichi, K., Gao, X. J., Beier, K. T., Weissbourd, B., DeLoach, K. E., Ren, J., Ibanes, S., Malenka, R. C., Kremer, E. J. & Luo, L. Viral-genetic tracing of the input–output organization of a central noradrenaline circuit. *Nature* **524,** 88–92 (2015).

95. Dong, H.-W. & Swanson, L. W. Projections from bed nuclei of the stria terminalis, magnocellular nucleus: Implications for cerebral hemisphere regulation of micturition, defecation, and penile erection. *J. Comp. Neurol.* **494,** 108–141 (2006).

96. Stone, E., Coote, J. H., Allard, J. & Lovick, T. A. GABAergic control of micturition within the periaqueductal grey matter of the male rat. *J. Physiol.* **589,** 2065–2078 (2011).

97. Dong, H.-W. & Swanson, L. W. Projections from bed nuclei of the stria terminalis, dorsomedial nucleus: Implications for cerebral hemisphere integration of neuroendocrine, autonomic, and drinking responses. *J. Comp. Neurol.* **494,** 75–107 (2006).

98. Dong, H.-W. & Swanson, L. W. Projections from bed nuclei of the stria terminalis, posterior division: Implications for cerebral hemisphere regulation of defensive and reproductive behaviors. *J. Comp. Neurol.* **471,** 396–433 (2004).

99. Guo, Y.-X., Li, D.-P., Chen, S.-R. & Pan, H.-L. Distinct intrinsic and synaptic properties of pre-sympathetic and pre-parasympathetic output neurons in Barrington's nucleus. *J. Neurochem.* **126,** 338–348 (2013).

100. Blok, B. F., Willemsen, A. T. & Holstege, G. A PET study on the brain control of micturition in humans. *Brain* **120,** 111–121 (1997).

101. Matsuura, S. & Downie, J. W. Effect of anesthetics on reflex micturition in the chronic cannula-implanted rat. *Neurourol. Urodyn.* **19,** 87–99 (2000).

102. Chang, H.-Y. & Havton, L. A. Differential effects of urethane and isoflurane on external urethral sphincter electromyography and cystometry in rats. *AJP Ren. Physiol.* **295,** F1248–F1253 (2008).

103. Smith, P. P., DeAngelis, A. M. & Kuchel, G. A. Evidence of central modulation of bladder compliance during filling phase. *Neurourol. Urodyn.* **31,** 30–35 (2012).

104. Cruz, Y. & Downie, J. W. Sexually dimorphic micturition in rats: relationship of perineal muscle activity to voiding pattern. *Am. J. Physiol.-Regul. Integr. Comp. Physiol.* **289,** R1307–R1318 (2005).

105. Nout, Y. S., Schmidt, M. H., Tovar, C. A., Culp, E., Beattie, M. S. & Bresnahan, J. C. Telemetric monitoring of corpus spongiosum penis pressure in conscious rats for assessment of micturition and sexual function following spinal cord contusion injury. *J. Neurotrauma* **22,** 429–441 (2005).

106. Krashes, M. J., Koda, S., Ye, C., Rogan, S. C., Adams, A. C., Cusher, D. S., Maratos-Flier, E., Roth, B. L. & Lowell, B. B. Rapid, reversible activation of AgRP neurons drives feeding behavior in mice. *J. Clin. Invest.* **121,** 1424–1428 (2011).

107. Achiraman, S., Archunan, G., SankarGanesh, D., Rajagopal, T., Rengarajan, R. L., Kokilavani, P., Kamalakkannan, S. & Kannan, S. Biochemical Analysis of Female Mice Urine with Reference to Endocrine Function: A Key Tool for Estrus Detection. *Zoolog. Sci.* **28,** 600–605 (2011).

108. Sipos, M. L., Wysocki, C. J., Nyby, J. G., Wysocki, L. & Nemura, T. A. An ephemeral pheromone of female house mice: Perception via the main and accessory olfactory systems. *Physiol. Behav.* **58,** 529–534 (1995).

109. Fu, X., Yan, Y., Xu, P. S., Geerlof-Vidavsky, I., Chong, W., Gross, M. L. & Holy, T. E. A Molecular Code for Identity in the Vomeronasal System. *Cell* **163,** 313–323 (2015).

110. Stowers, L., Holy, T. E., Meister, M., Dulac, C. & Koentges, G. Loss of Sex Discrimination and Male-Male Aggression in Mice Deficient for TRP2. *Science* **295,** 1493 (2002).

111. Pro-Sistiaga, P., Mohedano-Moriano, A., Ubeda-Bañon, I., del mar Arroyo-Jimenez, M., Marcos, P., Artacho-Pérula, E., Crespo, C., Insausti, R. & Martinez-Marcos, A. Convergence of olfactory and vomeronasal projections in the rat basal telencephalon. *J. Comp. Neurol.* **504,** 346–362 (2007).

112. Hayashi, S. & Kimura, T. Sex-attractant emitted by female mice. *Physiol. Behav.* **13,** 563–567 (1974).

113. McClintock, T. S., Adipietro, K., Titlow, W. B., Breheny, P., Walz, A., Mombaerts, P. & Matsunami, H. In Vivo Identification of Eugenol-Responsive and Muscone-Responsive Mouse Odorant Receptors. *J. Neurosci.* **34,** 15669–15678 (2014).

114. Jiang, Y., Gong, N. N., Hu, X. S., Ni, M. J., Pasi, R. & Matsunami, H. Molecular profiling of activated olfactory neurons identifies odorant receptors for odors in vivo. *Nat. Neurosci.* **18,** 1446–1454 (2015).

115. Nishizumi, H. & Sakano, H. Decoding and deorphanizing an olfactory map. *Nat. Neurosci.* **18,** 1432–1433 (2015).

116. Coquelin, A., Clancy, A., Macrides, F., Noble, E. & Gorski, R. Pheromonally induced release of luteinizing hormone in male mice: involvement of the vomeronasal system. *J. Neurosci.* **4,** 7 (1984).

117. Whitney, G., Alpern, M., Dizinno, G. & Horowitz, G. Female odors evoke ultrasounds from male mice. *Anim. Learn. Behav.* **2,** 13–18 (1974).

118. Holy, T. E. & Guo, Z. Ultrasonic Songs of Male Mice. *PLoS Biol.* **3,** e386 (2005).

119. Egnor, S. R. & Seagraves, K. M. The contribution of ultrasonic vocalizations to mouse courtship. *Curr. Opin. Neurobiol.* **38,** 1–5 (2016).

120. Kageyama, K. Regulation of gonadotropins by corticotropin-releasing factor and urocortin. *Front. Endocrinol.* **4,** (2013).

121. Deschênes, M., Moore, J. & Kleinfeld, D. Sniffing and whisking in rodents. *Curr. Opin. Neurobiol.* **22,** 243–250 (2012).

122. de Groat, W. C., Araki, I., Vizzard, M. A., Yoshiyama, M., Yoshimura, N., Sugaya, K., Tai, C. & Roppolo, J. R. Developmental and injury induced plasticity in the micturition reflex pathway. *Behav. Brain Res.* **92,** 127–140 (1998).

123. Koyama, Y., Imada, N., Kawauchi, A. & Kayama, Y. Firing of putative cholinergic neurons and micturition center neurons in the rat laterodorsal tegmentum during distention and contraction of urinary bladder. *Brain Res.* **840,** 45–55 (1999).

124. Sakakibara, R., Nakazawa, K., Shiba, K., Nakajima, Y., Uchiyama, T., Yoshiyama, M., Yamanishi, T. & Hattori, T. Firing patterns of micturition-related neurons in the pontine storage centre in cats. *Auton. Neurosci.* **99,** 24–30 (2002).

125. Sugaya, K., Ogawa, Y., Hatano, T., Nishijima, S., Matsuyama, K. & Mori, S. Ascending and descending brainstem neuronal activity during cystometry in decerebrate cats. *Neurourol. Urodyn.* **22,** 343–350 (2003).

126. Sasaki, M. Properties of Barrington's neurones in cats: units that fire inversely with micturition contraction. *Brain Res.* **1033,** 41–50 (2005).

127. Manohar, A., Curtis, A. L., Zderic, S. A. & Valentino, R. J. Brainstem network dynamics underlying the encoding of bladder information. *eLife* **6,** (2017).

128. Henneman, E. Relation between Size of Neurons and Their Susceptibility to Discharge. *Science* **126,** 1345–1347 (1957).

129. Ciesielska, A., Hadaczek, P., Mittermeyer, G., Zhou, S., Wright, J. F., Bankiewicz, K. S. & Forsayeth, J. Cerebral Infusion of AAV9 Vector-encoding Non-self Proteins Can Elicit Cell-mediated Immune Responses. *Mol. Ther.* **21,** 158–166 (2013).

130. Tang, Y., Rampin, O., Giuliano, F. & Ugolini, G. Spinal and brain circuits to motoneurons of the bulbospongiosus muscle: Retrograde transneuronal tracing with rabies virus. *J. Comp. Neurol.* **414,** 167–192 (1999).

131. Capelli, P., Pivetta, C., Soledad Esposito, M. & Arber, S. Locomotor speed control circuits in the caudal brainstem. *Nature* (2017). doi:10.1038/nature24064

132. Caggiano, V., Leiras, R., Goñi-Erro, H., Masini, D., Bellardita, C., Bouvier, J., Caldeira, V., Fisone, G. & Kiehn, O. Midbrain circuits that set locomotor speed and gait selection. *Nature* **553,** 455–460 (2018).

133. Danner, S. M., Shevtsova, N. A., Frigon, A. & Rybak, I. A. Computational modeling of spinal circuits controlling limb coordination and gaits in quadrupeds. *eLife* **6,** (2017).

134. Pavcovich, L. A. & Valentino, R. J. Central regulation of micturition in the rat by corticotropin-releasing hormone from Barrington's nucleus. *Neurosci. Lett.* **196,** 185–188 (1995).

135. Stengel, A. & Taché, Y. Neuroendocrine Control of the Gut During Stress: Corticotropin-Releasing Factor Signaling Pathways in the Spotlight. *Annu. Rev. Physiol.* **71,** 219–239 (2009).

136. Huynh, H. K., Willemsen, A. T. M., Lovick, T. A. & Holstege, G. Pontine Control of Ejaculation and Female Orgasm. *J. Sex. Med.* **10,** 3038–3048 (2013).

137. Martinez-Gomez, M., Luz, D., Cruz-Gomez, Y., Zempoalteca, R., Rodriguez-Antolin, J. & Castela, F. The Role of Pelvic and Perineal Muscles in Reproductive and Excretory Functions. in *Applications of EMG in Clinical and Sports Medicine* (ed. Steele, C.) (InTech, 2012). doi:10.5772/27393

138. Veening, J. G. & Coolen, L. M. Neural mechanisms of sexual behavior in the male rat: Emphasis on ejaculation-related circuits. *Pharmacol. Biochem. Behav.* **121,** 170–183 (2014).

139. Truitt, W. A. Identification of a Potential Ejaculation Generator in the Spinal Cord. *Science* **297,** 1566–1569 (2002).

140. Coolen, L., Allard, J., Truitt, W. & Mckenna, K. Central regulation of ejaculation. *Physiol. Behav.* **83,** 203–215 (2004).

141. Carro-Juárez, M. & Rodríguez-Manzo, G. The spinal pattern generator for ejaculation. *Brain Res. Rev.* **58,** 106–120 (2008).

142. Sakamoto, H. The gastrin-releasing peptide system in the spinal cord mediates masculine sexual function. *Anat. Sci. Int.* **86,** 19–29 (2011).

143. Coolen, L. M. Neural control of ejaculation. *J. Comp. Neurol.* **493,** 39–45 (2005).

144. Swanson, L. W. Neuropeptides - new vistas on synaptic transmission. *Trends Neurosci.* **6,** 294–295 (1983).

145. D'Amico, S. C. & Collins, W. F. External urethral sphincter motor unit recruitment patterns during micturition in the spinally intact and transected adult rat. *J. Neurophysiol.* **108,** 2554–2567 (2012).

146. Buffini, M., O'Halloran, K. D., O'Herlihy, C., O'Connell, P. R. & Jones, J. F. X. Comparison of the motor discharge to the voluntary sphincters of continence in the rat: Comparison of rat EUS and EAS. *Neurogastroenterol. Motil.* **24,** e175–e184 (2012).

147. Ashton-Miller, J. A. & DeLancey, J. O. L. On the Biomechanics of Vaginal Birth and Common Sequelae. *Annu. Rev. Biomed. Eng.* **11,** 163–176 (2009).

148. Nadelhaft, I., Vera, P. L., Card, J. P. & Miselis, R. R. Central nervous system neurons labelled following the injection of pseudorabies virus into the rat urinary bladder. *Neurosci. Lett.* **143,** 271–274 (1992).

149. Marson, L. Identification of central nervous system neurons that innervate the bladder body, bladder base, or external urethral sphincter of female rats: A transneuronal tracing study using pseudorabies virus. *J. Comp. Neurol.* **389,** 584–602 (1997).

150. Sugaya, K., Roppolo, J. R., Yoshimura, N., Card, J. P. & de Groat, W. C. The central neural pathways involved in micturition in the neonatal rat as revealed by the injection of pseudorabies virus into the urinary bladder. *Neurosci. Lett.* **223,** 197–200 (1997).

151. Grill, W. M., Erokwu, B. O., Hadziefendic, S. & Haxhiu, M. A. Extended survival time following pseudorabies virus injection labels the suprapontine neural network controlling the bladder and urethra in the rat. *Neurosci. Lett.* **270,** 63–66 (1999).

152. Nadelhaft, I. & Vera, P. L. Separate urinary bladder and external urethral sphincter neurons in the central nervous system of the rat: simultaneous labeling with two immunohistochemically distinguishable pseudorabies viruses. *Brain Res.* **903,** 33–44 (2001).

153. Im, Y. J., Hong, C. H., Jin, M. H., Lee, B. H. & Han, S. W. c-fos Expression in Bladder-Specific Spinal Neurons after Spinal Cord Injury Using Pseudorabies Virus. *Yonsei Med. J.* **49,** 479 (2008).

154. Nadelhaft, I. & Vera, P. L. Neurons in the rat brain and spinal cord labeled after pseudorabies virus injected into the external urethral sphincter. *J. Comp. Neurol.* **375,** 502–517 (1996).

155. Lee, J. W. & Erskine, M. S. Pseudorabies virus tracing of neural pathways between the uterine cervix and CNS: Effects of survival time, estrogen treatment, rhizotomy, and pelvic nerve transection. *J. Comp. Neurol.* **418,** 484–503 (2000).

156. Wiesel, O., Tóth, I. E., Boldogkői, Z., Hornyák, Á., Bokor, V., Halász, B. & Gerendai, I. Comparison of transsynaptic viral labeling of central nervous system structures from the uterine horn in virgin, pregnant, and lactating rats: CNS Connections of the Uterus. *Microsc. Res. Tech.* **63,** 244–252 (2004).

157. Papka, R. E., Williams, S., Miller, K. E., Copelin, T. & Puri, P. CNS location of uterine-related neurons revealed by trans-synaptic tracing with pseudorabies virus and their relation to estrogen receptor-immunoreactive neurons. *Neuroscience* **84,** 935–952 (1998).

158. Cano, G., Card, J. P., Rinaman, L. & Sved, A. F. Connections of Barrington's nucleus to the sympathetic nervous system in rats. *J. Auton. Nerv. Syst.* **79,** 117–128 (2000).

159. Marson, L. & McKenna, K. E. CNS cell groups involved in the control of the ischiocavernosus and bulbospongiosus muscles: A transneuronal tracing study using pseudorabies virus. *J. Comp. Neurol.* **374,** 161–179 (1996).

160. Xu, C., Giuliano, F., Yaici, E. D., Conrath, M., Trassard, O., Benoit, G. & Vergé, D. Identification of lumbar spinal neurons controlling simultaneously the prostate and the bulbospongiosus muscles in the rat. *Neuroscience* **138,** 561–573 (2006).

161. Dobberfuhl, A. D., Oti, T., Sakamoto, H. & Marson, L. Identification of CNS Neurons Innervating the Levator Ani and Ventral Bulbospongiosus Muscles in Male Rats. *J. Sex. Med.* **11,** 664–677 (2014).

162. Valentino, R. J., Kosboth, M., Colflesh, M. & Miselis, R. R. Transneuronal labeling from the rat distal colon: Anatomic evidence for regulation of distal colon function by a pontine corticotropin-releasing factor system. *J. Comp. Neurol.* **417,** 399–414 (2000).

163. Keast, J. R. Unusual Autonomic Ganglia: Connections, Chemistry, and Plasticity of Pelvic Ganglia. *Int. Rev. Cytol.* **193,** 1–69 (1999).

164. Keast, J. R. The autonomic nerve supply of male sex organs – an important target of circulating androgens. *Behav. Brain Res.* **105,** 81–92 (1999).

165. Keast, J. R., Booth, A. M. & de Groat, W. C. Distribution of neurons in the major pelvic ganglion of the rat which supply the bladder, colon or penis. *Cell Tissue Res.* **256,** 105–112 (1989).

166. Vizzard, M. A., Erdman, S. L., Förstermann, U. & de Groat, W. C. Differential distribution of nitric oxide synthase in neural pathways to the urogenital organs (urethra, penis, urinary bladder) of the rat. *Brain Res.* **646,** 279–291 (1994).

167. Keast, J. R. Patterns of co-existence of peptides and differences of nerve fibre types associated with noradrenergic and non-noradrenergic (putative cholinergic) neurons in the major pelvic ganglion of the male rat. *Cell Tissue Res.* **266,** 405–415 (1991).

168. Shafik, A. & El-Sibai, O. Effect of levator ani muscle contraction on urethrovesical and anorectal pressures and role of the muscle in urination and defecation. *Urology* **58,** 193–196 (2001).

169. Shafik, A. Levator ani muscle: new physioanatomical aspects and role in the micturition mechanism. *World J. Urol.* **17,** 266–273 (1999).

170. Shafik, A. Straining and its role in micturition. *Urology* **62,** 199–200 (2003).

171. Jiang, H.-H., Salcedo, L. B., Song, B. & Damaser, M. S. Pelvic Floor Muscles and the External Urethral Sphincter Have Different Responses to Applied Bladder Pressure During Continence. *Urology* **75,** 1515.e1-1515.e7 (2010).

172. Xicohténcatl-Rugerio, I., Corona-Quintanilla, D. L., Nicolás, L., Martínez-Gómez, M., Cuevas, E., Castelán, F. & Rodríguez-Antolín, J. The role of the pubococcygeus muscle in the urethrogenital reflex of male rats: Pelvic Muscles and Urethrogenital Reflex. *Neurourol. Urodyn.* **36,** 80–85 (2017).

173. Burden, H., Price, G., Renegar, R. & Hodson, C. Effects of peripheral nerve lesions during pregnancy on parturition in rats. *Anat. Embryol. (Berl.)* **182,** (1990).

174. Barnett, S. A., Dickson, R. G. & Warth, K. G. Social status, activity and preputial glands of wild and domestic house mice. *Zool. J. Linn. Soc.* **70,** 421–430 (1980).

175. Bronson, F. H. & Caroom, D. Preputial gland of the male mouse: attractant function. *Reproduction* **25,** 279–282 (1971).

176. Yoshikawa, K., Nakagawa, H., Mori, N., Watanabe, H. & Touhara, K. An unsaturated aliphatic alcohol as a natural ligand for a mouse odorant receptor. *Nat. Chem. Biol.* **9,** 160–162 (2013).

177. Wanigasekara, Y., Kepper, M. E. & Keast, J. R. Immunohistochemical characterisation of pelvic autonomic ganglia in male mice. *Cell Tissue Res.* **311,** 175–185 (2003).

178. Bartlett, M. J., Steeves, T. E., Gemmell, N. J. & Rosengrave, P. C. Sperm competition risk drives rapid ejaculate adjustments mediated by seminal fluid. *eLife* **6,** e28811 (2017).

179. Chen, X.-N., Zhu, H., Meng, Q.-Y. & Zhou, J.-N. Estrogen receptor-α and -β regulate the human corticotropin-releasing hormone gene through similar pathways. *Brain Res.* **1223,** 1–10 (2008).

180. Gutkowska, J., Jankowski, M., Mukaddam-Daher, S. & McCann, S. M. Corticotropin-releasing hormone causes antidiuresis and antinatriuresis by stimulating vasopressin and inhibiting atrial natriuretic peptide release in male rats. *Proc. Natl. Acad. Sci.* **97,** 483–488 (2000).

181. Potter, L. R., Yoder, A. R., Flora, D. R., Antos, L. K. & Dickey, D. M. Natriuretic Peptides: Their Structures, Receptors, Physiologic Functions and Therapeutic Applications. in *cGMP: Generators, Effectors and Therapeutic Implications* (eds. Schmidt, H. H. H. W., Hofmann, F. & Stasch, J.-P.) **191,** 341–366 (Springer Berlin Heidelberg, 2009).

182. Gutkowska, J., Antunes-Rodrigues, J. & McCann, S. M. Atrial natriuretic peptide in brain and pituitary gland. *Physiol. Rev.* **77,** 465–515 (1997).

183. Cheng, C.-L. & de Groat, W. C. Effect of Ovariectomy on External Urethral Sphincter Activity in Anesthetized Female Rats. *J. Urol.* **186,** 334–340 (2011).

184. Nilsson, M. E., Vandenput, L., Tivesten, Å., Norlén, A.-K., Lagerquist, M. K., Windahl, S. H., Börjesson, A. E., Farman, H. H., Poutanen, M., Benrick, A., Maliqueo, M., Stener-Victorin, E., Ryberg, H. & Ohlsson, C. Measurement of a Comprehensive Sex Steroid Profile in Rodent Serum by High-Sensitive Gas Chromatography-Tandem Mass Spectrometry. *Endocrinology* **156,** 2492–2502 (2015).

185. Streng, T. K., Talo, A., Andersson, K.-E. & Santti, R. A dose-dependent dual effect of oestrogen on voiding in the male mouse? *BJU Int.* **96,** 1126–1130 (2005).

186. Miller, V. M. & Duckles, S. P. Vascular Actions of Estrogens: Functional Implications. *Pharmacol. Rev.* **60,** 210–241 (2008).

187. Straub, R. H. The Complex Role of Estrogens in Inflammation. *Endocr. Rev.* **28,** 521–574 (2007).

188. Gould, S. J. & Lewontin, R. C. The spandrels of San Marco and the Panglossian paradigm: a critique of the adaptationist programme. *Proc. R. Soc. Lond. B Biol. Sci.* **205,** 581 (1979).

189. Mesiano, S. Roles of Estrogen and Progesterone in Human Parturition. in *Frontiers of Hormone Research* (ed. Smith, R.) **27,** 86–104 (Karger, 2001).

190. Grammatopoulos, D. K. & Hillhouse, E. W. Role of corticotropin-releasing hormone in onset of labour. *The Lancet* **354,** 1546–1549 (1999).

191. Yiou, R., Delmas, V., Carmeliet, P., Gherardi, R. K., Barlovatz-Meimon, G., Chopin, D. K., Abbou, C.-C. & Lefaucheur, J.-P. The pathophysiology of pelvic floor disorders: evidence from a histomorphologic study of the perineum and a mouse model of rectal prolapse. *J. Anat.* **199,** 599–607 (2001).

192. Wolff, P. R. & Powell, A. J. Urination patterns and estrous cycling in mice. *Behav. Neural Biol.* **27,** 379–383 (1979).

193. Wolff, P. R. & Powell, A. Urine patterns in mice: analysis of male/female counter-marking. *Anim. Behav.* 7 (1984).

194. Matochik, J. A., White, N. R. & Barfield, R. J. Variations in scent marking and ultrasonic vocalizations by Long-Evans rats across the estrous cycle. *Physiol. Behav.* **51,** 783–786 (1992).

195. Maruniak, J. A., Owen, K., Bronson, F. H. & Desjardins, C. Urinary marking in female house mice: Effects of ovarian steroids, sex experience, and type of stimulus. *Behav. Biol.* **13,** 211–217 (1975).

196. Kimura, T. & Hagiwara, Y. Regulation of urine marking in male and female mice: Effects of sex steroids. *Horm. Behav.* **19,** 64–70 (1985).

197. Coquelin, A. Urine-marking by female mice throughout their reproductive cycle. *Horm. Behav.* **26,** 255–271 (1992).

198. Watson, C. & Foundation, C. & D. R. *The Spinal cord a Christopher and Dana Reeve Foundation text and atlas*. (Amsterdam Elsevier/Academic Press, 2009).

199. Osman, N. I. & Chapple, C. R. Fowler's syndrome - a cause of unexplained urinary retention in young women? *Nat. Rev. Urol.* **11,** 87–98 (2014).

200. Bauer, S. B. The Hinman Syndrome. *J. Urol.* **197,** S132–S133 (2017).

201. Lovick, T. A. Central control of visceral pain and urinary tract function. *Auton. Neurosci.* **200,** 35–42 (2016).

202. Tai, C., Wang, J., Jin, T., Wang, P., Kim, S.-G., Roppolo, J. R. & de Groat, W. C. Brain Switch for Reflex Micturition Control Detected by fMRI in Rats. *J. Neurophysiol.* **102,** 2719–2730 (2009).

203. Lee, U., Chang, H. H., Christe, K. & Havton, L. Evoked voiding contractions and corresponding urethral sphincter electromyography in non-human primates differs from rodents. *J. Urol.* **189,** e13 (2013).

204. Langdale, C. L. & Grill, W. M. Phasic activation of the external urethral sphincter increases voiding efficiency in the rat and the cat. *Exp. Neurol.* **285,** 173–181 (2016).

205. Streng, T., Santti, R., Andersson, K.-E. & Talo, A. The role of the rhabdosphincter in female rat voiding. *BJU Int.* **94,** 138–142 (2004).

206. Coleman, A. M. & Sengelaub, D. R. Patterns of dye coupling in lumbar motor nuclei of the rat. *J. Comp. Neurol.* **454,** 34–41 (2002).

207. Streng, T., Santti, R. & Talo, A. Similarities and differences in female and male rat voiding. *Neurourol. Urodyn.* **21,** 136–141 (2002).

208. Streng, T., Santti, R. & Talo, A. Possible action of the proximal rhabdosphincter muscle in micturition of the adult male rat. *Neurourol. Urodyn.* **20,** 197–213 (2001).

209. Moldestad, O., Karlsen, P., Molden, S. & Storm, J. F. Tracheotomy improves experiment success rate in mice during urethane anesthesia and stereotaxic surgery. *J. Neurosci. Methods* **176,** 57–62 (2009).

210. Field, K. J. & Lang, C. M. Hazards of urethane (ethyl carbamate): a review of the literature. *Lab. Anim.* **22,** 255–262 (1988).

211. Noto, H., Roppolo, J. R., Steers, W. D. & de Groat, W. C. Excitatory and inhibitory influences on bladder activity elicited by electrical stimulation in the pontine micturition center in the rat. *Brain Res.* **492,** 99–115 (1989).

212. Takasaki, A., Hui, M. & Sasaki, M. Is the periaqueductal gray an essential relay center for the micturition reflex pathway in the cat? *Brain Res.* **1317,** 108–115 (2010).

213. Manzo, J., Garcia, L. I., Hernandez, M. E., Carrillo, P. & Pacheco, P. Neuroendocrine control of urine-marking behavior in male rats. *Physiol. Behav.* **75,** 25–32 (2002).

214. Becker, S. D. & Hurst, J. L. Female behaviour plays a critical role in controlling murine pregnancy block. *Proc. R. Soc. B Biol. Sci.* **276,** 1723–1729 (2009).

215. Tinbergen, N. *The Study of Instinct*. (Oxford University Press, 1951).

216. Hurst, J. L. & West, R. S. Taming anxiety in laboratory mice. *Nat. Methods* **7,** 825–826 (2010).

217. Matthews, M. K. Urinary marking and tendency to investigate novelty in Mus musculus. *Behav. Neural Biol.* **28,** 501–506 (1980).

218. Collins, S. A., Gosling, L. M., Watkins, R. W. & Cowan, D. P. Artificially increasing scent mark rate increases urogenital gland size in mice Mus musculus. *Physiol. Behav.* **74,** 517–522 (2001).

219. Smith, P. P., DeAngelis, A. & Simon, R. Evidence of increased centrally enhanced bladder compliance with ageing in a mouse model: FFT of ageing bladder compliance. *BJU Int.* **115,** 322–329 (2015).

220. Maruniak, J. A., Taylor, J. A. & Perrigo, G. Effects of Water Deprivation on Urine Marking and Aggression in Male House Mice. *Physiol. Behav.* **42,** 47–51 (1988).

221. Ogier, R., Tribollet, E., Suarez, P. & Raggenbass, M. Identified Motoneurons Involved in Sexual and Eliminative Functions in the Rat Are Powerfully Excited by Vasopressin and Tachykinins. *J. Neurosci.* **26,** 10717–10726 (2006).

222. Ueno, H., Kuno, M., Shintani, Y. & Kamo, I. Role of vasopressin V1A receptor in the urethral closure reflex in rats. *Am. J. Physiol.-Ren. Physiol.* **300,** F976–F982 (2011).

223. Kamo, I., Torimoto, K., Chancellor, M. B., de Groat, W. C. & Yoshimura, N. Urethral closure mechanisms under sneeze-induced stress condition in rats: a new animal model for evaluation of stress urinary incontinence. *Am. J. Physiol.-Regul. Integr. Comp. Physiol.* **285,** R356–R365 (2003).

224. Lenz, K. M. & Sengelaub, D. R. Maternal licking influences dendritic development of motoneurons in a sexually dimorphic neuromuscular system. *Brain Res.* **1092,** 87–99 (2006).

225. Ariely, D. *Predictably irrational: The hidden forces that shape our decisions.* (Harper Collins, 2008).

226. Kahneman, D. *Thinking, fast and slow*. (Farrar, Straus and Giroux, 2011).

227. Damasio, A. P. *Descartes' Error: Emotion, Reason, and the Human Brain*. (Avon, 1994).

228. Legenstein, R., Pecevski, D. & Maass, W. A Learning Theory for Reward-Modulated Spike-Timing-Dependent Plasticity with Application to Biofeedback. *PLoS Comput. Biol.* **4,** e1000180 (2008).

229. Minsky, M. Steps Toward Artificial Intelligence. *Proc. IRE* **49,** 8–30 (1961).

230. Atasoy, D., Betley, J. N., Su, H. H. & Sternson, S. M. Deconstruction of a neural circuit for hunger. *Nature* **488,** 172–177 (2012).

231. Chen, T.-W., Wardill, T. J., Sun, Y., Pulver, S. R., Renninger, S. L., Baohan, A., Schreiter, E. R., Kerr, R. A., Orger, M. B., Jayaraman, V., Looger, L. L., Svoboda, K. & Kim, D. S. Ultrasensitive fluorescent proteins for imaging neuronal activity. *Nature* **499,** 295–300 (2013).

232. Card, J. P. & Enquist, L. W. Transneuronal Circuit Analysis with Pseudorabies Viruses: Transneuronal Circuit Analysis with Pseudorabies Viruses. in *Current Protocols in Neuroscience* (eds. Gerfen, C. R., Holmes, A., Sibley, D., Skolnick, P. & Wray, S.) 1.5.1-1.5.39 (John Wiley & Sons, Inc., 2014). doi:10.1002/0471142301.ns0105s68

233. Cunningham, M. G., Donalds, R. A., Scouten, C. W. & Tresch, M. C. A versatile, low-cost adaptor for stereotaxic and electrophysiologic spinal preparations in juvenile and adult rodents. *Brain Res. Bull.* **68,** 157–162 (2005).

234. Harrison, M., O'Brien, A., Adams, L., Cowin, G., Ruitenberg, M. J., Sengul, G. & Watson, C. Vertebral landmarks for the identification of spinal cord segments in the mouse. *NeuroImage* **68,** 22–29 (2013).

235. Nadelhaft, I. & Vera, P. L. Neurons in the rat brain and spinal cord labeled after pseudorabies virus injected into the external urethral sphincter. *J. Comp. Neurol.* **375,** 502–517 (1996).

236. Holy, T. E., Dulac, C. & Meister, M. Responses of Vomeronasal Neurons to Natural Stimuli. *Science* **289,** 1569 (2000).

237. Kim, C. K., Yang, S. J., Pichamoorthy, N., Young, N. P., Kauvar, I., Jennings, J. H., Lerner, T. N., Berndt, A., Lee, S. Y., Ramakrishnan, C., Davidson, T. J., Inoue, M., Bito, H. & Deisseroth, K. Simultaneous fast measurement of circuit dynamics at multiple sites across the mammalian brain. *Nat. Methods* **13,** 325–328 (2016).

238. Soukhova-O'Hare, G. K., Schmidt, M. H., Nozdrachev, A. D. & Gozal, D. A novel mouse model for assessment of male sexual function. *Physiol. Behav.* **91,** 535–543 (2007).

239. Richner, M., Jager, S. B., Siupka, P. & Vaegter, C. B. Hydraulic Extrusion of the Spinal Cord and Isolation of Dorsal Root Ganglia in Rodents. *J. Vis. Exp.* (2017). doi:10.3791/55226

240. Saleh, T. M., Connell, B. J., McQuaid, T. & Cribb, A. E. Estrogen-induced neurochemical and electrophysiological changes in the parabrachial nucleus of the male rat. *Brain Res.* **990,** 58–65 (2003).